Contents

THEORETICAL AND EXPERIMENTAL DETERMINATION OF THE CRACK WIDTH IN REINFORCED CONCRETE AT VERY LOW TEMPERATURES

C. v.d. Veen
Delft University of Technology,
Faculty of Civil Engineering

This publication has been issued in close co-operation with the Netherlands Technology Foundation (STW).

Abstract

The compressive strength, the tensile splitting strength, the stress strain relationship and the thermal deformation of concrete are determined experimentally as a function of temperature.
Theoretical formulae are derived based on the classical bond stress-slip theory to predict crack width and spacing in a reinforced tension member at very low temperatures. This model is based on the local bond stress-slip relationship, which is determined experimentally as a function of temperature and curing conditions. It has been proven that realistic crack widths can be calculated using the tension member model. Furthermore a model is derived to predict the ultimate bond stress in case splitting failure occurred as a function of concrete cover and temperature. The lowest bond strength relative to the actual splitting strength is predicted at -40 and -80°C.

SUMMARY

Chapter 1 The introduction lists the avens of application for reinforced or prestressed concrete at low temperatures, e.g. in the Arctic environment and for the cryogenic storage of gases. Structural concrete always exhibits cracks in the service limit state. However, there is a lack of experimental and theoretical research on the crack width and the spacing at low temperatures. The typical feature of the splitting failure of the concrete cover as a function of temperature should be investigated. These subjects are the aim of the present study.

Chapter 2 The properties of concrete affected by low temperature are briefly reviewed. Besides the mechanical properties of concrete the thermal behaviour of concrete and steel are discussed. In general, an increase in strength is found at low temperatures. This increase depends mainly on the free moisture content of the concrete. Furthermore, the bond resistance increases very much at low temperatures. In all cases splitting failure occurs for a practical concrete cover at low temperatures.
High reinforcement ratios (3 to 4%) very greatly increase the crack spacing in water-saturated concrete tensile members at low temperatures. No increase in crack spacing was observed for sealed concrete at -165°C.

Chapter 3 In this chapter the theoretical formulae are derived to predict crack width and spacing in a reinforced tension member. This model is based on the local bond stress-slip relationship which should be approximated with the aid of a power function at various temperatures. What is termed the "first-generation crack" possesses a greater crack width than the crack width associated with a fully developed crack pattern, if a constant tensile strength is assumed. As a result of the thermal differences between concrete and reinforcement, restrained stresses are generated during cooling. The effect of this feature on the crack width and spacing is taken into account by considering the tensile member as pretensioned.
Subsequently, a theoretical model is developed for the splitting failure mechanism. In the model the softening behaviour of the concrete and the number of cracks are taken into account. A minimum cracking resistance relative to the actual tensile strength is calculated at around -70°C.

Chapter 4 The experimental programme and the equipment used are described. It was decided to divide the experiments into two main parts. In the first part the material properties of concrete were investigated as a function of temperature and moisture content. In the second part the bond stress-slip relationship was determined by means of a pull-out test. Furthermore, to study the effect of the temperature and moisture content on the crack width and the spacing, 12 centrically reinforced tension members of 1 m in length were tested at various temperatures.
The basic experimental programme comprised five temperatures, two concrete grades and three sets of curing conditions, namely water-saturated (S), sealed (W) and air-dry at 50% r.h. and 20°C (H). All the other experiments were performed for

one set of curing conditions, namely sealed. For both concrete mixes an investigation was made of the influence of the age (28 and 365 days), cooling rate and cyclic temperature loading on the bond stress-slip relationship. The effect on the bond resistance of the embedment length, the bar diameter and the type of reinforcement (plain bar, deformed) was also investigated.

Chapter 5 The increase in the compressive strength and the tensile splitting strength of concrete with lowering of the temperature is primarily a function of the free moisture content and is independent of the concrete grade and the age of the concrete. A higher cylinder to cubic strength ratio was found at low temperatures. Generally, the greater part of the increase in splitting strength occurs in the temperature range from 0 to -40°C, unlike the increase in compressive strength, which occurs mainly at temperatures from 0 to -120°C. Concrete tested at low temperatures and three different ages, namely 28, 90 and 365 days, showed about equal actual strengths. The static modulus of elasticity is found to increase at low temperatures, but to a far lesser extent than the (cylinder) compressive strength. A more or less linear elastic stress-strain relationship is found for concrete tested at -165°C.

After thermal cycling a reduction in strength of the sealed concrete is observed, which is most significant for the modulus of elasticity and least significant for the compressive strength. However, for the concrete mix with a low w/c ratio (0.40) hardly any reduction in strength is observed. Sealed and air-dry concrete exhibit thermal behaviour characterized by almost linear thermal deformation and perfect reversibility. This behaviour proved to be independent of the w/c ratio and the moisture content. Water-saturated concrete was found to undergo thermal expansion in the temperature range between -20 and -60°C. This expansion is clearly affected by the w/c ratio and it increases for higher ratios. Only limited stresses will be introduced in a reinforced concrete member during cooling as a result of the small differences between the coefficients of thermal expansion of the reinforcement and of the air-dry or sealed concrete. However, considerable stresses may develop in reinforced water-saturated concrete.

It has been proved that the bond resistance increases when the temperature is lowered. The main part of this increase takes place in the temperature range from 20 to -120°C. A typical phenomenon is observed at -165°C for slip values generally exceeding 0.02 mm. For higher bond stresses these slip values increase instantaneously, and these abrupt changes in the slip rapidly become larger.

For the mix with the low w/c ratio splitting failure is nearly always found to be the governing failure mechanism in the case of water-saturated concrete, whereas for the other concrete mix at low temperatures shear failure or yielding of the reinforcement determine the bond strength. For the one year old concrete a less pronounced effect of the temperature on the bond stress-slip relationship is observed and a different failure mode, splitting failure, is found at -165°C.

Thermal cycling proved to have no significant effect on the bond resistance for the mix with a low w/c ratio even after 10 temperature cycles. For the mix with a higher w/c ratio (0.60) a reduction in bond resistance is found which varied from 11 to 4%

for slip values from 0.025 to 0.20 mm. The bond strength of plain bars was found to increase by about 115% at -80 and -165°C in comparison with the bond strength found at 20°C. However, the bond stress measured at a slip value of 1.5 mm turns out to be relatively independent of the temperature.
The load at which a concrete element, subjected to direct tension, started to crack was found to increase markedly at lower temperatures particularly for water-saturated concrete. In all cases the crack widths found at low temperatures were smaller than those found at room temperature for the mix with the low w/c ratio (0.40), but greater crack widths were found for the mix with the high w/c ratio (0.60). Tension stiffening increases at lower temperatures and the major part of this increase occurs in the temperature range from 0 to -80°C. The greatest tension stiffening is observed for the water-saturated concrete tension members.

Chapter 6 The experimentally found bond stress-slip relationships are predicted analytically and a reasonable agreement with the results obtained from other research is found. Splitting failure can be predicted theoretically with the model, whilst the typical phenomenon, a lower bond strength to tensile strength ratio found at -40 and -80°C, is predicted as well. The bond strength limited by the shear failure mode is expressed as a bond strength to compressive strength ratio and amounts to 0.51.
Crack width can be calculated as a function of temperature with the aid of the tension member model. It can also take into account the "prestressing effect" in the case of water-saturated concrete. It is necessary to apply transverse reinforcement at low temperatures to avoid splitting failure. The maximum crack width is limited to 0.2 mm at -120 and -165°C and 0.5 mm at the higher temperatures.

Chapter 7 The main results of the study are reviewed and suggestions are given for supplementary research. The material properties and bond stress-slip relationships found can be used in a finite element package to analyze the cracking behaviour of structures at low temperatures.

1. INTRODUCTION

1.1. Scope of the research

Since the Second World War the growth in the world economy has led to a greater demand for energy. Particularly the use of natural gas has undergone exponential growth leading to an increase in its use for both domestic and industrial applications. Because of this development a growing need has arisen for the exploitation of large gas reservoirs in the Arctic and the sub-Arctic and for suitable storage and transportation equipment. The application of reinforced concrete structures in the Arctic environment is very effective in withstanding the severe loading conditions characterized by temperatures down to about 50 degrees Celsius below zero, and by icefields and icebergs. Natural gas can be stored both in the gaseous phase and in liquefied form. Nowadays gases are in general preferably stored in liquid form at atmospheric pressure. Therefore gases are cooled to their boiling point, which for most gases is below 0°C, Table 1, Turner [1].

Table 1 Some physical properties of liquefied gases, [1].

liquefied gases	boiling point °C	volume reduction factor
Butane	- 11	1/240
Ammonia	- 33	1/950
Propane	- 42	1/310
Ethane	- 89	1/430
Methane (LNG)	- 162	1/620
Oxygen	- 183	1/800
Nitrogen	- 196	1/690

Liquefied Natural Gas (LNG) consists of 80-90% (by vol.) of methane.
Liquefied Petroleum Gas (LPG) consists mostly of propane and/or butane.

Natural gas undergoes a decrease in volume in a ratio of 620:1 as a result of liquefaction at -162°C and is then commonly referred to as L.N.G. For safety reasons a double-walled tank is normally used for the bulk storage of large quantities of L.N.G. The most common systems comprise an inner tank of 9% nickel steel, to maintain ductility at the very low operating temperature, and a carbon steel outer tank. Thermal insulation in the gap between the outer and inner tank minimizes the loss of energy. In recent years the use of increasingly larger tanks, combined with the introduction of even more stringent safety regulations, has led to a new design philosophy and the introduction of composite tanks using prestressed concrete, Bruggeling [2]. Such a tank comprises an inner tank made of nickel steel or prestressed concrete and a steel liner and an outer tank with a concrete roof both constructed of prestressed concrete, [3-5], see Fig. 1.1.

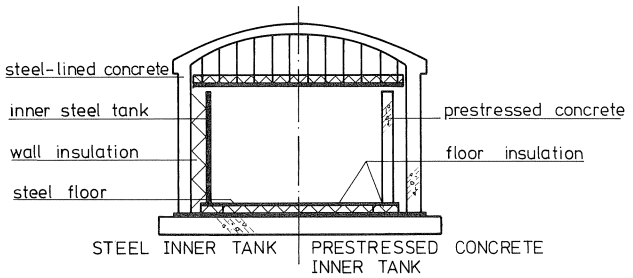

Fig. 1.1 Basic principles for the construction of a double-wall tank [4].

However, the application of reinforced concrete in the structures mentioned above strongly depends on a thorough understanding of the material properties under these conditions. As reinforced concrete comprises two different materials, i.e. steel and concrete, the bond between the reinforcement and the concrete at different temperatures determines the ductility, safety and durability of the structures.
The typical features associated with very low temperatures have stimulated active research all over the world. However, mostly the compressive and the tensile splitting strength of concrete were investigated at low temperatures. Only a limited number of research projects took account of the cryogenic bond stress-slip characteristic, which is the main factor that determines crack width and crack spacing. To calculate crack width and spacing much more information on the typical bond stress-slip characteristic is needed.

1.2. Aim of the research programme

The classical bond-slip theory e.g. Noakowski [6],Bruggeling [7] is used to determine the most important parameters which affect crack width and spacing. This theory assumes that, when the tensile capacity of the concrete is reached, the concrete cracks. The force can be transferred to the concrete per unit of length of each bar and is given by the circumferential area multiplied by the mean bond stress ($\pi\, d_s \tau_{b,av}$). Hence the tensile strength will again be reached at a distance ℓ_{st} from the crack.
This defines the minimum distance ℓ_{st} at which cracks can form, formula 1.1.

$$\ell_{st} = \frac{f_{ct}\, A_c}{\pi\, \tau_{b,av} d_s} \quad \text{mm} \qquad (1.1)$$

The average bond stress $\tau_{b,av}$ can be calculated if the local bond stress-slip relationship is known. This formula holds true if the thermal expansion of the concrete and the reinforcement is almost the same, which is the case in the temperature range from -20 to +60°C. However, when the application of reinforced concrete is not confined to this temperature range, the thermal deformation may differ considerably. For this reason the thermal behaviour of concrete and the reinforcement is also examined.

At room temperature it is common practice to assume a linear relation between the bond stress and the compressive strength. To verify this relationship at low temperatures, the compressive strength of concrete is also investigated.
Thus the aim of the research programme is to determine at least the bond stress-slip relationship, the tensile (splitting) strength, the compressive strength and the thermal behaviour of the concrete at various temperatures. The classical bond-slip theory is also expected to be valid at low temperatures, which fact should be proven analytically and experimentally. Furthermore, much attention is paid to the modelling of the splitting failure mechanism as a function of temperature. In practice this failure mode should be prevented because failure takes place in a brittle way.

2. SURVEY OF THE LITERATURE

2.1. Introduction

The properties of concrete are greatly affected at (very) low temperatures. The main conclusions of a comprehensive literature survey, Van der Veen [8] with regard to the properties mentioned above are briefly reviewed. More attention is paid to the bond behaviour between the reinforcement and the concrete as well as the influence of temperature on crack width and spacing. For more detailed information the reader is referred to the literature survey [8].

2.2. Cryogenic properties of concrete

Various authors [9-18] have surveyed literature concerning, among other features, the mechanical properties of concrete in the range between ambient and cryogenic temperatures. Generally, it is found that the strength of concrete increases as the temperature is lower. This increase will be greater in concretes with higher moisture contents. Furthermore, this increase in strength associated with a lowering of the temperature is primarily a function of the free moisture content of the concrete, regardless of concrete grade, aggregate type (dense or lightweight), degree of air entrainment, type of cement (ordinary Portland cement, fly-ash, blast-furnace slag), or whether or not admixtures are used.
It has been found that the compressive strength increase is hardly affected by the concrete's strength at room temperature and that this increase is directly proportional to the free moisture content of the concrete, see Fig. 2.1.
In practice the free moisture content of thick concrete structures will roughly range from 4 to 6% by mass and at -165°C a strength increase of approximately 60 N/mm^2 will be found.
Research [19-24] has showed that the tensile splitting strength increases at lower temperatures but to a less pronounced extent compared to the compressive strength.

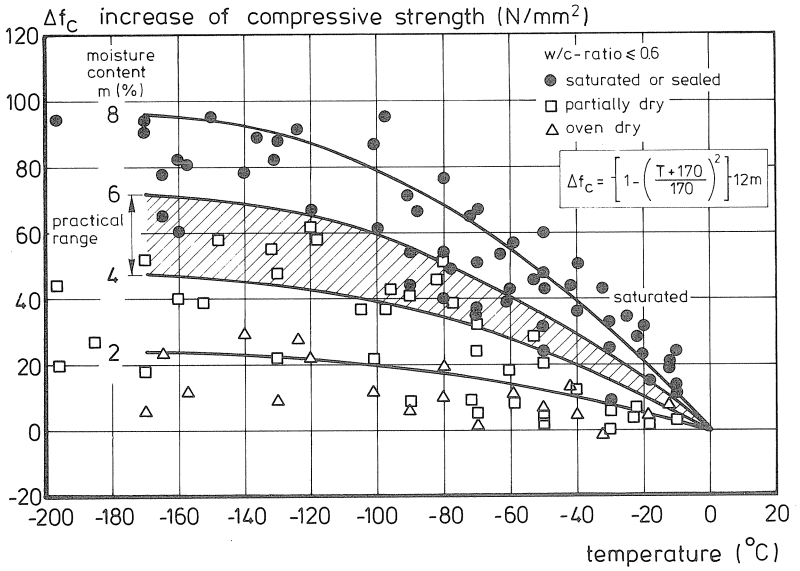

Fig. 2.1 Increase in compressive strength as a function of temperature and moisture content, Van der Veen [8].

Generally, the greatest part of the increase in splitting strength takes place in the temperature range from 0 to -40°C, as contrasted with the increase in compressive strength, which takes place mainly from 0 to -100°C. In general a maximum value was observed at -80°C, whilst at lower temperatures the increase in strength remained constant or even a small decrease was observed.

Young's modulus of elasticity has been studied by various investigators [23,25-28]. For water-saturated and sealed concrete the elastic modulus similarly increases when the temperature is lowered, but to a far lesser extent than the compressive strength. As a result, the initial tangent modulus of elasticity increases by approximately 80, 50 and 15% for saturated, sealed and air-dry concrete respectively at -160°C on the basis of commonly used concrete. Significant losses of concrete strength occur for water-saturated concrete with high w/c ratios due to thermal cycling, Rostásy and Wiedemann [29], particularly for the modulus of elasticity.

In order to quantify the coefficient of thermal expansion $\alpha(T)$, concrete is divided into two main classes. The first comprises concrete with a moisture content corresponding to storage at 86% relative humidity (r.h.) and ranging down to oven-dry concrete. In this class, changes in moisture content have virtually no effect on thermal deformation. Thus the type of aggregate is the governing quantity, see Fig. 2.2. The second class comprises concrete stored at above 86% relative humidity to equilibrium and ranging up to water-saturated concrete. Here an expansion is found in the transition range from -20 to -60°C, and this expansion is highly dependent on the moisture content, see Fig. 2.3. When moist concrete is reheated, $\alpha_c(T)$ shows a hysteresis.

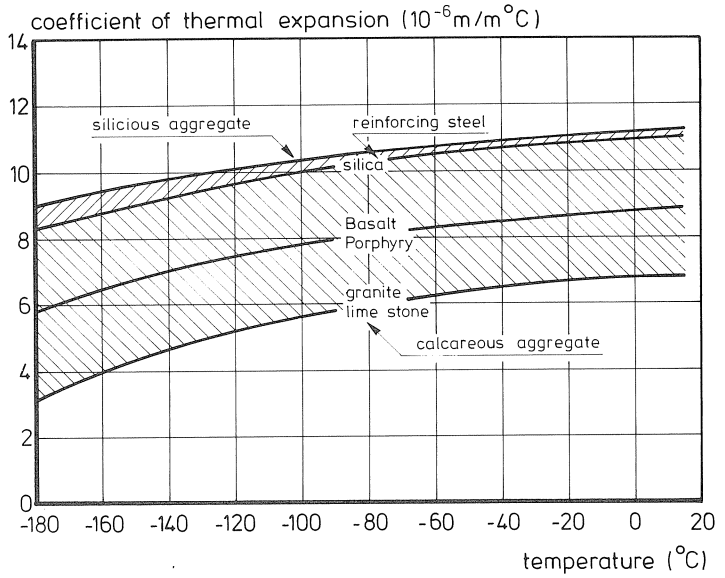

Fig. 2.2 Coefficient of thermal expansion for dry to moderately moist concrete and for reinforcement [30].

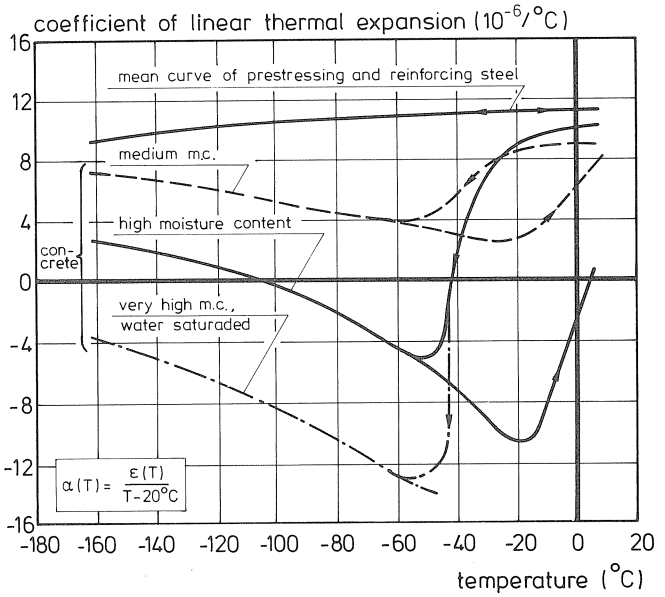

Fig. 2.3 Coefficient of thermal expansion for concrete of high moisture content [30].

2.3. Bond strength

Bond behaviour has been studied for many years. In general, it is investigated by means of pull-out tests, because this type of experiment is fairly simple to perform. What is usually determined is the relationship between the bond stresses (τ_b) at a certain point of a reinforcing bar, averaged over the distance between a few ribs, and the associated relative displacement of the bar (Δ) in relation to the surrounding concrete, commonly called the slip. Several bond mechanisms can be distinguished at room temperature. At extremely small slip values, only a few microns, the level of adhesion is reached, which is a result of such factors as mechanical interlock of the hardened cement paste at the surface irregularities of the bar. Only low bond stresses of approximately 0.05 f_{ccm} can be resisted. For higher bond stresses adhesion will be destroyed, and load transfer will now take place by friction between the concrete and the bar surface and, in the case of a deformed bar, by compressive forces acting on the ribs of the bar. Consequently, the bond resistance can increase after the adhesion has been destroyed for deformed bars as contrasted with plain bars, see Fig. 2.4.

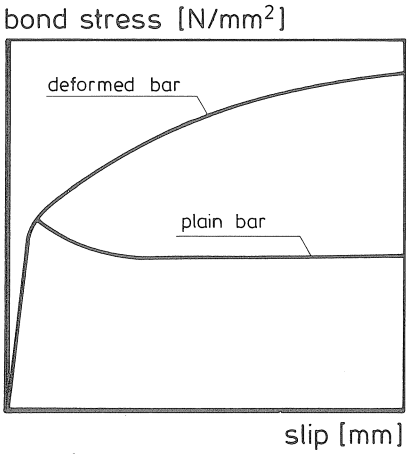

Fig. 2.4 Basic bond stress-slip relations.

The magnitude of the ultimate bond stress of deformed bars depends upon the failure mode. Concrete can fail in two different ways, by splitting failure or by shearing along a plane just around the bar. In practice the first failure mode should be prevented because failure takes place in a brittle way, while in the second failure mode bond failure occurs in consequence of a gradual slip-through of the deformed bar, in which case the maximum bond stress will be attained. However, the alternative possibility is that the bond strength will be determined by the yield strength of the reinforcement instead of the concrete itself. This will happen when the embedment length is (too) long and when there is a high concrete strength. For the reason stated above, most researchers who studied the bond behaviour at

cryogenic temperatures with the aid of a pull-out test used a low-grade concrete and/or a small embedment length. Cryogenic bond behaviour has been studied on a large scale from the mid-seventies in Japan [18,23] and subsequently in a few other countries [19,9,31-34]. Not all the important parameters which influence the bond behaviour at room temperature (see Rehm [35]) have been investigated at cryogenic temperatures. These governing parameters are: the relative rib area represented by the coefficient f_R, the concrete grade, and the casting direction versus the reinforcing direction.
On the basis of the results mentioned in the preceding Section, the moisture content can also be expected to be the governing quantity with regard to the bond behaviour at very low temperatures. This subject as well as the influence of temperature on crack width and spacing will be dealt with in the next Section.

2.3.1. Influence of the curing conditions

Various investigators, Kasami et al. [36], Pfützenreuter [37], Rostásy and Scheuermann [19] and Vandewalle [31] studied the influence of the curing conditions upon the bond strength. For deformed bars the bond stress was usually reported for a

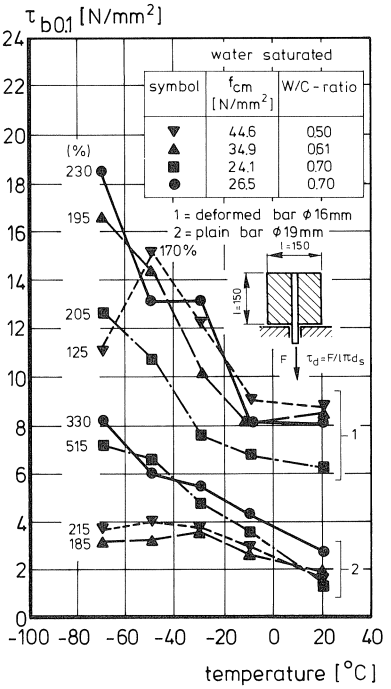

Fig. 2.5 Bond stress at 0.1 mm slip as a function of temperature for water-saturated concrete [36].

measured slip value of 0.1 mm. Only Rostásy/Scheuermann [19] and Pfützenreuter [37] reported the characteristic bond stress-slip curves, and Kasami et al. [36] also investigated the bond behaviour of plain bars at low temperatures. Two curing conditions, water-saturated and air-dry (45% r.h.), were used by Kasami et al. [36] to investigate the bond behaviour of plain bars 19 mm in diameter embedded horizontally in 150 mm concrete cubes at an age of 90 days. The embedment length was 150 mm or 7.9 d_s. The bond strength (failure by slip-through) of plain bars in water-saturated concrete increased very greatly when the temperature was lowered. For the ratios of the actual bond stresses at low temperature to the bond stress at 20°C, the values found were 4.1 and 5.8 at -70°C and -196°C respectively. A small increase of 40% at -196°C was observed for the air-dry condition. In a second part of the experimental programme, the bond behaviour of plain bars as well as deformed bars was studied in the temperature range from +20 to -70°C for four different concrete mixes. The experimental results are shown in Fig. 2.5, in which the change of the bond stress due to low temperatures is expressed by reference to the bond stresses for 0.1 mm end slip. It appears that the bond stress at -70°C increases by approximately 100% for the deformed bars, while for the plain bars two to five higher values are observed in relation to values determined at room temperature. Usually, the bond stress is related to the compressive strength, Noakowski [6]. Because the compressive strength increases by approximately 200% at -70°C, it follows that the bond stress for deformed bars increases to a lesser extent.

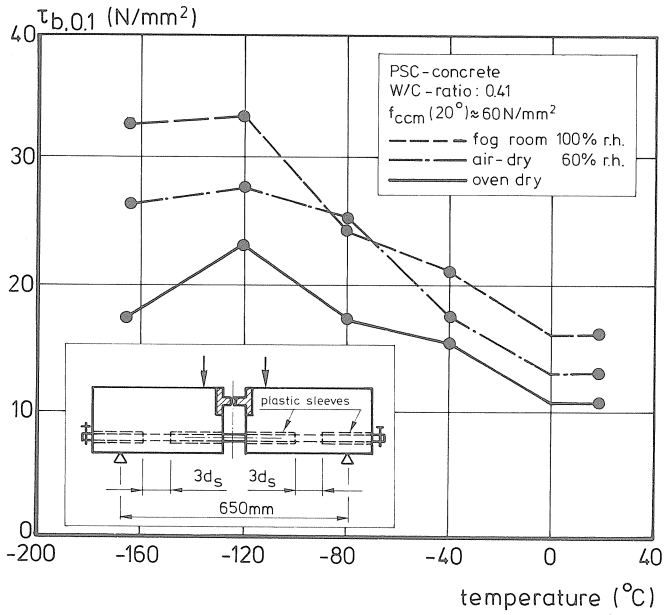

Fig. 2.6 Bond stress determined by means of a beam test at 0.1 mm slip for different curing conditions versus temperature [31].

Vandewalle and Mortelmans [31,38] determined the bond between reinforcement and concrete by means of a beam test according to RILEM. To prevent yielding of the reinforcement during the experiment, the embedment length was reduced from 10 d_s to 3 d_s. The concrete mix with a w/c ratio 0.41 was made with Portland blast furnace cement (PSC). Three different curing conditions were used: in a fog room at 100%, air-dry at 60% r.h. and oven-dry. Experiments were performed at an age of 28 days, the bar diameter was 25 mm and the concrete cover of 37.5 mm was 1.5 d_s. Some typical results are shown in Fig. 2.6. As can be clearly seen, the maximum bond stress is attained at -120°C.
On comparing the relative bond stress ratio $\tau_b(T)/\tau_b(20°C)$ with the relative strength ratio $f_{ccm}(T)/f_{ccm}(20°C)$, the following conclusions can be drawn:

- The bond stress ratios increase at low temperatures to a lesser extent than the compressive strength ratios for moist concrete. However, the bond stress ratios increase proportionally to, and are greater than, the compressive strength ratios for air-dry and oven-dry concrete respectively.
- All the specimens failed because of splitting of the concrete cover.

The bond characteristics were defined by Vandewalle [32] with the aid of a regression analysis:

$$\tau_b(T) = \tau_{bu}(T)\ (1 - 0.78 \exp(-9.78\ \Delta)) \qquad N/mm^2 \qquad (2.1)$$

It appeared that this bond stress-slip relationship depends solely on the bond strength $\tau_{bu}(T)$, which is determined by the splitting strength of the concrete cover in practical cases.

Rostásy and Scheuermann [19] performed a large number of pull-out tests on 16 mm diameter reinforcing bars with f_R = 0.067, centrically embedded over a length of 3 d_s. The pull-out specimen was ϕ172x192 mm cylindrical in shape; the pull-out direction was the same as the casting direction. Tests were performed after cooling at a rate of 0.5°C/min at an age of 150 days. The influence of three different curing conditions (water-saturated, sealed and air-dry 65% r.h.) on the bond-stress relationship was studied. It should be noted that mostly a high w/c ratio of 0.8 was used to obtain a low-grade concrete in order to prevent yielding of the reinforcement during the experiments. For small slip values Δ = 0.01 mm the researchers observed the effect of low temperatures upon the bond stress only for saturated concrete. In this case the bond stress increased.
For larger slip values the influence of the temperature upon the bond stress is more pronounced for all the curing conditions. At a slip value of 0.1 mm the bond stresses appeared to be proportional to the actual compressive strength for the air-dry and sealed concrete. The researchers observed a marked increase in bond stress for the saturated concrete which exceeds the increase in compressive strength. This conclusion is in agreement with the results of Vandewalle and Mortelmans [31]. Furthermore, all the specimens failed by shearing-off, except for the water-

saturated concrete at temperatures lower than -100°C, because the yield strength of the reinforcement was reached before the concrete could fail. Some bond stress-slip curves at different temperatures and curing conditions found experimentally by Rostásy and Scheuermann [19] are shown in Fig. 2.7. A typical phenomenon was found at -170°C for slip values larger than 0.03 and 0.12 mm for the water-saturated and sealed specimens respectively. The slip values increased instantaneously and these abrupt changes in slip rapidly increased at higher bond stresses and finally led to failure. This phenomenon agrees well with the observations of Pfützenreuter [37]. According to Scheuermann [39], such abrupt changes in slip are associated with the sudden initiation of internal longitudinal splitting cracks. For the air-dry concrete specimens the investigators observed a continuous bond stress-slip curve which finally resulted in abrupt failure. Based on their experimental observations, Rostásy and Scheuermann [19] derived local bond stress-slip relationships in the form:

$$\tau_b(T) = a(T)\Delta^{b(T)} \qquad N/mm^2 \qquad (2.2a)$$

in which $\Delta < 0.3$ mm.

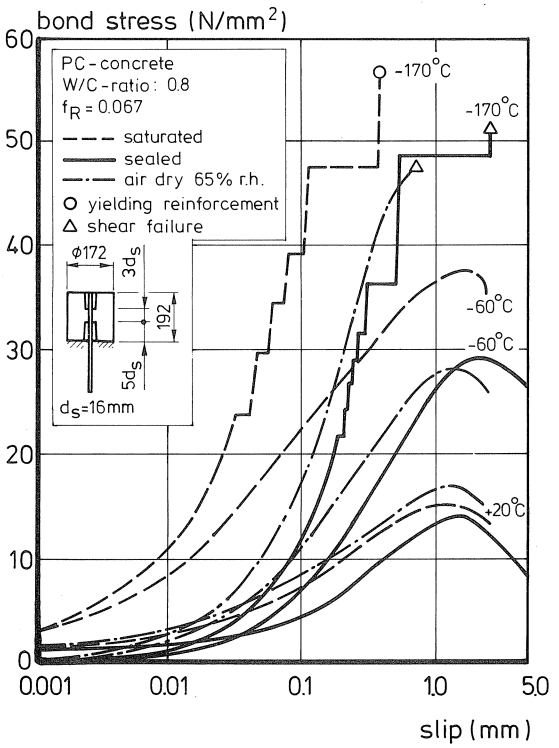

Fig. 2.7 Bond stress-slip relationship for different curing conditions and temperatures [19].

Typical factors of the bond stress-slip relationships are shown in Fig. 2.8.
Based on curve-fitting, formula 2.2a was generalised by Scheuermann [33] in the following expression:

$$a(T) = f_{ccyl}(T)\ (0.06 + C_1 f_R)\ (1 - 0.68\ \frac{T - 20}{190}) \qquad (2.2b)$$

$$b(T) = C_2(1 - 0.39\ \frac{T - 20}{190}) \qquad (2.2c)$$

in which

$C_1 = 8.64 \pm 2.0$ and $C_2 = 0.46 \pm 1.0$

f_R = specific rib area $\quad 0.058 \leq f_R \leq 0.087$

Formulae 2.2a to 2.2c are valid for a concrete cover from 2 to 5 d_s and for bond stress up to the bond strength (τ_{bu}), which is governed by the failure mode. In case of shear failure the ultimate bond stress is equal to:

$$\tau_{bu}(T) = 0.47\ f_{ccyl}(T) \qquad N/mm^2 \qquad (2.3)$$

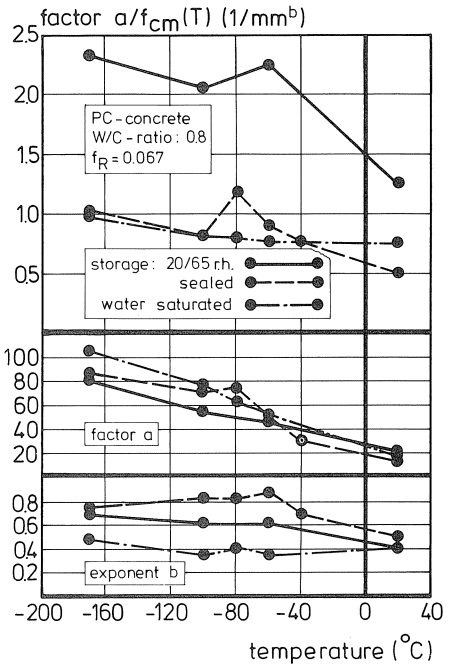

Fig. 2.8 Factors of the bond stress-slip relationships versus temperature and curing conditions [19].

If splitting of the concrete cover takes place, the bond strength can be determined with formula 2.4:

$$\tau_{bu}(T) = 0.66\, f_{csp\ell}(T)\, (2\,\frac{c}{d_s} + 1) \qquad N/mm^2 \qquad (2.4)$$

Note: From the experimental results [33] it was found that after cracking was observed the pull-out force could be increased by 10 per cent before failure occurred, except at -40 and -80°C where no further increase was possible. Thus at these two temperatures expression 2.4 should be multiplied by 0.91.

According to Scheuermann [33] one should use formula 2.3 for a concrete cover greater than 3 d_s.

Bamforth et al. [9] measured the bond strength by means of pull-out tests. Specimens comprised 150 mm cubes with a cast-in 20 mm diameter reinforcing bar embedded over 150 mm. Four different concrete mixes were sealed and tested at an age of 3 months over the temperature range from 20 to -165°C. The bond strength increased by 3-4 times when the concrete was cooled to -165°C, regardless of the mix composition. The maximum bond stress was attained at -120°C. Ratios of tensile strength to bond strength $f_{ctm}(T)/\tau_{bu}(T)$ were calculated, and it appeared that these values decreased with lower temperature. Furthermore, the lowest values of this ratio were obtained for the lightweight concrete.

Goto and Miura [21] performed bond tests on saturated specimens representing the end zone of a beam, see Fig. 2.9. The transverse pressure due to the bearing reaction was eliminated by means of a plastic sleeve placed over the end of the 22 mm diameter deformed bar. Two types of specimens (A or B) were used for investigating the failure load and the corresponding type of failure. For any anchorage length in the case of type A failure occurred by splitting.

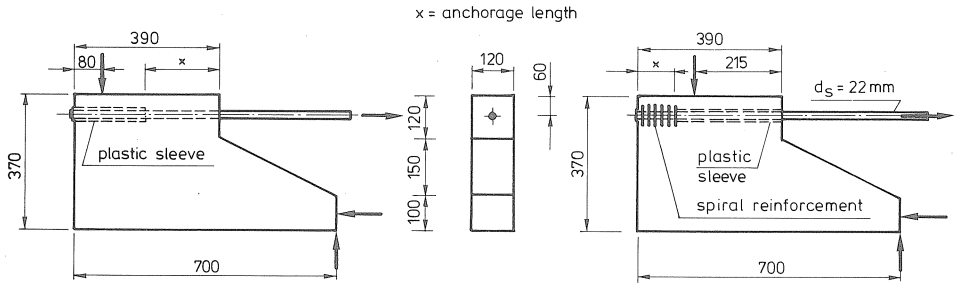

Fig. 2.9 Specimens for anchorage test [21].

The average bond stress at splitting failure increased with the lowering of the temperature by a factor of approximately 2.4 at -160°C. Tests were performed with a very short anchorage length of 50 mm and a spiral reinforcement cage surrounding the embedded bar to obviate splitting, (specimen type B). Very high bond stresses were measured at slip-through failure at -160°C. However, a factor of about 2.5 was again found for the ratio $\tau_{bu}(-160°C)/\tau_{bu}(20°C)$. Both factors are in agreement with the relative tensile strength at -160°C related to the tensile strength at +20°C. Apparently, therefore, the bond strength is affected at low temperatures in a similar way as the tensile strength. Note that the relative concrete strength $f_{cm}(-160°C)/f_{cm}(20°C) = 3.45$ is much higher than the relative bond strength (2.5) at -160°C, which was also observed by other previously mentioned investigators.

2.3.2. Effect of thermal cycling

Only two papers giving information on the effect of thermal cycling upon the bond strength were found in the literature. Kasami et al. [36] investigated this effect upon the bond strength of plain bars with the aid of pull-out tests which were performed with 19 mm reinforcing bars with an embedment length of 150 mm. Four different concrete mixes were used. The temperature was varied from +20 to -40°C and the bond strength was determined after 0, 1 and 30 thermal cycles at room temperature. Results are shown in Fig. 2.10 and are expressed as a percentage ratio to the initial bond strength as a function of the number of thermal cycles. It appeared that the bond strength was very greatly reduced for the water-saturated concrete with high w/c ratios. After one cycle a reduction of 30% was observed which increased to about 50% after 30 cycles.

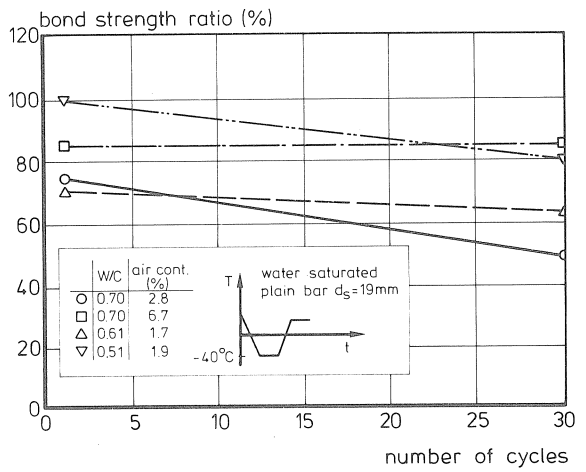

Fig. 2.10 Bond strength ratio of plain bars versus the number of thermal cycles [36].

Concrete with the lowest w/c ratio (0.51) or concrete with a high air content (6.7%) showed a reduction in bond strength which was about half that mentioned above. However, Wiedemann [30] found that most of the reduction occurred in the temperature range from +20 to -70°C. Consequently, a larger reduction could be expected.
The effect of thermal cycles upon the bond strength of deformed bars was studied by Scheuermann [33]. Only specimens of sealed concrete were used in the experiments, because curing under these conditions roughly simulates practical conditions. Experiments were performed at room temperature after thermal cycling in the range from +20 to -92°C. The bond strength was determined at different slip values Δ after 0, 1, 3, 5, 10 and 15 thermal cycles. Only a very small reduction in bond strength was found for the concrete with a w/c ratio of 0.80. However, a reduction by about 35% after 15 thermal cycles was found for a concrete with a w/c ratio of 0.82.

2.4. Crack width and spacing

Various investigators studied the influence of low temperatures upon the crack spacing and crack width, more particularly by means of experiments on reinforced concrete members loaded in pure tension or in pure bending. Some investigators, Schäper [17], Iványi and Fastabend [40] and Schnell [18,41], tried to explain the observed typical phenomena at low temperatures. Furthermore, an attempt was made to predict crack spacing and crack width with the aid of formulae originally developed for normal conditions (room temperature). The next Section deals with these matters.

2.4.1. Concrete elements subjected to direct tension

To study the influence of low temperatures on crack spacing, Goto and Miura [21] performed a number of experiments on centrically reinforced specimens of about 900 mm in length. These specimens, with 100x100 mm or 120x120 mm square cross-section, were reinforced with one bar of 22 mm diameter and subjected to direct tension at +20 and -160°C, see Fig. 2.11. The experiments were conducted on water-saturated specimens with a moisture content of about 7% at an age of 7 days.

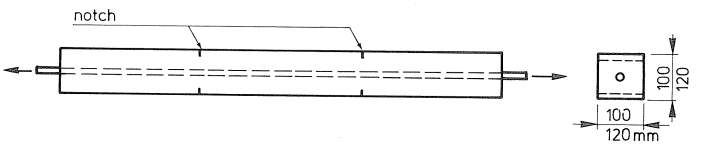

temperature (°C)	crack spacing (mm) Φ100mm²	(mm) Φ120mm²
+20°C	100 - 110	125 - 150
-160°C	150 - 180	270 - 290

Fig. 2.11 Long pull-out specimen for determining crack spacing [21].

The researchers found that at low temperatures the crack spacing increases considerably, Fig. 2.11. Unfortunately, no values relating to the crack widths were reported.

Both crack width and crack spacing were measured on long pull-out specimens in the experimental programme reported by Scheuermann [39]. Crack phenomena have been studied on reinforced sealed concrete members (200x400x3500 mm) at different temperatures. The reinforcement ratio was varied between 1.01×10^{-2} and 1.94×10^{-2}. It was found that the load at which cracking of the member started increased markedly due to the increase in tensile strength at low temperatures. Consequently, the steel stress $\sigma_{s,cr}$ after cracking also increases at low temperatures. This feature is shown in Fig. 2.12.

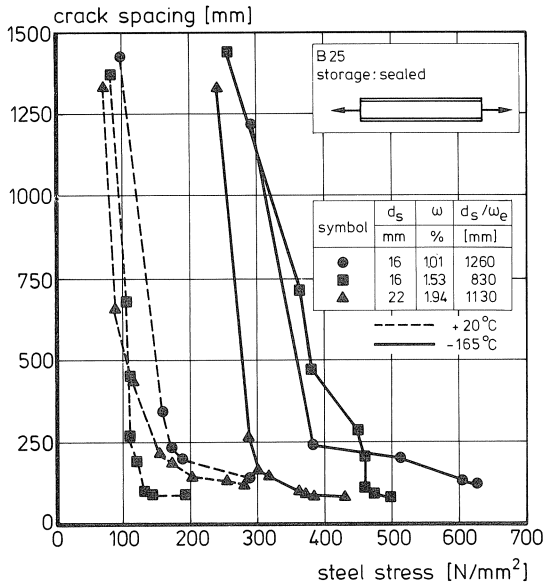

Fig. 2.12 Crack spacing versus steel stress σ_s at the crack, at various temperatures and reinforcement ratios [39].

The development of the crack pattern during the load increase after cracking began was observed to occur in the usual way, regardless of the temperature. Thus, initial cracking passes into final cracking, in which the visible mean crack spacing $\Delta\ell$ becomes apparent. It seems that this mean crack spacing $\Delta\ell$ decreases slightly at low temperatures, in contrast with what was observed by Goto and Miura [21].
Also, the crack width was measured at different temperatures. This can be seen in Fig. 2.13, which shows that at low temperatures the crack width decreases in comparison with the crack width at room temperature for a certain steel stress at the crack.

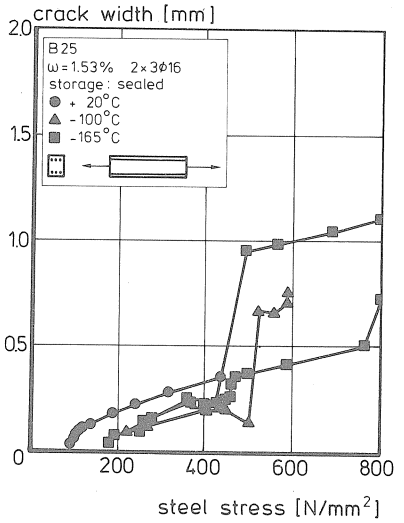

Fig. 2.13 Crack width versus steel stress at the crack for different temperatures [39].

However, with increasing steel stress an abrupt slip increase was observed at low temperature, leading to greater crack widths than at room temperature. Therefore, according to Scheuermann [39], the actual steel stress at the crack should be limited in order to avoid abrupt changes in the slip values.

2.4.2. Concrete elements subjected to pure flexure

Results of bending experiments on reinforced concrete beams at very low temperatures were reported by, among others, Iványi and Schäper [42] and Iványi and Fastabend [40]. The first-mentioned investigators performed experiments on 200x300x2000 mm beams with varying reinforcement (d_s = 16 mm and d_s = 10 mm) at two temperatures: +20°C and -175°C respectively. The free moisture content of the concrete was about 4.6% and the specimens were stored in a shed, i.e. were probably air-dry. Some typical results concerning the crack pattern are shown in Fig. 2.14.

At low temperature the crack spacing increases by about 30% in comparison with room temperature. As a result of the thermal differences between concrete and the reinforcement, internal stresses developed in the beam. Consequently, the cracking moment increased. To investigate the influence of the temperature on the crack width, one experiment was carried out in which attention was focused more particularly on the crack width. A beam similar to type B1 (Fig. 2.14) was loaded at room temperature. The corresponding average crack width and maximum crack width were approximately 0.2 and 0.25 mm respectively. After loading, the beam was

cooled to -175°C. The measured average and maximum crack widths were found to decrease to 0.1 and 0.15 mm respectively. The crack pattern remained unaltered at low temperatures. The internal stresses that were introduced thus appeared to reduce the crack width considerably.

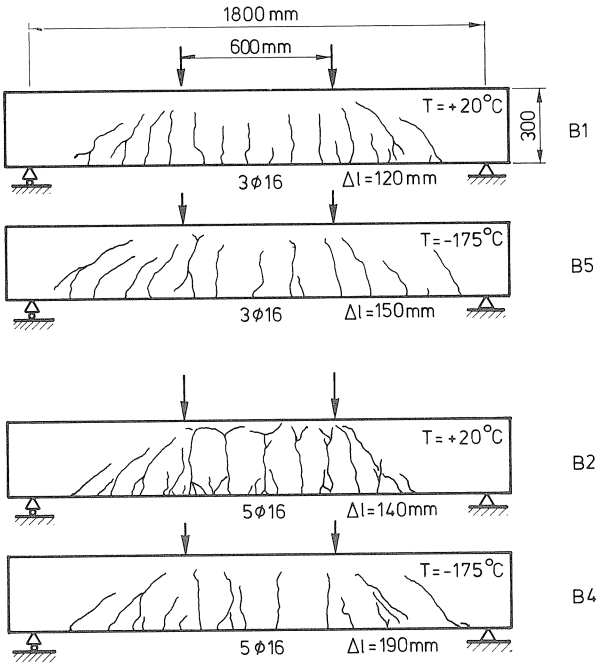

Fig. 2.14 Influence of the temperature on crack spacing for different reinforcement ratios [42].

Similar research was conducted by Iványi and Fastabend [40]. They found that crack spacing in a feebly reinforced beam loaded at low temperatures was always smaller than in the comparable experiments at room temperature. However, more highly reinforced beams always exhibited larger crack spacings when tested at low temperatures than when tested at room temperature.
The feebly reinforced beams (0.3 and 0.35%) exibited smaller crack widths when tested at low temperature than those tested at room temperature. More highly reinforced beams (0.59 and 1.1%), however, always exhibited larger crack widths at low temperatures than at room temperature.

2.4.3. Discussion and analysis of the experimental results

The classical bond-slip theory is used to analyse the experimental results. This theory assumes that the concrete cracks when its tensile strain capacity is reached.

The force can be transferred to the concrete per unit of length of each bar and is given by $\tau_b \pi d_s$. Hence, the tensile strength will be reached at a distance ℓ_{st} from the crack. This defines the minimum distance ℓ_{st} at which cracks can form:

$$\ell_{st} = \frac{f_{ct} A_c}{\tau_{b,av} d_s \pi} \quad \text{mm} \qquad (2.5)$$

in which $\tau_{b,av}$ is the average bond stress over the transfer length ℓ_{st}. Usually a value of 1.5 ℓ_{st} is adopted for the mean crack spacing $\Delta\ell$. At low temperatures both the tensile strength f_{ct} and the bond strength represented by the average bond stress $\tau_{b,av}$, increase considerably. In fact, the ratio of tensile strength to bond stress should be considered as a function of temperature. This ratio was experimentally investigated for sealed concrete specimens by Bamforth et al. [9]. They found that in general the ratio $f_{ct}/\tau_{b,av}$ decreases with temperature. Consequently, crack spacing and widths will also decrease. This conclusion agrees well with the observations of Scheuermann [39] who found a slight reduction in crack spacing at low temperatures, but it seems to disagree with the other experimental results. However, most of the researchers performed experiments on specimens of very moist concrete and only Scheuermann [39] carried out experiments on sealed concrete. Consequently, different thermal strains between concrete and reinforcement will exist for the moist concrete but will be negligible for the sealed concrete. As a result of the differences in thermal strain, restrained stresses are generated during cooling. These stresses can be predicted for a long concrete specimen with a centrically embedded steel bar:

$$\sigma_{sT} = \frac{E_s(T)}{(1 + n\rho)} \Delta T \, (\alpha_s(T) - \alpha_c(T)) \quad \text{N/mm}^2 \qquad (2.6)$$

whilst the compressive stress simultaneously generated in the concrete is:

$$\sigma_{cT} = -\sigma_{sT} \rho \quad \text{N/mm}^2 \qquad (2.7)$$

Depending on the reinforcement ratio, the steel stresses varied between 0 and 400 N/mm^2. The associated concrete stresses resulting from the internal prestressing varied between 0 and -4 N/mm^2. These compressive concrete stresses increase in proportion to the reinforcement ratio, as follows from formula 2.7. The experimental results of crack spacing mentioned above are assembled in Table 2.1.
In order to compare the reinforcement of the beams subjected to purely flexural loading with the beam loaded in tension, the reinforcements of the former beams were converted to the concrete area of the effective zone, according to Bruggeling and De Bruijn [43]. From Table 2.1 it can be concluded that, if internal prestressing exists, an increase in crack spacing is observed for an effective reinforcement percentage higher than 1.3%. This crack spacing will tend towards a value which is twice as large as that found in observations at room temperature, when the effective reinforcement is about 4 per cent. How the internal prestressing affects the crack spacing is not yet understood.

Table 2.1 Experimental results of crack spacing at low temperatures.

investigator(s)	experiment	reinforcement %	prestressing $\alpha_s \neq \alpha_c$	$\frac{\Delta\ell(T)}{\Delta\ell(20^\circ C)}$
Goto/Miura	tension	3.36 ; 3.80	yes	1.4-1.8
Iványi/Fastabend	flexure	0.65 ; 1.00 (1.95)* ; (3.00)	yes	1.3
Iványi/Schäper	flexure	0.59 ; 1.10 (2.23)* ; (4.16)*	yes	1.5-1.8
	flexure	0.30 ; 0.36 (1.13)* ; (1.36)*	yes	0.7-1.1
Scheuermann	tension	1.01 ; 1.53;1.94	no	0.9

* reinforcement percentage has been converted to the effective reinforcement percentage according to Bruggeling and De Bruijn [43].

However, there also seems to be another reason why crack spacing tends to increase at low temperatures. Schnell [18] used the bond-slip theory developed by Krips [44], which may be regarded as an extension of Noakowski's [6] theory, to explain the increasing crack spacing at low temperatures. The crack spacing depends on the ratio of the actual steel stress σ_s to the steel stress after cracking $\sigma_{s,cr}$, according to Krips [44]. Because $\sigma_{s,cr}$ increases considerably at low temperatures, the ratio $\sigma_s/\sigma_{s,cr}$ will decrease, which results in greater crack spacing at a certain stress level σ_s.
For steel stresses lower than about 400 N/mm^2 and concrete members with a low reinforcement ratio the crack width is always smaller at low temperature than at room temperature [39,40]. For higher steel stress Scheuermann [39] found abrupt increases in crack width. This phenomenon cannot be predicted by the crack formulae usually adopted. Therefore he suggested that the steel stress at the crack should be limited at low temperatures in order to avoid this typical feature.
Concrete members with high reinforcement ratios show larger crack widths at low temperatures than at room temperature. It seems that crack widths and spacing can be predicted with existing formulae at low temperatures [40].

2.5. Conclusions

From the experimental results reported and discussed above the following conclusions can be drawn:

- The cryogenic bond stress increases to a lesser extent than the actual compressive strength for saturated concrete, while this increase in cryogenic bond is proportional to, and greater than, the actual compressive strength for air-dry and oven-dry concrete respectively. Consequently, the bond strength is affected mainly by the moisture content of the concrete at low temperatures.

- At -170°C the slip values increase instantaneously, and these abrupt changes become rapidly larger at higher bond stresses, finally leading to failure. Such abrupt changes are probably caused by sudden initiation of internal longitudinal splitting cracks.
- Thermal cycling causes a reduction in bond strength and bond resistance for water-saturated concrete.
- High (effective) reinforcement ratios (3 to 4%) very greatly increase the crack spacing in saturated concrete members at low temperatures. Consequently, the crack width will be larger at low temperatures than at room temperature for a certain steel stress.
- Low (effective) reinforcement ratios (0.5 to 1.5%) in saturated concrete members result in smaller crack widths at low temperatures in comparison with crack widths observed at room temperature.
- The crack spacing and width can probably be calculated by using the classical concept of a unique bond stress-slip curve. However, for moist concrete we have to take account of the internal prestressing of the concrete as a result of the differential thermal strain between concrete and reinforcement.
- There is a lack of information about the local bond stress-displacement characteristic of concrete with a low w/c ratio (0.40) as is commonly used in practice. The results can be compared with Scheuermann's experiments which were mainly performed on concretes with higher w/c ratios.
- Less experimental information about crack widths at low temperature is available, particularly for sealed concrete.
- It should be checked whether crack spacing and crack width can be calculated with simple formulae valid at room and low temperatures. Until now an adapted local bond stress-displacement curve was mostly used in the analysis. This would seem to indicate that such a calculation is possible.
- Splitting failure always occurs for a practical concrete cover at low temperatures. Furthermore, the local bond stress-displacement curves are valid until splitting failure occurs. Therefore much attention should be paid to the development of a model enabling prediction of the bond stress level at which splitting occurs.
- Experimental information about plain bars is rather limited.

3. THEORETICAL MODELLING OF BOND PHENOMENA AND THE SPLITTING FAILURE MECHANISM

3.1. Introduction

Bond between the reinforcement and the concrete is one of the essential properties which makes reinforced concrete possible. Cracks will always exist in reinforced concrete or generally in structural concrete, Bruggeling [7]. These cracked concrete parts will be tied together by the reinforcement crossing the cracks and this reinforcement controls the crack width too. In order to understand the behaviour of cracked concrete it is essential to know the way in which the tensile force applied on

a bar reinforcement is transferred into the surrounding concrete. The length of the transfer zone can be calculated using an analytical method based on a local bond stress-displacement relationship. To use the valid displacement (slip) values of this relationship the associated bond strength should be known as a function of the concrete cover. The magnitude of the ultimate bond stress of deformed bars depends upon the failure mode. Much attention is paid to the splitting failure mode, because it usually determines the bond strength in the case of concrete covers commonly used in practice.
In this chapter the theoretical formulae are first derived to predict crack width and spacing in a reinforced tension member. Second, an analytical model is derived to predict the splitting failure of the concrete cover.

3.2. Model for the tension member of reinforced concrete

The behaviour of the reinforced concrete tension member under increasing load will be described here. The characteristic force-deformation relationship for this tension member can be divided into three parts, see Fig. 3.1. In the first part, the uncracked tension member, a tensile force is resisted by concrete as well as reinforcement. At a certain magnitude of the tensile force the tensile strength σ_{cr-1} of the concrete and its strain capacity ε_{cr} will be reached in the weakest parts of the tension member. The second part is formed by the mean strains at the initiation of the first crack (ε_{cr}) and where the crack pattern is fully developed (ε_{max}). The mean tensile strength of the concrete (f_{ctm}) varies randomly over the length of the tension member. Consequently, the tension member is cracked at its weakest place. It is assumed that the external force causing a fully developed crack pattern (N_{cr-2}) is 20% larger than the external tensile force causing the first crack (N_{cr-1}).

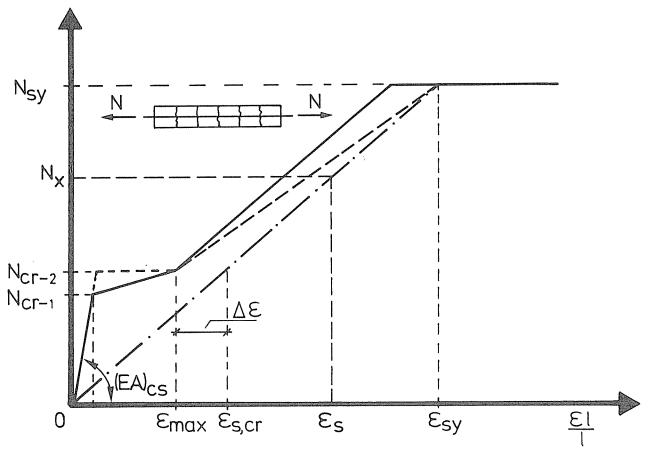

Fig. 3.1 The force-mean strain relationship of a reinforced concrete tension member.

In the calculation the tensile strength σ_{cr-1} and σ_{cr-2} are taken to be 0.62 f_{ctm} and 0.75 f_{ctm} respectively. However, to make the calculation as simple as possible a constant tensile strength ($\sigma_{cr-1} = \sigma_{cr-2}$) is assumed. Furthermore, it is assumed that the mean spacing of cracks is 1.5 ℓ_{st} if ℓ_{st} is the transfer length.
In the third part the number of cracks, i.e. the mean crack spacing, and the tension stiffening effect $\Delta\varepsilon$ are kept constant. Both assumptions are approximations of reality. The first assumption is accepted in general and for the second assumption various models exist. However, with regard to crack width this tension stiffening effect is only of minor importance. In order to keep the calculation as simple as possible a constant $\Delta\varepsilon$ is chosen, which can be used in the service limit state.

3.2.1. Bond stress-slip relationship

The bond stress-slip relationship of reinforcing bars can be experimentally determined with the aid of a pull-out test, see Fig. 3.2. The simplest way to approximate this relationship was given by Lutz [45] who used a linear relation, $\tau_b = a\ \Delta$. A bi-linear relation was used by Tanner [46], by which means a maximum bond stress was obtained. The function used by Vandewalle [32] contains a maximum too. Consequently calculations in the ultimate limit state could also be considered. Functions with a close fit to the actual curve were given by Vandewalle [32], Nilson [47], Rehm [35], Martin [48] and Noakowski [6], Fig. 3.3.

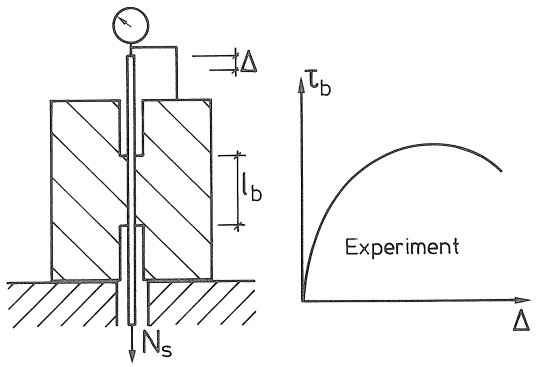

Fig. 3.2 Bond stress-slip curve determined with a pull-out test.

Note that three researchers [6,35,48] determined a linear relation between the bond stress and the mean cubic compressive strength f_{ccm}.
It was proved analytically by Noakowski [6] that for the first generation of cracks a solution exists for the crack width (w_{cr-1}) and transfer length if the bond stress-slip curve is approximated by $\tau_b = a\ \Delta^b$. This relationship is the starting point from which a model is developed.
Based on several experiments two mean bond characteristics were used by Bruggeling [43].

general case $\tau_b = 0.38\ f_{ccm}\ \Delta^{0.18}$

upper case $\tau_b = 0.32\ f_{ccm}\ \Delta^{0.28}$

These above mentioned values are given for the case of bars with sufficient concrete cover ($2\ d_s$).

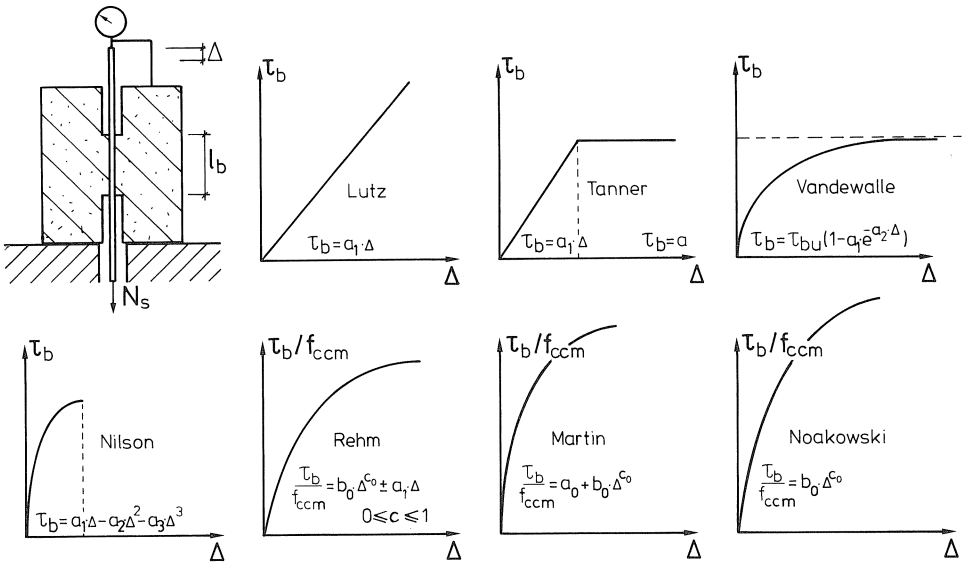

Fig. 3.3 Approximations for the bond stress-slip relationship.

3.2.2. Theoretical modelling of the tension member of reinforced concrete

In the following it will be shown briefly how the distribution of stresses and deformation along a zone starting from a crack in reinforced concrete can be determined. For more detailed information the reader is referred to Noakowski [6] and Van der Veen [50]. This theory mentioned above is based on actual displacement or local deformations in the bond zone near the surface of the reinforcement. Figure 3.4 shows a stressed tension member and the different deformations, in which ℓ_{st} is the transfer length. The tensile force $A_c\sigma_{cr} + A_s\sigma_{so}$ outside the transfer zone is resisted in the crack by the tensile force $A_s\sigma_{s,cr}$ in the reinforcement. Therefore the tensile force $A_s(\sigma_{s,cr} - \sigma_{so})$ is transferred by bond to the concrete in the transfer zone. Hence the tensile strength σ_{cr} is reached at a distance ℓ_{st} from the crack, which defines the minimum distance ℓ_{st} at which cracks can form. Let the x-axis coincide with the bar and let it begin at a distance ℓ_{st} from the crack where the concrete and steel deformation are equal ($\varepsilon_c = \varepsilon_s$).

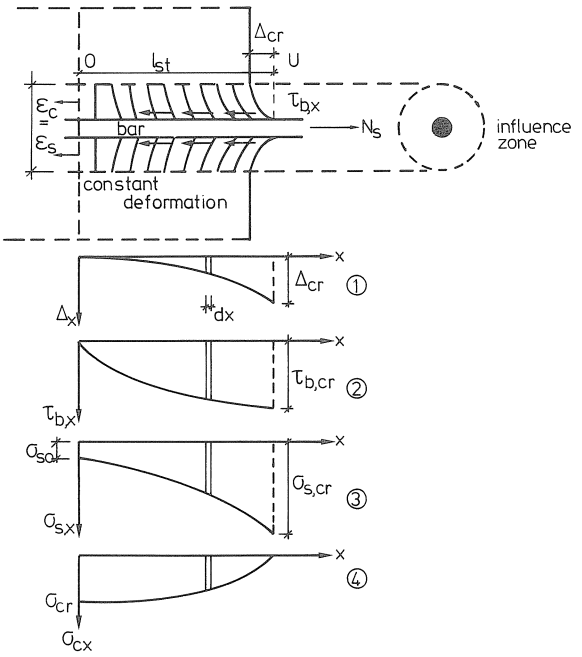

Fig. 3.4 Stresses in steel and concrete over one half of the transfer zone.

The equilibrium condition for each cross-section in the length is:

$$\sigma_{s,cr} A_s = \sigma_{sx} A_s + \sigma_{cx} A_c \tag{3.1}$$

Equilibrium at an element with size dx gives equations 3.2.

$$\frac{d\,\sigma_{sx}}{dx} = \frac{4}{d_s}\tau_{bx} \quad \text{and} \quad \frac{d\,\sigma_{cx}}{dx} = \frac{-4\rho}{d_s}\tau_{bx} \tag{3.2}$$

The bond stress $\tau_b(x)$ (= τ_{bx}) depends on the relative displacement (= slip) $\Delta(x)$ (= Δ_x) between reinforcement bar and concrete. This bond stress-slip relationship is measured in experimental tests and given in equation 3.3.

$$\tau_{bx} = a\,\Delta_x^{\,b} \tag{3.3}$$

Note that the index denoting temperature (T) is omitted from the variable so as to keep the equations clear.
It is generally assumed that this relation is valid for each element dx and is constant along the transfer length. The change of the relative displacement along the length dx is the difference between the deformations of steel and concrete.

$$\frac{d\,\Delta_x}{dx} = \frac{\sigma_{sx}}{E_s} - \frac{\sigma_{cx}}{E_c} \tag{3.4}$$

Differentiation of equation (3.4) and insertion of equation (3.2) and (3.3) gives

$$\frac{d^2\Delta_x}{dx^2} = \frac{4}{d_s} \frac{(1 + n\rho)}{E_s} a \Delta_x^b \tag{3.5}$$

in which

$n = \frac{E_s}{E_c}$ (linear elastic behaviour assumed)

$\rho = \frac{A_s}{A_c}$ reinforcement ratio.

The general solution of this non-linear differential equation is given by, among others, Noakowski [6] and Krips [44] and yields:

$$\Delta_x = \left\{\frac{2(1+n\rho)}{E_s d_s} a \frac{(1-b)^2}{(1+b)}\right\}^{\frac{1}{1-b}} x^{\frac{2}{1-b}} \tag{3.6}$$

The transfer length ℓ_{st} and the crack width w_{cr-1} is found indirectly by the steel stress distribution over the transfer zone and the two boundary conditions [6]:

$\sigma_s\ (x=o) = \sigma_{s,cr} \frac{n\rho}{(1+n\rho)}$ and

$\sigma_s\ (x=\ell_{st}) = \sigma_{s,cr}$, the steel stress in the crack.

Note, that the steel stress jump ($\sigma_{s,cr} - \sigma_{so}$) determines the transfer length ℓ_{st}. Thus the transfer length is independent of the steel stress level $\sigma_{s,cr}$.
In the crack at a distance ℓ_{st} from O, see Fig. 3.4, the relative diplacement amounts to

$$\Delta_{cr} = \left(\frac{1+b}{2} \frac{d_s}{4} \frac{1}{a E_s} \frac{\sigma_{s,cr}^2}{(1+n\rho)}\right)^{\frac{1}{1+b}} \tag{3.7a}$$

in which

$$\sigma_{s,cr} = \sigma_{cr} \left(\frac{1}{\rho} + n\right)$$

Thus the crack width is known because the crack width w_{cr-1} equals twice the slip value Δ_{cr}.

$$w_{cr-1} = 2\ \Delta_{cr} \tag{3.7b}$$

The transfer length is given by equation 3.8.

$$\ell_{st} = \frac{w_{cr-1}}{(1-b)} \frac{E_s}{\sigma_{s,cr}} \tag{3.8}$$

The above formulae are derived in another way by Van der Veen [50] and are valid in a tensile member where the transfer zones do not overlap one another. Thus the cracks are situated at a distance of at least 2 ℓ_{st} from each other. Cracks of this type are called "first-generation cracks", Bruggeling [49]. However, with continuing deformation of the tensile member, intermediate cracks are formed. These cracks are called "second-generation cracks, i.e. cracks which occur when the transfer zones associated with the "first-generation cracks" encounter one another. In order to take the step towards the treatment of the "second-generation cracks" a so-called shape factor $S\sigma$ is introduced. The shape factors $S\sigma_s$ and $S\sigma_c$ are defined as the ratio:

$$S\sigma_s = \frac{\int_0^{\ell_{st}} (\sigma_{sx}-\sigma_{so})dx}{(\sigma_{s,cr}-\sigma_{so})\ell_{st}} \quad \text{shape factor for the steel stress} \tag{3.9}$$

$$S\sigma_c = \frac{\int_0^{\ell_{st}} \sigma_{cx}\, dx}{\sigma_{cr}\, \ell_{st}} \quad \text{shape factor for the concrete stress} \tag{3.10}$$

The magnitude of the shape factors is dependent only on the factor b in the exponential curve of the bond-slip relationship [6,50].

$$S\sigma_s = \frac{(1-b)}{2} \quad \text{and} \quad S\sigma_c = \frac{(1+b)}{2} \tag{3.11}$$

Notice that

$$S\sigma_s + S\sigma_c = 1 \tag{3.12}$$

It is now simple to find and to understand equation (3.8). The relative displacement Δ_{cr} is determined by the extra elongation of the reinforcing bar and the shortening of the concrete over the transfer zone with a length ℓ_{st}. Therefore:

$$\Delta_{cr} = S\sigma_s \left(\frac{\sigma_{s,cr}-\sigma_{so}}{E_s} + \frac{\sigma_{cr}}{E_c}\right) \ell_{st} \quad \text{and} \quad \frac{\sigma_{so}}{E_s} = \frac{\sigma_{cr}}{E_c} \tag{3.13}$$

$$w_{cr-1} = S\sigma_s \frac{\sigma_{s,cr}}{E_s} \Delta\ell \quad \text{in which } \Delta\ell \text{ is } 2\ \ell_{st} \tag{3.13a}$$

Finally, substituting equation (3.11) gives equation (3.8).

The mean strain of a tension member of reinforced concrete over the transfer length ℓ_{st} can be calculated by using the associated distribution of stresses:

$$\varepsilon_{mean\ 1} = \frac{1}{E_s} \left(S\sigma_s\ (\sigma_{s,cr}-\sigma_{so}) + \sigma_{so}\right)$$

$$\varepsilon_{mean\ 1} = \frac{1}{E_s} \left(S\sigma_s\ (\sigma_{s,cr}-\sigma_{so}) + (S\sigma_s+S\sigma_c)\ \sigma_{so}\right)$$

$$\varepsilon_{mean\ 1} = \frac{1}{E_s} (S\sigma_s\ \sigma_{s,cr} + S\sigma_c\ \sigma_{so}) \tag{3.14}$$

Substituting equation 3.11 yields:

$$\varepsilon_{mean\ 1} = \frac{1}{E_s} \left(\frac{(1-b)}{2}\ \sigma_{s,cr} + \frac{(1+b)}{2}\ \sigma_{so}\right) \tag{3.15}$$

The solving method with shape factors will also prove useful in the case of "second-generation cracks".
Consider a special case of "second-generation cracks" in which the crack distance is ℓ_{st}. If the steel stress distribution over half ℓ_{st} is known, a crack width w_{cr-2} and mean strain $\varepsilon_{mean\ 2}$ can be calculated with the aid of shape factors. Therefore, two particular bond stress-slip relations, namely b = 0 and b = 1, and the associated stress distributions are examined more closely, see Fig. 3.5.

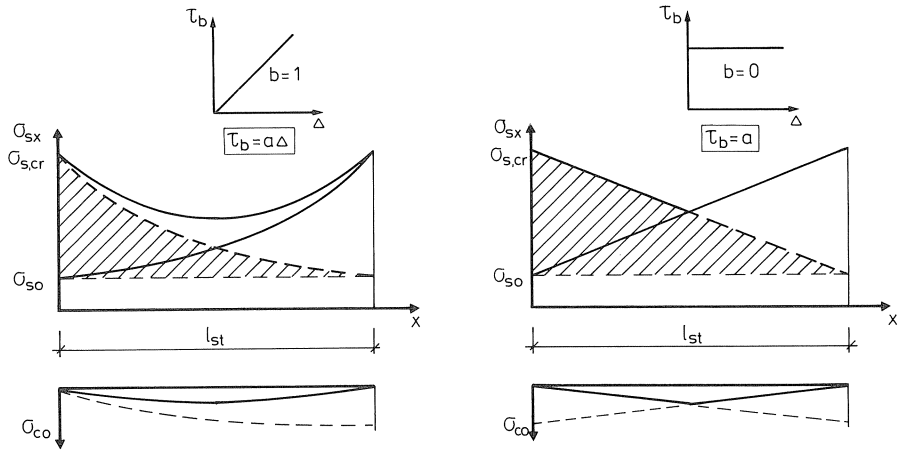

Fig. 3.5 Overlap of the transfer zone (distortion zone) for two bond stress-slip relations.

First, the relationship with b = 0 is considered. Consequently, a constant bond stress independent of the slip value exists. If the transfer length is 0.5 ℓ_{st}, only half of the tensile force A_s $(\sigma_{s,cr}-\sigma_{so})$ is transferred by bond to the concrete in the distortion zone. As a result the mean strain over the distortion zone of 0.5 ℓ_{st} equals equation (3.15a).

$$\varepsilon_{mean\ 2} = \frac{1}{E_s} \{\sigma_{so} + 1.5\ (\sigma_{s,cr}-\sigma_{so})\ S\sigma_s\} \tag{3.15a}$$

Second, for the linear bond stress-slip relationship a superposition of the steel stress distribution is valid. Consequently, the mean strain over the distortion zone of 0.5 ℓ_{st} amounts to:

$$\varepsilon_{mean\ 2} = \frac{1}{E_s} \{\sigma_{so} + 2\ (\sigma_{s,cr}-\sigma_{so})S\sigma_s\} \tag{3.15b}$$

Both equations can be determined directly from figure 3.5 by calculating the mean steel stress strain over $0.5\ \ell_{st}$.
When formulae (3.15a) and (3.15b) are compared, the factor in front of $(\sigma_{s,cr}-\sigma_{so})$ changes from 1.5 to 2.0 for b is 0 and 1 respectively. This factor can be generalized if a linear distribution is assumed for this factor associated for $0 \leq b \leq 1$ resulting in formula 3.16.

$$\varepsilon_{mean\ 2} = \frac{1}{E_s}\left\{\sigma_{so} + \frac{(3+b)}{2}\,(\sigma_{s,cr}-\sigma_{so})\ S\sigma_s\right\} \tag{3.16}$$

Substituting equations (3.11) and (3.12) gives:

$$\varepsilon_{mean\ 2} = \frac{1}{E_s}\left\{\frac{(1+b)^2}{4}\sigma_{so} + \frac{1}{4}\,(3+b)\,(1-b)\,\sigma_{s,cr}\right\} \tag{3.17}$$

Now we have also found the shape factors in the case of "second-generation cracks" (compare equations 3.14 and 3.15) resulting in:

$$S\sigma_{s2} = \frac{(3+b)\,(1-b)}{4} \quad \text{and} \quad S\sigma_{c2} = \frac{(1+b)^2}{4} \tag{3.18}$$

The crack width w_{cr-2} can be calculated as shown in equation (3.13a) in which $\Delta\ell = \ell_{st}$ and $S\sigma_s = S\sigma_{s2}$.

$$w_{cr-2} = \frac{(3+b)\,(1-b)}{4}\,\ell_{st}\,\frac{\sigma_{s,cr}}{E_s} \tag{3.19}$$

The ratio w_{cr-2} over w_{cr-1} amounts to:

$$\frac{w_{cr-2}}{w_{cr-1}} = \frac{(3+b)}{4}$$

This ratio was also found by Krips [44], albeit using a different method. If we substitute a commonly used value b = 0.18 [43], then we find a crack width about 20% smaller: $w_{cr-2} = 0.8\ w_{cr-1}$ .This is confirmed by the theoretical results of Vandewalle [32].
Of course, an idealized case is described for a crack distance of ℓ_{st}. The crack distance $\Delta\ell$ varies between ℓ_{st} and $2\ \ell_{st}$ if a so-called maximum mean strain (ε_{max}) of the tension member is reached. It is generally accepted that the mean crack distance $\Delta\ell$ amounts to $1.5\ \ell_{st}$ if ε_{max} is reached.
Therefore the mean strain of the reinforced tension member (see Fig. 3.6.) amounts to:

$$\varepsilon_{max} = \frac{2\ \varepsilon_{mean\ 1} + \varepsilon_{mean\ 2}}{3}$$

Substituting equations (3.15) and (3.17) gives:

$$\varepsilon_{max} = \frac{1}{12\ E_s}\left\{(1-b)\ (7+b)\ \sigma_{s,cr} + (1+b)\ (5+b))\ \sigma_{so}\right\} \tag{3.20}$$

The shape factors are found again and yield:

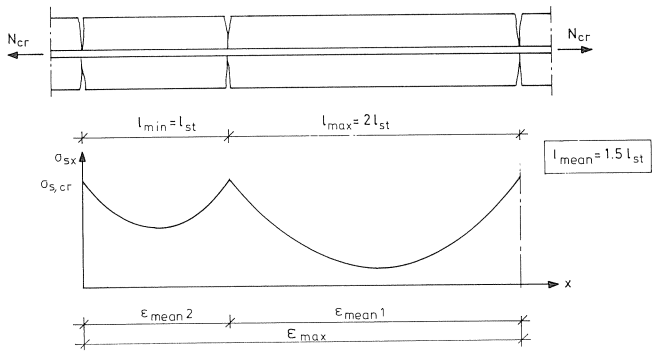

Fig. 3.6 Overlap of the distortion zone.

$$S\sigma_{s-max} = \frac{(1-b)\,(7+b)}{12} \quad \text{and} \quad S\sigma_{c-max} = \frac{(1+b)\,(5+b)}{12} \tag{3.21}$$

The mean crack width w_{cr} can be calculated as shown in equation (3.13a) in which $\Delta\ell = 1.5\ \ell_{st}$ and $S\sigma_s = S\sigma_{s-max}$.

$$w_{cr} = \frac{1}{8}\,\ell_{st}\,\frac{\sigma_{s,cr}}{E_s}\,(1-b)\,(7+b) \tag{3.22}$$

If a constant tensile strength is assumed during the generation of cracks the ratio w_{cr} over w_{cr-1} yields:

$$\frac{w_{cr}}{w_{cr-1}} = \frac{(7+b)}{8} \tag{3.23}$$

Thus the mean crack width w_{cr} after completing the crack pattern amounts about 90% of w_{cr-1}. This result is in accordance with the results of Krips [44].
It is assumed that a further increase in the elongation (or load) above ε_{max} does not change the crack pattern and the so-called tension stiffening $\Delta\varepsilon$, see Fig. 3.7. The degree of stiffening effect is defined by

$$\Delta\varepsilon = \varepsilon_{s,cr} - \varepsilon_{max} \tag{3.24}$$

Substituting equation (3.20) results in equation (3.25)

$$\Delta\varepsilon = \frac{(1+b)\,(5+b)}{12}\,(\varepsilon_{s,cr}-\varepsilon_{so}) \tag{3.25}$$

For $\varepsilon > \varepsilon_{max}$ the mean crack width w_x can be predicted with

$$w_x = \Delta\ell\,(\varepsilon_s-\Delta\varepsilon-\varepsilon_{cm})$$

in which ε_{cm} is the mean concrete strain over the distorsion zone and yields $\varepsilon_{cm} = S\sigma_{c-max}\ \varepsilon_{so}$

Finally, this results in equation (3.26).

$$w_x = \Delta\ell \left(\varepsilon_s - \frac{(1+b)}{12}\frac{(5+b)}{} \varepsilon_{s,cr}\right) \qquad (3.26)$$

If we assume $\sigma_{cr-1} = \sigma_{cr-2}$ the calculation procedure can be summarized as given below.

1st. crack pattern not fully developed, thus $\Delta\ell > 2\ \ell_{st}$
calculate w_{cr-1} and ℓ_{st} with formulae (3.7) and (3.8).

2nd. crack pattern fully developed, $\varepsilon \simeq \varepsilon_{max}$ and $\Delta\ell = 1.5\ \ell_{st}$
calculate w_{cr} and ε_{max} with formulae (3.22) and (3.20).

3rd. crack width in the service limit state
calculate $\Delta\varepsilon$ and w_x with formulae (3.25) and (3.26).

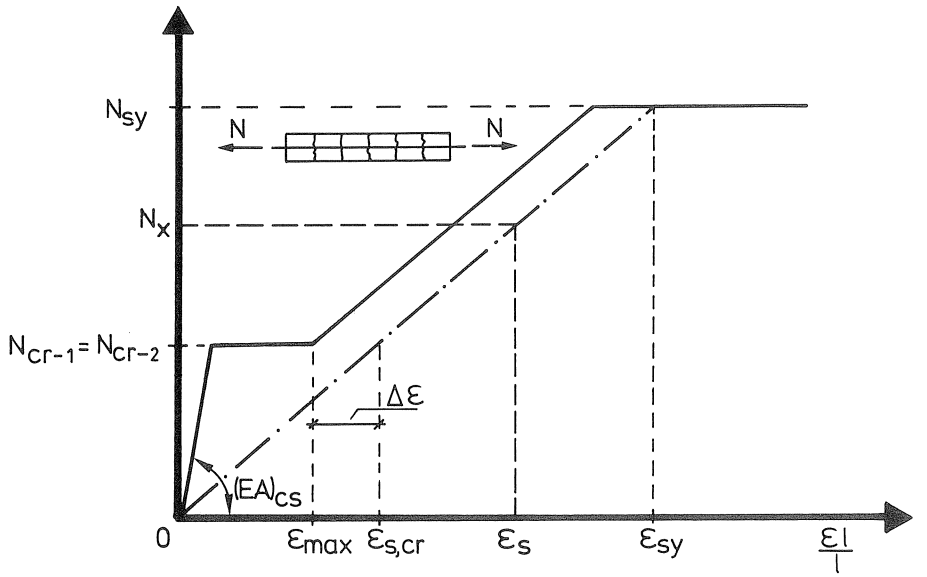

Fig. 3.7 The force-mean strain relationship of a reinforced concrete tension member.

Remark: In a first attempt to solve the problem of the crack width w_{cr-2} ("second-generation cracks") the principle of superposition of stresses, formula (3.15b), was used by the author [50,51], regardless the value of the exponent b. This method results in equal crack widths $w_{cr-1} = w_{cr-2} = w_{cr}$ ($\sigma_{cr-1} = \sigma_{cr-2}$) and in an overestimation of w_{cr} by about 10% at room temperature. Nevertheless, this method proved to be very successful in predicting crack widths, Van der Veen and Pruijssers [51].

3.2.3. Effect of different thermal strain between concrete and reinforcement

It was found in the literature [8] that for very moist concrete the thermal coefficient of expansion is different for concrete and the reinforcement at low temperatures, see Fig. 2.3. As a result of the thermal differences, restrained stresses are generated during cooling. These stresses can be predicted with formulae (2.6) and (2.7) and are valid for the middle part of a long tension member. At both ends of this tension member slip of the reinforcement will occur over the transmission (transfer) length ℓ_{sT}. In fact this problem is similar to the transmission length of pretensioned prestressing steel, Bruggeling [52]. The slip at the end of the tension member can be predicted with formula (3.7). Substitution of $\sigma_{s,cr} = \Delta T\ (\alpha_s - \alpha_c)\ E_s$ yields (see Fig. 3.8):.

$$\Delta_{cT} = \left\{\frac{(1+b)}{2}\,\frac{d_s}{4}\,\frac{1}{a}\,\frac{E_s}{(1+n\rho)}\,\Delta T^2(\alpha_s-\alpha_c)^2\right\}^{\frac{1}{1+b}} \tag{3.27}$$

The transmission length can be predicted with formula (3.8) which gives equation 3.28.

$$\ell_{sT} = \frac{2\,\Delta_{cT}\,E_s}{(1-b)\,\sigma_{sT}(1+n\rho)} \tag{3.28}$$

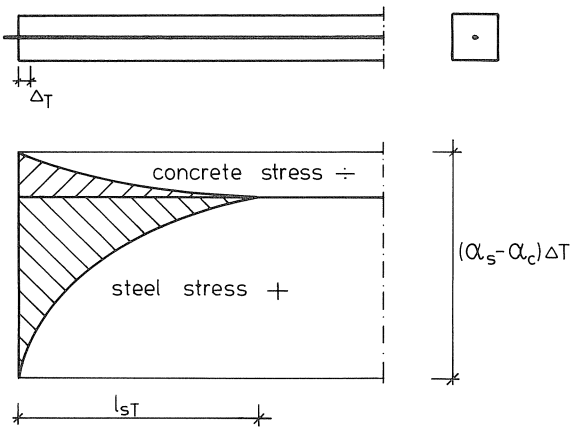

Fig. 3.8 The transmission length at the end of a reinforced member after cooling.

As a result of a compressive stress σ_{cT} in the concrete, which is simultaneously generated during cooling, a higher external force is necessary before cracking is initiated. This force $N_{s,cr}$ can be calculated by superimposing the compressive stress σ_{cT} calculated using formulae (2.6) and (2.7) and the tensile strength σ_{cr}.

$$N_{s,cr} = (\sigma_{cr}-\sigma_{cT})\ (\tfrac{1}{\rho} + n)\ A_s \tag{3.29}$$

The stress distribution over the transmission length is given in Fig. 3.9.

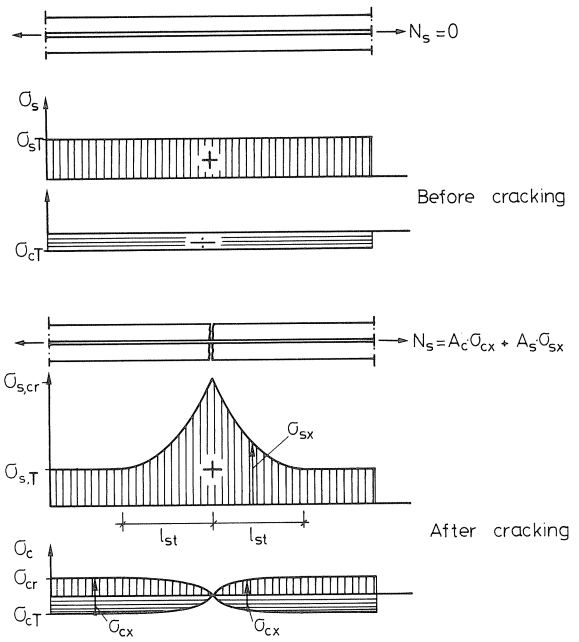

Fig. 3.9 Stress distribution over the transmission length.

Before cracking the steel stress in the reinforcement amounts to σ_{sT} and is calculated with formula (2.6). After cracking, the steel stress in the crack increases to $\sigma_{s,cr}$ and is calculated with formula (3.29). Consequently, the jump in steel stress $\Delta\sigma_{s,cr}$ amounts to:

$$\Delta\sigma_{s,cr} = N_{s,cr}/A_s - \sigma_{sT} \qquad N/mm^2 \qquad (3.30a)$$

Substituting formulae (3.29) and (2.7) into equation (3.30a) yields:

$$\Delta\sigma_{s,cr} = \sigma_{cr}\left(\frac{1}{\rho} + n\right) - n\,\sigma_{cT} \qquad N/mm^2 \qquad (3.30b)$$

The factor $n\,\sigma_{cT}$ represents the effect of the prestressing and is of minor influence on the magnitude of the steel stress jump $\Delta\sigma_{s,cr}$. It is now possible to calculate crack width, crack distance and tension stiffening in the same way as for reinforced concrete by substituting $\sigma_{s,cr}$ into $\Delta\sigma_{s,cr}$ and $\varepsilon_{s,cr}$ into $\Delta\varepsilon_{s,cr}$, see Bruggeling [7]. The initial steel stress σ_{sT} is added to the steel stress jump to calculate the actual force-elongation relationship.
Because of the minor effect of the "prestress" on the steel stress jump, the transfer length and hence the crack distance are hardly affected. Probably there is another reason why crack spacing increases very greatly in the case of water-saturated concrete, which feature was found in the literature, see Table 2.1. This is the subject of Section 6.5.2.

3.3. Theoretical model for the splitting failure mechanism

It is generally accepted that bond forces (stresses) of deformed bars radiate out into the surrounding concrete at some inclination α from the bonding surface of the bar, see Fig. 3.10. The bond stresses can be divided into radial (σ_r) and tangential (σ_t)

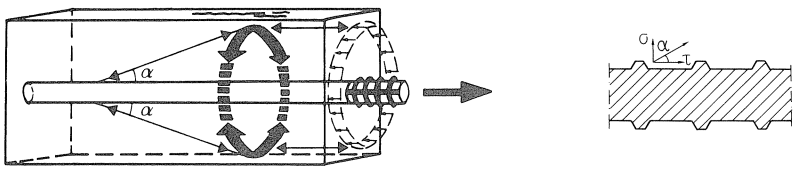

Fig. 3.10 Bond behaviour of deformed bars; the radial components of the bond stresses are balanced by tensile stresses in the uncracked concrete ring, Tepfers [53].

components. The radial compressive components of the bond forces are balanced by tensile stress rings in the concrete, according to Tepfers [53]. He stated that the radial component of the bond forces, $\tau_b \tan \alpha$, can be regarded as a hydraulic pressure acting on a thick walled concrete ring formed by the concrete surrounding the bar. The wall thickness of the ring is determined by the smallest possible dimension, the least thickness of the cover (c). For determination of the cracking resistance he applies three theories which, as regards the distribution of the stresses, refer to the elastic (3.31), partly cracked elastic (3.32) and plastic stages (3.33), see Fig. 3.11.

elastic stage
$$\tau_{br} = \frac{f_{ct}}{\tan \alpha} \frac{(c+d_s/2)^2 - (d_s/2)^2}{(c+d_s/2)^2 + (d_s/2)^2} \qquad (3.31)$$

partly cracked elastic stage
$$\tau_{br} = \frac{f_{ct}}{\tan \alpha} \frac{(c+d_s/2)}{1.664\, d_s} \qquad (3.32)$$

plastic stage
$$\tau_{br} = \frac{f_{ct}}{\tan \alpha} \frac{2\, c}{d_s} \qquad (3.33)$$

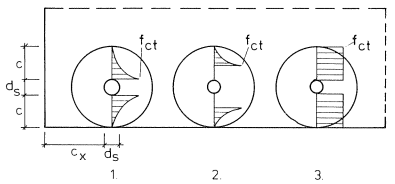

Fig. 3.11 The distribution of the tangential tensile stresses in the elastic, partly cracked elastic and plastic stages, Tepfers [53].

The elastic and plastic stages give the lowest and highest cracking resistance respectively.
Tepfers [53] showed that the load capacity of the concrete ring is not exhausted when cracking starts at the inner surface, but is reached later when the cracks penetrate some distance into the ring. In actual fact the elastic stage gives the load when cracking starts from the bond surface between the concrete and the reinforcing bar, while the partly cracked elastic stage gives the load when the longitudinal crack goes right through the concrete cover. However, the softening behaviour of the concrete was disregarded in the model. Consequently, no tensile stresses were allowed to transfer in the crack.
In the model presented here we also take into account the softening behaviour of the concrete according to Reinhardt et al. [54]. In the next Section the softening behaviour of concrete is first described as found in literature and then the equations of the model are given. Furthermore, the model is simplified and the effect of low temperature on the failure load is examined.

3.3.1. Softening behaviour of concrete

The stress-elongation diagram of a deformation-controlled uniaxial test of concrete is, in the fracture mechanics approach, split up into a strain part and the remainder, which is defined as the crack opening displacement δ, see Fig. 3.12. The strain part consists of a reversible strain and an irreversible strain. In comparison with the crack opening displacement δ, the irreversible strain part is negligible. Consequently, the uncracked material behaves in a linear elastic manner and all non-linearities are comprised in the discrete crack. Several functions were used for the fitting of the data points, Wolinski et al. [55]. However, the power function (3.34) as proposed by Reinhardt [56] is chosen because of its simplicity.

$$\frac{\sigma}{f_{ct}} = 1 - \left(\frac{\delta}{\delta_o}\right)^k \tag{3.34}$$

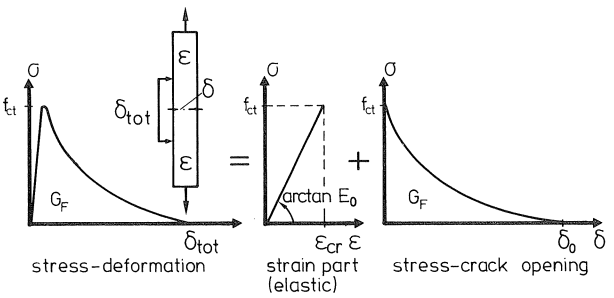

Fig. 3.12 Stress-deformation curve of a uniaxial test split into two parts, i.e. elastic part and the stress-crack opening.

The coefficient k is assumed to be a material constant, δ_o is the crack opening where stress no longer can be transferred and f_{ct} is the tensile stength. The total fracture energy G_F represents the area under the complete stress-deformation curve and is given by formula (3.35).

$$G_F = f_{ct}\ \delta_o\ \frac{k}{1+k} \tag{3.35}$$

Typical material values for concretes made with a maximum aggregate size D_{max} of 32, 16 or 8 mm respectively are given by Wolinski et al. [55].

f_{ct} = 2.86 N/mm^2 (f_{ccm} = 49.1 N/mm^2) δ_o = 0.2 mm

E_{co} = 32550 N/mm^2 k = 0.248

G_F = 109.6 N/m (experimental) G_F = 113.7 N/m (analytical)

It was found by Petersson [57] and in a literature survey made by Hordijk et al. [58] that the fracture energy decreases with increasing w/c ratio. Thus the decreasing concrete quality, due to an increasing w/c ratio, affected the fracture energy and the tensile strength in an analogous way, at least for w/c ratios between 0.6 and 0.4, see Fig. 3.13. Based on these observations it is assumed by the author that the fracture energy depends linearly on the tensile strength. Consequently, δ_o becomes independent of the concrete quality.

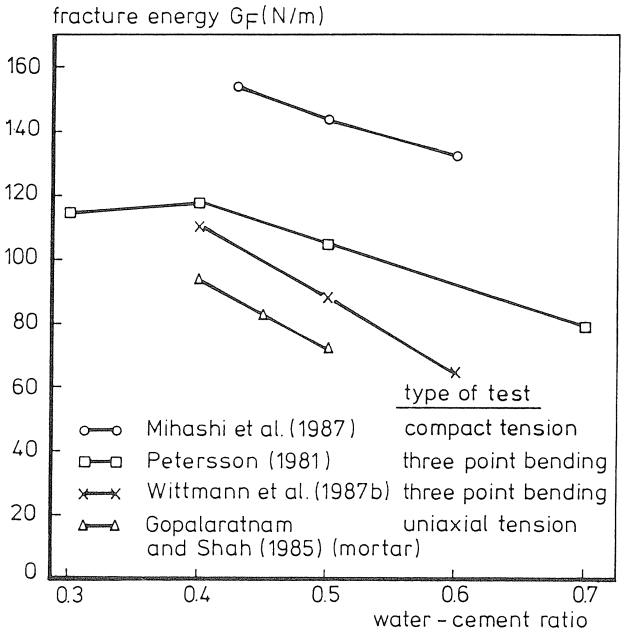

Fig. 3.13 Fracture energy as function of w/c ratio, Hordijk et al. [58].

3.3.2. Basic equations

A model is derived for the tangential stress distribution over the cross section of a thick-walled concrete ring taking into account the softening of the concrete after cracking. The radial stress $\tau_b \tan \alpha$ due to bond action on the concrete is regarded as a hydraulic pressure against a thick-walled concrete ring. Consider the concrete ring with internal cracks, see Fig. 3.14.
The resistance of the uncracked part of the concrete ring was given by Tepfers [53].

$$\tau_{br} \tan \alpha = f_{ct} \frac{2\,e}{d_s} \frac{(c + \frac{d_s}{2})^2 - e^2}{(c + \frac{d_s}{2})^2 + e^2} \tag{3.36}$$

in which e = crack depth and c = concrete cover.
Consider now the cracked part of the concrete ring. As a result of the cracks only a one-dimensional approach in the tangential (t) direction is applied. At a radial distance r the total tangential elongation δ_{tot} consists of an elastic part and n cracks. Thus the following deformation occurs.

$$\varepsilon_t 2\pi r + n\,\delta_o \left(1 - \frac{\sigma_t}{f_{ct}}\right)^{\frac{1}{k}} = \delta_{tot} \tag{3.37}$$

in which n is the number of cracks.

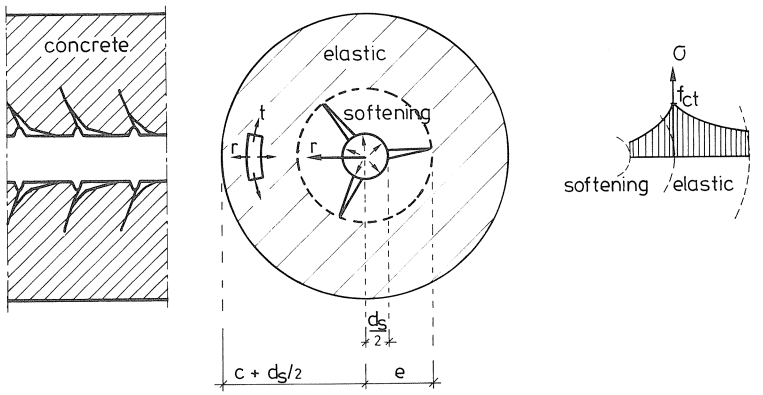

Fig. 3.14 Concrete ring with internal cracks surrounding a reinforcing bar.

At a radial distance e where the tensile strength has been reached and no cracks exist (in the elastic part) the total tangential elongation amounts approximately to:

$$\varepsilon_t\, 2\pi e \simeq \frac{f_{ct}}{E_c} 2\pi e \quad \text{(no effect of Poisson's ratio)} \tag{3.38}$$

Remark: According to Timoshenko [59] the tangential strain ε_t for plane stress amounts to:

$$\varepsilon_t = (\sigma_t - \nu\sigma_r)/E_{co} \tag{3.39}$$

in which σ_r is always a compressive stress and σ_t a tensile stress. Assuming a crack depth of about 0.5 times the concrete cover and a Poisson's ratio of 0.2, the tangential strain will be about:

$$\varepsilon_t = 1.1 \frac{f_{ct}}{E_{co}} \tag{3.40}$$

Thus about 10% of the strain is neglected in the case of perfect linear elastic behaviour. Because of the non-linearities between stress and strain for tensile stresses above 0.6 f_{ct} the static modulus instead of the initial modulus of elasticity is used, as is usually done in engineering practice.

Consequently, the total tangential elongation δ_{tot} at a radial distance e amounts to:

$$\delta_{tot} = \varepsilon_{cr}\, 2\pi e \qquad (\varepsilon_{cr} = \frac{f_{ct}}{E_c}) \tag{3.41}$$

The associated radial displacement amounts $u_r = \varepsilon_{cr}e$. To simplify the problem we assume a constant radial displacement for the cracked part $u_r = \varepsilon_{cr}e$. Thus also the total tangential displacement δ_{tot} is constant and is in fact imposed by the outer elastic concrete ring if no stresses exist in the cracked zone. Consequently, a rigid body translation in the radial direction $u_r = \varepsilon_{cr}e$ occurs for the cracked part, see Fig. 3.15a. As a result of the elastic deformation due to the actual tangential stresses in the cracked part, the "gap" δ_{tot} is just closed at the crack tip (r = e) where the tensile strength is just reached, see Fig. 3.15b.

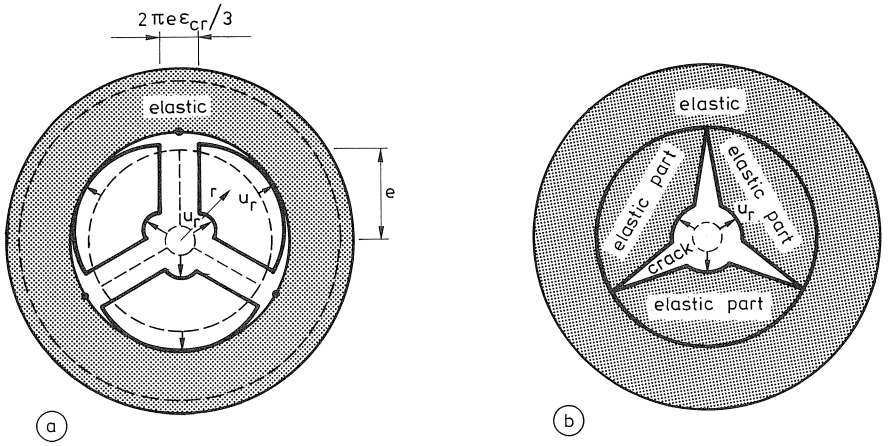

Fig. 3.15 Rigid body translation in the radial direction (a) and the deformed cracked parts loaded with a constant tangential stress equal to the tensile strength (b).

However, even if it is assumed that for $r < e$ the tangential stresses equal the tensile strength ($\sigma_t(r < e) = f_{ct}$) the associated elastic tangential deformation is still not able to close the gap δ_{tot}, particularly for small values of r. Thus, a crack opening always exists and this is the point of departure from which the model is developed. Substituting expression (3.41) in equation 3.37 gives:

$$\varepsilon_t \, 2\pi r + n \, \delta_o \, (1 - \frac{\sigma_t}{f_{ct}})^{\frac{1}{k}} = \varepsilon_{cr} \, 2\pi e \tag{3.42}$$

rearranging equation (3.42) gives:

$$\sigma_t = f_{ct} \, [1 - \{\frac{2\pi}{n \, \delta_o} \, (e \, \varepsilon_{cr} - r \, \varepsilon_t)\}^k] \tag{3.43}$$

Note: $\sigma_t = \sigma_t(r)$

It is assumed that $\varepsilon_t = \varepsilon_{cr}$ for $r \leq e$. This is (more or less) correct for $r = e$, but for smaller values of r the strain ε_t is overestimated. However, the expansion in tangential direction due to the radial compressive stress is not taken into account, which feature caused a smaller difference in the estimated ε_t and the real magnitude of ε_t. Furthermore, the stress is calculated from the stress-crack opening curve from which it follows that only small differences in stresses occur, see Fig. 3.16.

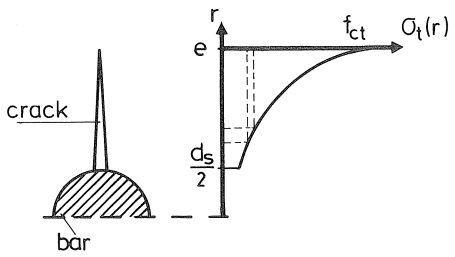

Fig. 3.16 Minor influence on stresses as a result of a small change in crack opening.

Substituting $\varepsilon_t = \varepsilon_{cr}$ in equation 3.43 gives:

$$\sigma_t = f_{ct} \, [1 - \{\frac{2\pi \, \varepsilon_{cr}}{n \, \delta_o} \, (e - r)\}^k] \tag{3.44}$$

The force developed in the cracked zone (softening) follows from the integral:

$$\int_{r=\frac{d_s}{2}}^{r=e} \sigma_t dr = f_{ct} \int_{r=\frac{d_s}{2}}^{r=e} dr - (\frac{2\pi \, \varepsilon_{cr}}{n \, \delta_o})^k \, f_{ct} \int_{r=\frac{d_s}{2}}^{r=e} (e - r)^k dr$$

$$\int_{r=\frac{d_s}{2}}^{r=e} \sigma_t dr = f_{ct} \, (e - \frac{d_s}{2}) \, [1 - \{(\frac{2\pi \, \varepsilon_{cr}}{n \, \delta_o}) \, (e - \frac{d_s}{2})\}^k \, \frac{1}{k+1}] \tag{3.45}$$

Thus the cracking resistance developed by the softening amounts to:

$$\tau_{br}\tan\alpha = \frac{2\ f_{ct}}{d_s}\ (e - \frac{d_s}{2})\ [1 - \{(\frac{2\pi\ \varepsilon_{cr}}{n\ \delta_o})\ (e - \frac{d_s}{2})\}^k\ \frac{1}{k+1}] \qquad (3.46)$$

Note that only stress is transferred in the total crack length if equation (3.47) is satisfied,

$$2\pi\ \varepsilon_{cr}\ (e - \frac{d_s}{2}) \leq n\ \delta_o \qquad (3.47)$$

otherwise we must adjust the lower integration boundary of the integral in equation 3.45 to x. This new lower integration boundary can be calculated from equation 3.48.

$$2\pi\ \varepsilon_{cr}\ (e - x) = n\ \delta_o \text{ (if equation 3.47 is not satisfied)} \qquad (3.48)$$

$$x = e - \frac{n\ \delta_o}{2\pi\ \varepsilon_{cr}} \qquad (3.49)$$

In this case there is a part of the crack where no stress is transferred. The total cracking resistance consists of the elastic part (formula 3.36) and the softening part formula 3.46.

$$\tau_{br}\tan\alpha = \frac{f_{ct}}{d_s}\frac{2e\ (c+\frac{d_s}{2})^2-e^2}{(c+\frac{d_s}{2})^2+e^2} + \frac{2\ f_{ct}}{d_s}(e - \frac{d_s}{2})[1-\{(\frac{2\pi\ \varepsilon_{cr}}{n\ \delta_o})\ (e - \frac{d_s}{2})\}^k\ \frac{1}{k+1}] \qquad (3.50)$$

in which

ε_{cr} = $\frac{f_{ct}}{E_c}$ (ultimate strain)
e = crack depth
c = concrete cover
n = number of cracks
δ_o = 0.2 mm and k = 0.248

The number of cracks is an important variable in formula 3.50. If the number of cracks increases to infinite $n \to \infty$ the cracking resistance changes to the plastic case; cracks penetrating the concrete cover, thus $e = c + \frac{d_s}{2}$ and only softening exist.

$$\lim_{n \to \infty} \frac{2\ f_{ct}}{d_s}\ (e - \frac{d_s}{2})[1 - (\frac{2\pi\ \varepsilon_{cr}}{n\ \delta_o})^k\ (e - \frac{d_s}{2})^k\ \frac{1}{k+1}] = \frac{2\ f_{ct}}{d_s}\ (e - \frac{d_s}{2})$$

Thus,

$$t_{br}\tan\alpha = \frac{2\ f_{ct}}{d_s}\ (e - \frac{d_s}{2}) = \frac{2\ f_{ct}\,c}{d_s} \text{ (compare with formula 3.33)}$$

This feature is clear when we consider that the total tangential displacement remains constant as it is imposed by the still elastic outer concrete ring. If several cracks exist, each crack is not able to open as far as a single crack. Consequently, more stress can be transferred over the smaller crack openings. A minimum is obtained if only a single crack (n = 1) exists, and this is the most important solution for practical applications, because this now gives us the lowest crack resistance.

3.3.3 Comparison of the model with results at room temperature

It is not possible to find a general applicable maximum for formula (3.50), because it depends not only on the crack depth e but also on the ultimate strain ε_{cr}, the concrete cover c and the bar diameter d_s. Consequently, a maximum can only be obtained if ε_{cr}, c and d_s are given. Calculations are made with 3 different bar diameters, 10, 20 and 30 mm respectively, 5 different concrete covers 0.5, 1.5, 2.5, 3.5 and 4.5 d_s respectively and an average ultimate concrete strain $\varepsilon_{cr} = 85 \times 10^{-6}$. The latter was calculated from $\varepsilon_{cr} = \frac{f_{ct}}{E_c}$ and the tensile strength f_{ct} was calculated from the splitting strength. The ratio between these two values can be obtained from the results of Heilmann [60] and amounts to:

$$f_{ct}\ (28\ \text{days}) = 0.9\ f_{cspl}\ (28\ \text{days}) \tag{3.51a}$$

$$f_{ct}\ (90\ \text{days}) = \quad f_{cspl}\ (90\ \text{days}) \tag{3.51b}$$

For commonly used concrete ε_{cr} varies between 100 and 70 x 10^{-6} and an average value of 85 x 10^{-6} was used for the calculations. The results obtained with one crack (n = 1) are collected in Fig. 3.17 where the bond stress to the tensile strength of the concrete is plotted as a function of the cover to bar diameter ratio. For comparison purposes only, the angle α is assumed to be constant 45°. The model predicts values between the partly cracked elastic and plastic stage just as the experimental values. It is clearly shown that the cracking resistance (relative to the tensile strength) is higher for smaller bar diameters. To understand this feature one should realize that the crack opening depends on the elastic deformation of the elastic outer concrete ring. If the crack depth equals e.g. d_s (= e) then the crack opening equals $2\pi (d_s - r)\varepsilon_{cr}$. Thus at the bar surface ($r = \frac{d_s}{2}$) the crack opening equals $\pi d_s \varepsilon_{cr}$. Hence, for a smaller bar diameter d_s a smaller crack opening is found and a higher stress could be transferred. However, it should be noted that the differences are small (12%) in the practical area for a concrete cover c = 1.5 d_s. Thus it is difficult to find experimental evidence because of the large scatter of results.

The predicted results are influenced very much by the value of α, which is assumed to be 45° for comparison reasons only. To obtain more information Martin [48] performed a numerical study on the stress distribution around a bar with lateral ribs. From Martin's results Eligehausen [64] calculated the average values of α given in Table 3.1.

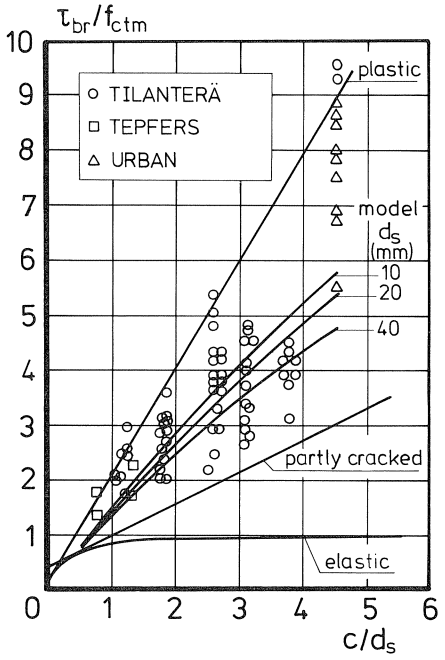

Fig. 3.17 Effect of thickness of concrete cover and bond capacity of the pull-out specimens on the occurrence of longitudinal cracking of the concrete cover.

This calculation shows that α is independent of the concrete quality and varies between 45° and 26°. With increasing bar diameter and increasing cover to bar diameter ratio the value of α decreases. However, Eligehausen states that the calculated angle α will, with increasing slip, increase to about 45° due to the wedge action of the crushed concrete in front of the ribs.

Table 3.1 Average value of the angle α from the analysis of Martin, Eligehausen [48,64].

d_s (mm)	cover c/d_s 1	2	3
10	44.3	40.9	34.2
16	34.5	33.8	31.5
26	26.5	29.5	-

Probably the best way to estimate the angle α is to use the results of the pull-out tests. Based on the results of Urban [62] an angle $\alpha = 35^\circ$ is calculated for $\frac{c}{d_s} = 4.5$ and from the results of Tepfers and angle $\alpha = 40^\circ$ is found for $1 \leq \frac{c}{d_s} \leq 2$. The latter angle is the most important one from a practical point of view and the first angle $\alpha = 35^\circ$ can be used for analyzing pull-out experiments with a large concrete cover. Note that the tendency in angles is the same as that found by Eligehausen.

Influence of the number of cracks

In Fig. 3.17 the effect of the bond capacity on the occurrence of longitudinal splitting cracking is given. However, it is evident that cracking of the cover does not imply that the ultimate bond stress has been reached. Some increase in load till failure is reported by Schmidt-Thrö [65] +15% and could be calculated from the results of Tepfers [53] +19%.

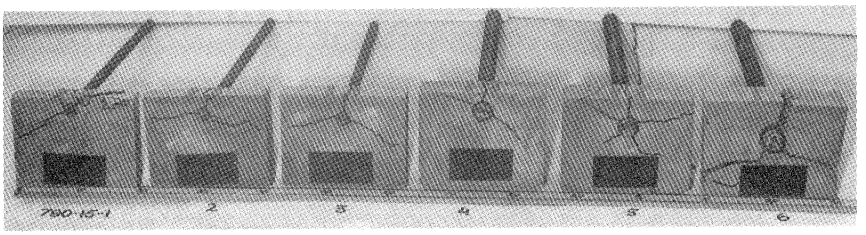

Fig. 3.18 Formation of internal and external longitudinal cracks, Tepfers [53].

As already discussed, the number of cracks is important to calculate the maximum (failure) load. The solution with one crack is compared with the experimental results in Fig. 3.17 and gives the lowest value. In order to calculate the ultimate load the number of cracks should be known. Schmidt-Thrö and Tepfers found that nearly always at least three cracks appeared, see Fig. 3.18.
When a fresh calculation was made with formula 3.50 and n = 3, an increase of about 5 to 10% was found for practical concrete covers, which fact seems to agree more or less with the experimental results.

3.3.4 Simplification of the model

Based on the average ultimate tensile strain $\varepsilon_{cr} = 85 \times 10^{-6}$, $\delta_o = 0.2$ mm and $k = 0.248$ the cracking resistance of the softening part in formula 3.50 can be simplified to:

$$\tau_b \tan \alpha = \frac{f_{ct}}{d_s} (2e - d_s) \left\{1 - 0.155 \left(\frac{2e - d_s}{n}\right)^{0.248}\right\} \qquad (3.52)$$

If we write $e = \beta (c + \frac{d_s}{2})$ for the crack depth and $n = 1$ and substitute formula

3.52 into formula 3.50, the following expression is obtained:

$$\tau_b \tan \alpha = \frac{f_{ct}}{d_s} 2\beta \left(c + \frac{d_s}{2}\right) \frac{(1 - \beta^2)}{(1 + \beta^2)} + \frac{f_{ct}}{d_s} \{2 \beta c - d_s (1 - \beta)\} \{1 - 0.155 (2 \beta c - d_s (1 - \beta))^{0.248}\} \quad (3.53)$$

A maximum cracking resistance is obtained for a crack depth $\beta(c + \frac{d_s}{2})$ which depends on the concrete cover and bar diameter. Values of the optimum β are collected in Table 3.2.

Table 3.2 Optimum values of β (n = 1)

d_s	c/d_s			
(mm)	1.5	2.5	3.5	4.5
10	0.73	0.70	0.68	0.67
20	0.69	0.67	0.65	0.63
40	0.66	0.63	0.61	0.59

Assuming an average value of $\beta = 0.70$ and substituting this value in formula 3.53 gives the total cracking resistance

$$\tau_b \tan \alpha = 0.48 \frac{f_{ct}}{d_s} (c + \frac{d_s}{2}) + \frac{f_{ct}}{d_s} \frac{1.4}{} (c - 0.21 d_s) \{1 - 0.168 (c - 0.21 d_s)^{0.248}\} \quad (3.54)$$

This formula approximates formula 3.50 closely enough for practical use. For a concrete cover smaller than 2 d_s the angle α is 40°. Substituting tan 40° into formula 3.54 gives the bond stress level at which longitudinal cracking starts.

$$\tau_{br} = 0.57 \frac{f_{ct}}{d_s} (c + \frac{d_s}{2}) + 1.67 \frac{f_{ct}}{d_s} (c - 0.21 d_s) \{1 - 0.168 (c - 0.21 d_s)^{0.248}\} \quad (3.55)$$

3.3.5 Effect of low temperature on the failure load

Only one investigation, Körmeling [66] concerning the softening behaviour at low temperatures is known by the author. The stress-crack opening displacement curves show the same tendency at both temperatures, i.e. 20 and -170°C. The fracture energy increases by about 45% and the tensile strength by about 29% at -170°C. From formula 3.35 it follows that the factor $\frac{k}{1+k}$ should be multiplied by $\frac{1.45}{1.29}$. Hence k = 0.315, which means that a higher relative cracking resistance can be expected.

Nevertheless the same assumption holds true for room and low temperatures because of the lack of information for temperatures below zero.
Because the tensile stength increases more than the modulus of elasticity at lower temperatures, the ultimate tensile strain ε_{cr} increases too. A maximum value was found at -70°C by Bamforth [34] which was about 100 to 185% greater than at room temperature. This is due to the fact that the major part of the increase in the tensile (splitting) strength occurred in the temperature range from 0 to -60°C. Consequently, the crack opening (n = 1) given by the equation

$$\delta(r) = 2\ \pi\ (e - r)\ \varepsilon_{cr}(T)$$

will reach its maximum value at around -70°C and results in the lowest contribution of the softening part to the cracking resistance. Thus in general a lower (relative) cracking resistance will be found if $\varepsilon_{cr}(T)$ is larger than $\varepsilon_{cr}(20°C)$. This statement is in agreement with the experimental observations of Scheuermann [33], who observed a 10% lower splitting failure load at -40 and -80°C, see formula (2.4).

3.4. Conclusions

- Prediction of crack width and crack spacing is possible at low temperatures if the local bond stress-displacement characteristic, found experimentally, is approximated with the aid of a power function at various temperatures.
- The so-called "first-generation crack" possesses a greater crack width than the crack width associated with a fully developed crack pattern if a constant tensile strength is assumed.
- Initially, where the thermal coefficient of expansion is different for concrete and reinforcement, a greater crack distance will be found at low temperature.
- Splitting failure can be predicted as a function of temperature by means of a model which includes the softening behaviour of concrete. A minimum relative cracking resistance relative to the tensile strength is calculated at around -70°C.
- If the bar diameter increases by 100% an approximately 10 to 15% lower relative cracking resistance against splitting failure is calculated.

4. EXPERIMENTAL PROGRAMME AND TESTING EQUIPMENT

4.1. Introduction

It was concluded in Section 2 that mainly the temperature and the moisture content of the concrete affect the mechanical properties of concrete. Therefore the temperature and the moisture content affected by the w/c ratio and the curing conditions are the main variables to be investigated. It was decided to divide the experiments into two main parts. In the first part the material properties of concrete, such as the compressive strength $f_{ccm}(T)$, the tensile splitting strength

$f_{cspl}(T)$, the modulus of elasticity $E_c(T)$ and the thermal behaviour $\varepsilon_c(T)$ (and $\varepsilon_s(T)$), are investigated as a function of temperature and moisture content.
In the second part the bond stress-slip relationship was determined by means of a pull-out test with an embedment length of 3 times the bar diameter. Furthermore, 12 experiments were performed on centrically reinforced tension members of 1 m in length. Section 5 deals with these subjects.
The present Section describes the experimental programme and the equipment used. More detailed information on this subject is presented in Van der Veen [67,68]

4.2. Experimental programme

Besides the determination of the material properties, the experimental programme comprised the pull-out and reinforced tension member tests. First, a survey of the pull-out tests is presented, then a survey of the tension member tests.

4.2.1. Pull-out experiments

Each batch comprised, among other types of specimen, six ϕ200x200 mm pull-out specimens with a centrically embedded steel bar. The experiments were conducted at an age of 90 days and using a 20 mm diameter reinforcing bar with an embedment length of $3d_s$ for the major part of the test series.
Because the temperature was the main variable to be investigated, five different temperatures, +20, -40, -80, -120 and -165°C respectively, were used. During the experiments the temperature was lowered at a rate of 1°C/min. The basic experimental programme comprised five temperatures, two concrete grades and three curing conditions, namely water-saturated (S), sealed (W) and air-dry at 50% r.h. and 20°C (H). A total of 96 pull-out specimens, 8 batches for both concrete grades, were investigated for the basic programme. It should be noted that each parameter was investigated in three experiments in order to get an idea of the scatter of results. All the other experiments were performed for one single set of curing conditions, namely sealed. For both concrete mixes the influence of the age (28 and 365 days), cooling rate and cyclic temperature loading on the bond stress-slip relationship was investigated. Furthermore, the embedment length (3 and $2d_s$) and the diameter (20 and 10 mm) were varied in mix 2 (low concrete grade), while the type of reinforcement (plain bar and Tempcore steel) was investigated in mix 1 (high concrete grade). In all, 198 pull-out tests were performed divided among 33 batches. A survey of the tests is given in Table 4.1.
Each experiment is described in detail in Van der Veen [69]. All the experimental results have been assigned an identifying code indicating the type of experiment.This code is composed as follows. First, a number indicates the type of mix employed, namely, 1 for mix 1 and 2 for mix 2. Second, a letter indicates the curing conditions: W, S and H for sealed, saturated and air-dry concrete respectively.

Table 4.1 Survey of the pull-out experiments.

Mix 1			Mix 2		
batch no.	main variable		batch no.	main variable	
1	curing conditions	: sealed	1	curing conditions	: sealed
2		sealed	2		sealed
3		sealed	3		sealed
4		sealed	4		sealed
5		saturated	5		saturated
6		saturated	6		saturated
7		air-dry	7		air-dry
8		air-dry	8		air-dry
9	age	: 28 days	9	age	: 28 days
10		365 days	10		28 days
11	type of bar	: plain bar	11		365 days
12		plain bar	12		365 days
13		plain bar	13	embedment length	: $2d_s$
14		plain bar	14		$2d_s$
15	temperature loading	: cyclic	15	bar diameter	: 10 mm
16*	type of bar	: Tempcore	16		10 mm
			17	temperature loading	: cyclic

* cured in a fog room; tested at an age of 28 days.

Third, a number indicates the age of the concrete in days: 28, 90 or 365. The temperature is always indicated separately. The following is an example of this identifying code:

temperature: -80°C
code 1/W/90

4.2.2. Reinforced tension members

Besides the control cubes, each batch comprised two centrically reinforced tension members of 1 m in length, with 100x100 mm square cross-section and a 20 mm deformed bar. The experiments were conducted at an age of 90 days. Four different temperatures, +20, -40, -80 and -165°C respectively, two concrete mixes and two curing conditions, namely sealed (W) and water-saturated (S) were used. Eight tension members of sealed concrete and four of water-saturated concrete were tested. For the latter curing condition only the effect of two temperatures, namely -80 and -165°C, was investigated for both mixes.

4.2.3. Concrete mix and curing conditions

Two different mixes were used. Both mixes were composed of Portland B cement and glacial river gravel aggregates with a maximum particle size of 16 mm. The mix composition is given in Table 4.2 and Appendix I.

Table 4.2 Mix proportions and 28 day mechanical properties at 20°C.

	Mix 1	Mix 2
cement content [kg/m^3]	400	275
water cement ratio	0.40	0.60
compaction index (Walz)	1.21	1.11
air content [%]	1.1 - 1.7	0.6 - 1.1
fresh density [kg/m^3]	2403	2404
cube compressive strength* [N/mm^2]	61.3 (5.2%)**	39.9 (8.0%)**
cube splitting strength* [N/mm^2]	3.4 (9.6%)**	2.6 (9.1%)**
Young's Modulus [N/mm^2]	34950 (4.5%)**	32100 (7.1%)**

*) curing condition: sealed concrete
**) coefficient of variation

Pull-out specimens as well as cubes were cast in synthetic moulds. The long tension specimens were cast in timber moulds. Immediately after casting, all the specimens and cubes were kept wet and covered with plastic sheets. After two days the specimens and cubes were demoulded and stored until testing. The specimens and cubes were cured in water (S), or wrapped in aluminium foil (W) or placed in a room at 50% relative humidity at 20°C (H), depending on the curing conditions. The free moisture content of both concrete grades was determined by drying samples of concrete at 110°C for 8 days, at an age of 28, 90 and 365 days. The free moisture content m is expressed as a percentage of the dry weight. The mean values of m are given in Table 4.3.
The free moisture content m is the governing quantity for determining the concrete strength. At an age of 90 days the free moisture content varied between 4.1 and 4.8% for mix 1 and between 3.7 and 5.5% for mix 2. Thus, the range of moisture contents used in practice is covered.
In order to measure the thermal deformation of concrete as a function of temperature ϕ60x150 mm cylindrical specimens were drilled from 200 mm cubes parallel to the casting direction. These cubes were cast in steel moulds, demoulded after two days and stored for two weeks under the prescribed conditions (saturated,

Table 4.3 Free moisture content of the cubes, in % by mass.

age	saturated		sealed		air-dry 50% r.h.	
	Mix 1	Mix 2	Mix 1	Mix 2	Mix 1	Mix 2
days	m(%)	m(%)	m(%)	m(%)	m(%)	m(%)
28	-	4.9	4.5	5.0	-	4.2
90	4.8	5.5	4.4	4.5	4.1	3.7
365	-	-	3.6	4.2	-	-

sealed or air-dry at 50% r.h.). The cylinders were then drilled and sawn to the required length and returned to the prescribed curing conditions until testing, generally at 90 days. At the time of testing the free moisture content of the cylinders was measured in the same way as in the cubes mentioned above. The mean values of the free moisture content are given in Table 4.4.

Table 4.4 Free moisture content (m) of the ϕ60x150 mm cylinders.

			Mix 1		Mix 2	
		age (days):	90	365	90	365
curing conditions			m(%)	m(%)	m(%)	m(%)
saturated	(S)		4.6	-	5.4	-
sealed	(W)		4.0	3.8	4.0	3.1
air-dry, 50% r.h.	(H)		3.0	-	3.4	-

In general, the free moisture content of the cylinders varied over a wider range in comparison with the cubes, because the dimensions of the cylinders were smaller than those of the cubes.

4.2.4. Preparation of the specimens

Cylindrical concrete specimens ϕ200x200 mm were used for the axial concentric pull-out tests. In accordance with the RILEM-CEB-FIP recommendations [70] the diameter of the specimens was chosen as about 10 times the bar diameter d_s. In general, the 20 mm diameter deformed steel bar was embedded centrically over a length of 60 mm, i.e. three times the bar diameter. To obtain a constant temperature distribution over the bond zone, a non-bonded length of 3.5 d_s was provided at both ends (the non-loaded and loaded end) of the bar. Fig. 4.1 shows the specimen geometry.

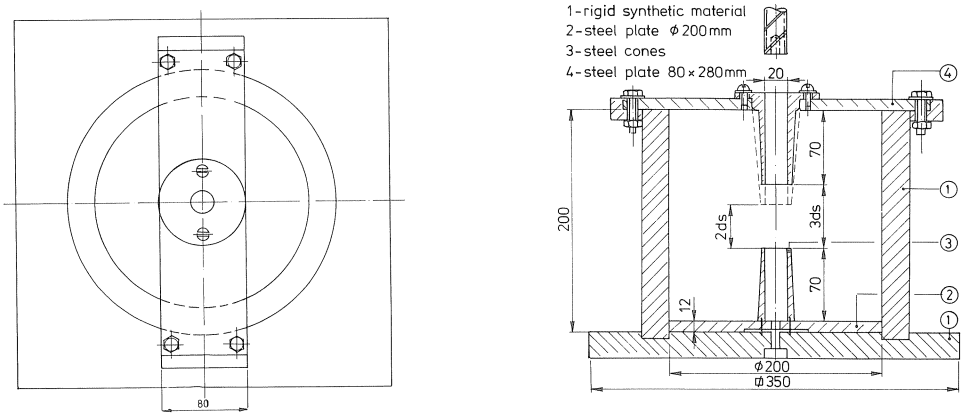

Fig. 4.1 Mould for pull-out specimen. View in plan and cross-section.

The mould was made of a rigid synthetic material. Demountable steel cones were attached to 12 mm thick steel plates that were located at the bottom and top of the mould. These conical spaces reduced the bond length of the steel bar and also kept the bar centrically positioned during casting. The bar was firmly attached to the steel bottom plate with one bolt. Space left at the interface of the bar and the cones was filled with wax, which was liquefied by heating. Two days after casting, the cylinder was demoulded with the aid of compressed air which entered the mould through the bottom hole. The specimen was further demoulded by removing the cones and was then stored in the vertical position under the prescribed curing conditions until testing. Before testing, the top concrete surface of the pull-out specimen was smoothed by means of a grinding machine. Next, the specimen was placed in the testing equipment in such a way that the pull was applied in the opposite direction to the casting direction (so-called vertical position).
The 1 m long tension specimens were demoulded two days after casting and stored horizontally under water (S) or sealed in aluminium foil (W) until testing.

4.3. Testing equipment

4.3.1. Hydraulic equipment

To perform the pull-out test at a prescribed low temperature a special test rig was built, see Fig. 4.2.
The testing equipment consisted of a hydraulic jack (range 400 kN) and a steel frame on which a cooling vat (D) was mounted. In the cooling vat the pull-out specimen was placed on a 100 mm thick load bearing disk of insulating material. At one end of the

reinforcing bar a screw thread was cut in the ribs only over a length of 100 mm, leaving the core intact. Thus, a nut (J) can be screwed on to the bar. This end of the bar is fixed to the jaws (H) of the jack by means of a nut. The axial force in the steel bar is measured by a load cell (K), range 400 kN.

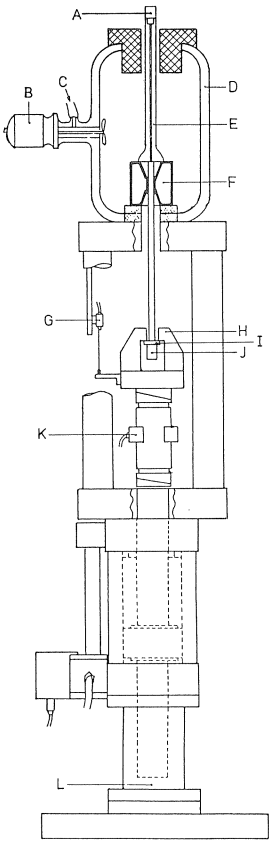

A - displacement transducer
B - fan motor
C - LN_2 injection
D - thermos container
E - dilato meter(invar)
F - pull-out specimen
G - displacement transducer
H - jaws
I - ball-joint
J - nut
K - load-cell
L - displacement transducer

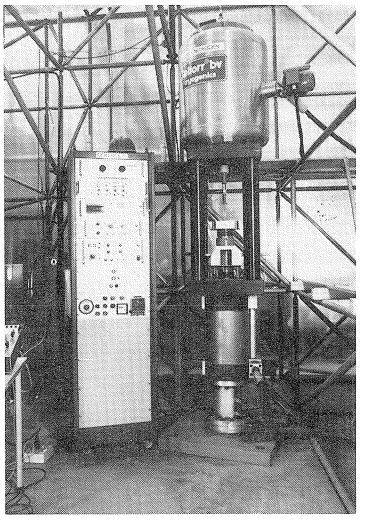

Fig. 4.2 View of test rig.

The experiment was performed under displacement-controlled conditions using transducer G in Fig. 4.2 at a displacement rate of 1 mm/min. End slip values of the pull-out bar were measured by a linear voltage displacement transducer (A) located at the free end of the embedded bar.

Because most of the tests were carried out at extremely low temperatures, the displacement transducer (A) was mounted on a dilatometer (E) outside the cooling vat. This dilatometer consisted of a tube and an internal solid pin, both made of a special kind of nickel steel, see Section 4.4.2. Thus the relative displacement between the steel bar and the concrete was transmitted by the dilatometer and

measured outside the cooling vat. The measuring signals of force (K) and end slip (A) were amplified and recorded by a two-channel transient recorder (Nicolet, Explorer II) with a maximum measuring frequency of two million samples per second and a core of 4k. A sampling time rate of 5 seconds was used for the tests described. After each test the results were stored on a floppy disk and afterwards processed by the HP21MX laboratory computer. After synchronisation, force (bond stress) slip relations were plotted and analysed.
The test rig for the long member is shown in Fig. 4.3. This testing equipment consisted of a hydraulic jack (range 200 kN) and a double steel frame which enclosed the cooling box in which the tension members were placed. Steel tension rods were screwed onto both ends of the reinforcing bar. These rods were fixed via the load cell and the hydraulic jack to the steel frame, which was constructed in a double layer to ensure axial loading. The experiments were performed under load-controlled conditions using the load cell. The load was applied to the tension member via a number of load steps. Two minutes after each load step, the load, the total elongation and the crack widths were measured, stored and processed by the laboratory computer.

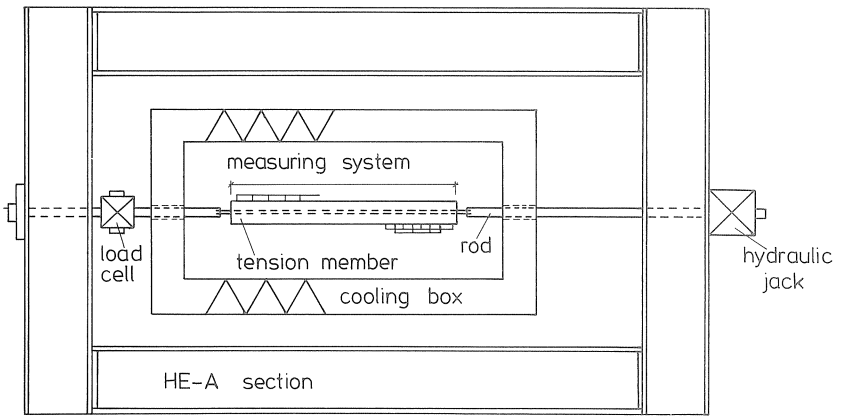

Fig. 4.3 Top-view of test rig which consisting of the cooling box enclosed by a steel frame.

4.3.2. Cooling process and thermal cycling

A common method for generating low temperatures is to use liquefied nitrogen (LN_2), which is produced and sold in bulk. It possesses a boiling temperature of -196°C, which is more than 30°C below that of liquefied natural gas (LNG); it is also non-inflammable and non-toxic.
The operation of LN_2-operated cooling boxes with continuous temperature adjustment is based on the principle of injecting a certain amount of LN_2 which is atomized in the interior around the test specimen and subsequently evaporates.

The amount of heat required for evaporation is withdrawn from the interior of the cooling box and from the specimen, resulting in a cooling effect.
How the cooling process operated is shown schematically in Fig. 4.4. A temperature controller briefly opened the solenoid valve installed in the rear wall. As a result, LN_2 from a storage vessel was sprayed on the fan and entered the interior of the cooling vat.
This fan, driven by an exterior electric motor, rotated behind a screen in the cooling vat, into which it discharged the mixture of air and gas. A temperature sensor in the vat provided temperature control with the aid of a Commodore 64 Micro computer. An analog-digital convertor was necessary for translating the analog temperatures into digital values for the computer, and vice versa. In the computer program developed for these tests the parameters such as the cooling rate in (°C/min) and the desired low temperature could be freely chosen. The cooling rate was controlled by the computer via longer or shorter opening time of the valve.

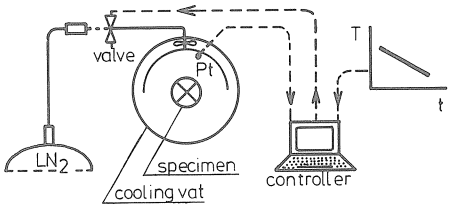

Fig. 4.4 Schematic view of the cooling process.

All the measured temperatures were displayed on a monitor screen and were printed. To make temperature cycling possible a tubular radiator with a capacity of 1800 W was fitted concentrically on the fan.

4.3.3. Temperature conditioned test coolers

The starting point for the development of the cooling box in which control cubes and cylinders were to be cooled was that the testing of the cubes and cylinders must take place outside this box. Because 1m long centrically reinforced concrete members uniaxially loaded must also be tested, the inside dimensions were 0.6x0.6x1.35 m. The double-walled stainless steel cooling box was insulated with 150 mm foam (Roofmate). A hinged cover at the top gave access to the interior of the box. Inside the cooling box was a second box which could be opened at the top to insert the specimens. The front of this box was open. Cooling was effected by spraying liquefied nitrogen upon two fans, which produced a continuous cold forced draught between the inner box and the wall of the cooling box. Through holes in the back of the inner box this cold gas was drawn from the front of the box past the specimens to the back, see Fig. 4.5.
In the bottom of the cooling box and around the two fans were three electrical heating elements with a total capacity of 7000 W for increasing the temperature.

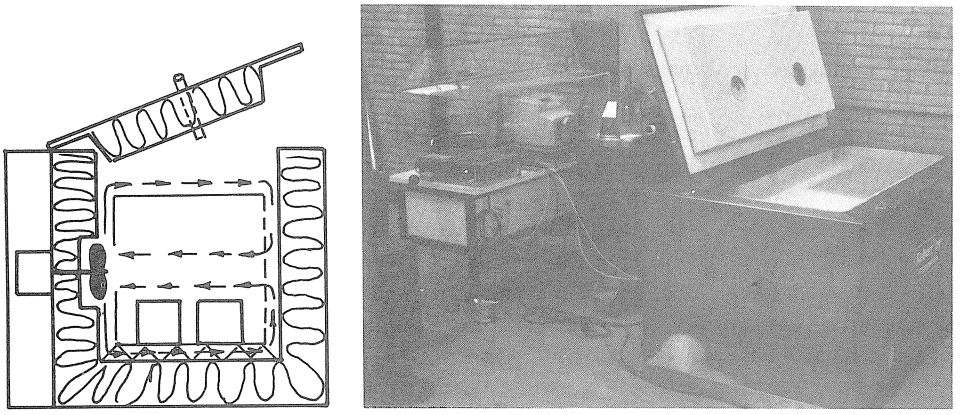

Fig. 4.5 View of large cooling box.

Good interadjustment of cooling and heating made it possible to perform tests with temperature cycles.
Despite the 150 mm thick insulation in the cooling box mentioned above, a considerable quantity of liquid nitrogen was used. Therefore the insulation of the second cooling box was based on the principle of a storage container for liquefied gases. A cylindrical shape was chosen to allow high-vacuum and super-insulation. This thermos container is shown schematically in Fig. 4.6. All the pull-out and thermal deformation tests were performed in this container.

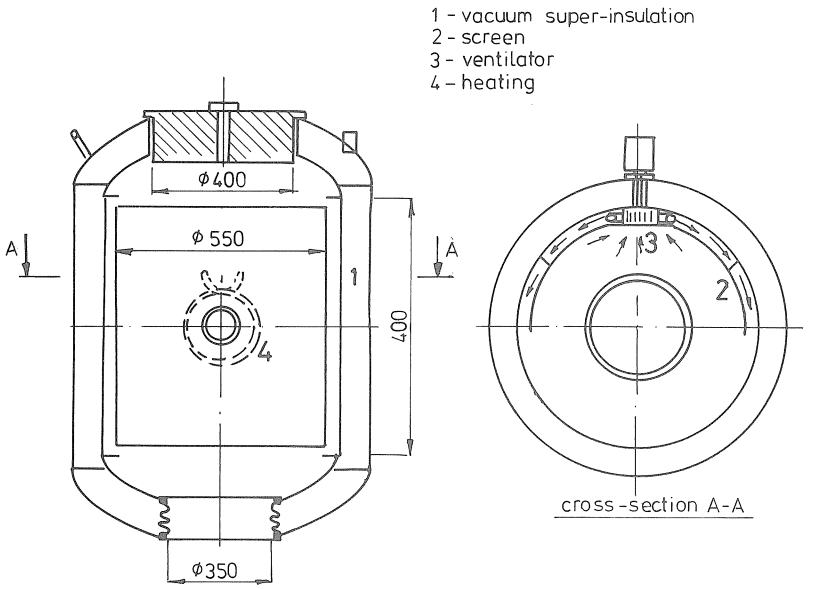

Fig. 4.6 Schematic view of the thermos container.

4.4. Measuring systems at low temperature

4.4.1. Temperature measurements

Generally, a thermocouple is used for determining the temperature. These are available for a wide range of temperatures. However, under cryogenic conditions the copper-constantan type (Cu-Cu/Ni) is the only one which can be used. Very accurate and stable temperature measurements can be obtained with metal resistance thermometers. A platinum type can be used between -260 en +850°C. In the cooling box (container) one single platinum resistor was used for accurate and stable temperature control, while for temperature measurements inside the specimen the cheap thermocouple was used.

4.4.2. Displacement measurements

For measuring the thermal contraction and expansion behaviour a ϕ60x150 mm cylindrical specimen of concrete or a reinforcing bar 150 mm in length was mounted within a frame formed of quartz rods, see Fig. 4.7a, placed in a thermos container.

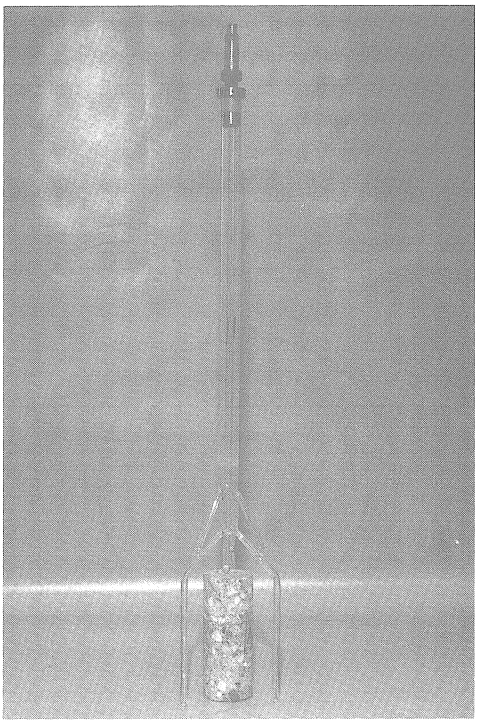

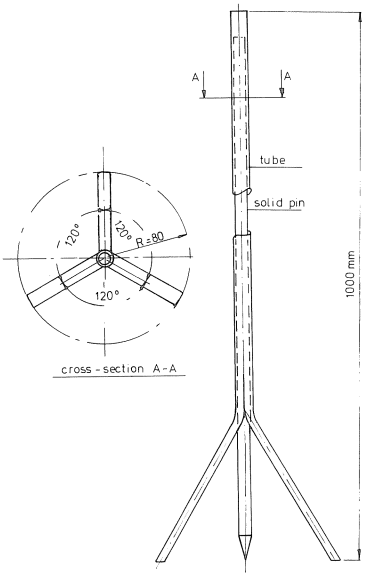

Fig. 4.7 a. Dilatometer made of quartz glass;

b. Dilatometer for measuring slip values.

The specimen was subjected to controlled cooling at a constant rate (1°C/min) and the relative displacement of the two opposite end faces was recorded with the aid of quartz glass rods. This displacement was transmitted by a SiO_2 glass rod to a displacement transducer (LVDT) located outside the cooling box. This type of test rig was possible because quartz glass possesses a very low coefficient of thermal expansion. The same method was used in the pull-out test for measuring the relative displacement (slip) between the steel bar and the surrounding concrete. Unfortunately, splitting failure of the pull-out specimen caused damage to the dilatometer made of SiO_2. Therefore a new dilatometer was made of a low-expansion 36% nickel-iron alloy, a material which possesses a mean coefficient of linear expansion of 2.2×10^{-6} m/m°C in the temperature range from -250 to 0°C. This dilatometer is shown in Fig. 4.7b.

4.4.3. Crack width measurements

It is not possible to measure crack width visually at low temperatures. Therefore, two series of electro-mechanical extensometers were situated along both sides of the reinforced tension member, see Fig. 4.8a. This type of extensometer was developed at Delft University and consists of a steel spring which is clamped between two angles, and two strain gauges in the mid-section, see Fig. 4.8b. A measuring length of 110 mm was used with a measuring range of 2 mm and a general accuracy smaller than 0.01 mm.

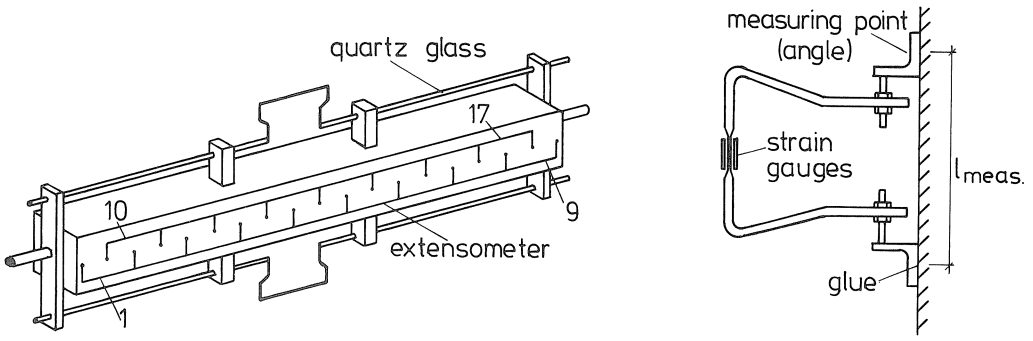

Fig. 4.8 a. Measuring system for crack width and total elongation;
b. Detail of the electro-mechanical extensometer.

The crack width is defined as the relative displacement between two measuring points (angle) on the tension member. In order to measure the total elongation of the tension member the same type of extensometers were used. These two extensometers were situated between two quartz rods which were connected to the ends of the reinforcement, see Fig. 4.8a.

5. EXPERIMENTAL RESULTS

5.1. Introduction

This Section is devoted to the experimental results of the standard, pull-out and reinforced tension member tests. First, the results of the standard tests which relate to the compressive strength and tensile splitting strength of the concrete, the stress-strain relationship, the thermal deformation and some material properties of the reinforcing steel as a function of temperature are discussed. Second, the results of the pull-out experiments are dealt with in Section 5.6. Third, in Section 5.7 attention is paid to the measurements performed on the reinforced concrete tension members, such as crack width and crack spacing. All type of experiments were performed at different temperatures and curing conditions as mentioned in Section 4.2.

5.2. Compressive strength and splitting strength at various temperatures

The average strength results of the standard tests conducted at 20°C and 90 days old are summarized in Table 5.1. In all, three different curing conditions were examined: water-saturated, sealed and air-dry (50% r.h.) concrete.

Table 5.1. Test results at room temperature at an age of 90 days.

Mix	curing conditions	number (.)	f_{ccm} (N/mm^2)	c.v.* (%)	number (.)	$f_{cspl,m}$ (N/mm^2)	c.v.* (%)
1	sealed	39	68.4	6.3	33	3.56	8.4
	saturated	6	68.4	2.9	6	3.75	8.2
	air-dry	6	64.3	2.7	6	3.45	4.9
2	sealed	37	45.3	8.1	4.0	2.93	8.5
	saturated	6	48.1	2.9	6	3.07	3.2
	air-dry	6	44.7	4.3	6	3.00	6.3

* coefficient of variation

Investigations have shown that the compressive strength increases as the temperature is lower. This increase is hardly affected by the strength at room temperature, see Section 2.2. For this reason the mean compressive strength at low temperatures can be expressed as:

$$f_{cm}(T;m) = f_{cm}(20°C) + \Delta f_{cm}(T;m) \qquad N/mm^2 \qquad (5.1)$$

in which the strength increase depends on temperature and moisture content only. A formula was derived by Rostásy and Scheuermann [19] to predict the increase in compressive cylinder strength:

$$\Delta f_{cm}(T;m) = \{1 - (\frac{T+170}{170})^2\}12\ m \quad \text{(cylinder)} \qquad N/mm^2 \qquad (5.2)$$

in which m = moisture content % (by wt)
T = temperature

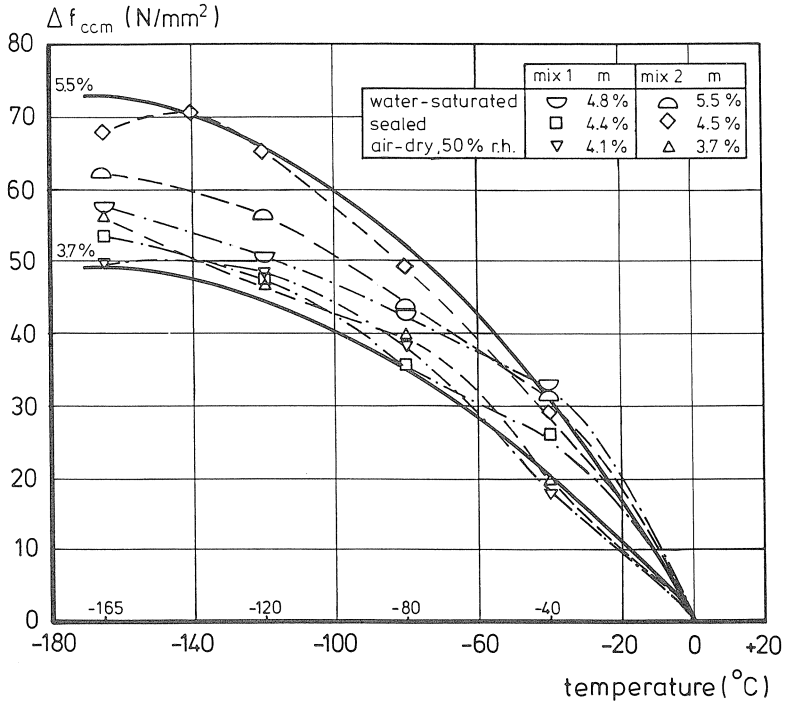

Fig. 5.1 Increase in cubic strength at 90 days for different curing conditions versus temperature.

From a regression analysis of the test results, see Fig. 5.1., a formula has been found for the cubic compressive strength increase $\Delta f_{ccm}(T;m)$:

$$\Delta f_{ccm}(T;m) = \{1 - (\frac{T+170}{170})^2\}13.2\ m \qquad N/mm^2 \qquad (5.3)$$

A higher cylinder to cubic strength ratio (about 0.9) was found at low temperatures than at room temperature, which fact was also observed at room temperature for high concrete grades by Neville [71]. Formula 5.3 shows reasonably good agreement with the experimental values for both mixes as presented in Fig. 5.1. The lowest increase was found for the air-dry cubes for both mixes and the highest increase for the sealed cubes only for mix 2.
Also an increase in tensile splitting strength was observed at very low temperatures. Experimental values are shown in Figs. 5.2 and 5.3 for mix 1 and mix 2 respectively.

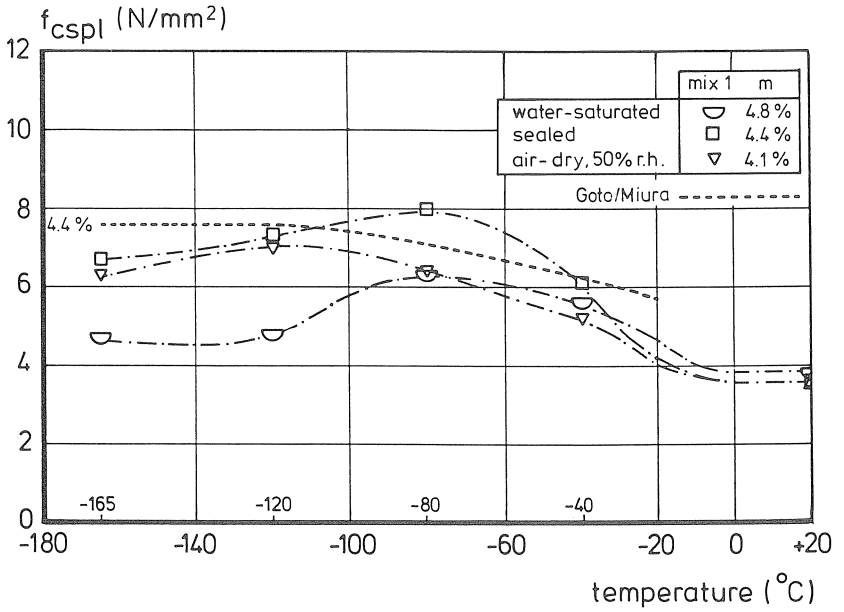

Fig. 5.2 Tensile splitting strength for mix 1 with different moisture content versus temperature.

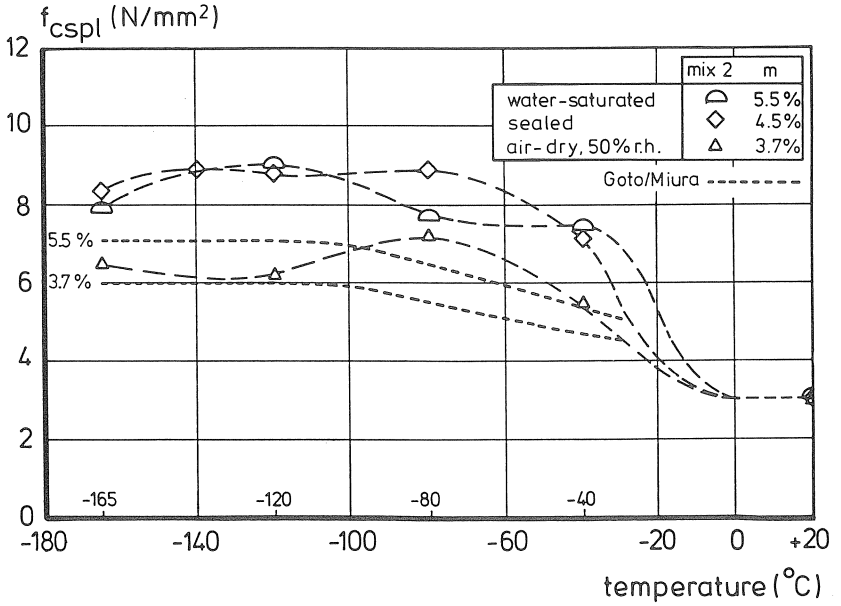

Fig. 5.3 Tensile splitting strength for mix 2 with different moisture content versus temperature.

The tensile splitting strength shows a marked increase for the water-saturated and sealed concrete in the temperature range from 0 to -40°C, particularly for mix 2. In general a maximum value was observed at -80°C. At lower temperatures the increase in strength remained constant or even a small decrease was observed, as shown in Fig. 5.2. The tensile splitting strength can be estimated from the cylinder compressive strength according to Goto/Miura [22]:

$$f_{cspl,m}(T) = 0.214\ f_{cm}(T)^{0.75} \qquad N/mm^2 \qquad (5.4)$$

in which $f_{cm}(T)$ can be predicted with the aid of formulae (5.1) and (5.2). When the splitting strength is calculated from the cubic strength, the factor 0.214 in formula 5.4 should be converted to 0.181. In this case the usual ratio between cylinder and cubic strength is applied. Unfortunately, the experimental results exhibit a wide scatter, so that only poor agreement is obtained with this prediction.
Generally, the major part of the increase in splitting strength occurred in the temperature range from 0 to -40°C, unlike the increase in compressive strength, which occurred mainly from 0 to -100°C. Consequently, the increase in strength is not similar for the compressive strength and the tensile splitting strength. Hence, it will be difficult to find a relation between the mean tensile splitting strength and the mean compressive strength which is valid at low temperatures.

5.2.1 Influence of the age of the concrete

It is a well known fact that the strength of concrete increases as a function of age under normal conditions (room temperature). To investigate simultaneously the

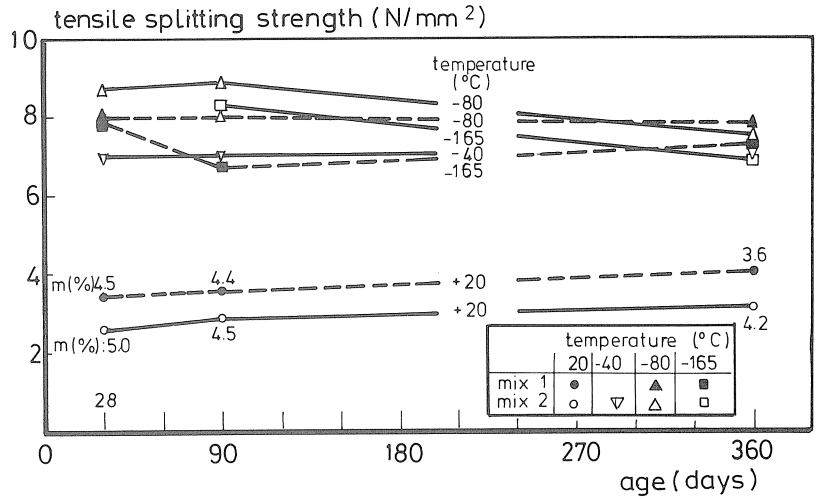

Fig. 5.4 Tensile splitting strength of sealed concrete as a function of temperature and age.

influence of the age of the concrete and the low temperature, a number of experiments were performed at different ages, namely 28, 90 and 365 days.As a result of the hydratation process the amount of free water in the sealed concrete will decrease. Consequently, a smaller increase in strength at low temperatures will be observed.

At an age of 365 days the same (mix 1) and a lower (mix 2) actual splitting strength was observed, see Fig. 5.4. It should be noted, however, that the differences in strength are only small. The compressive strength showed a different behaviour.

The actual compressive strength for both mixes is shown in Fig. 5.5. Approximately the same actual strength at different ages was found at -80 and -165°C for mix 1. For mix 2 (water/cement ratio 0.60) the same or a slightly increased actual strength at an age of one year was observed.

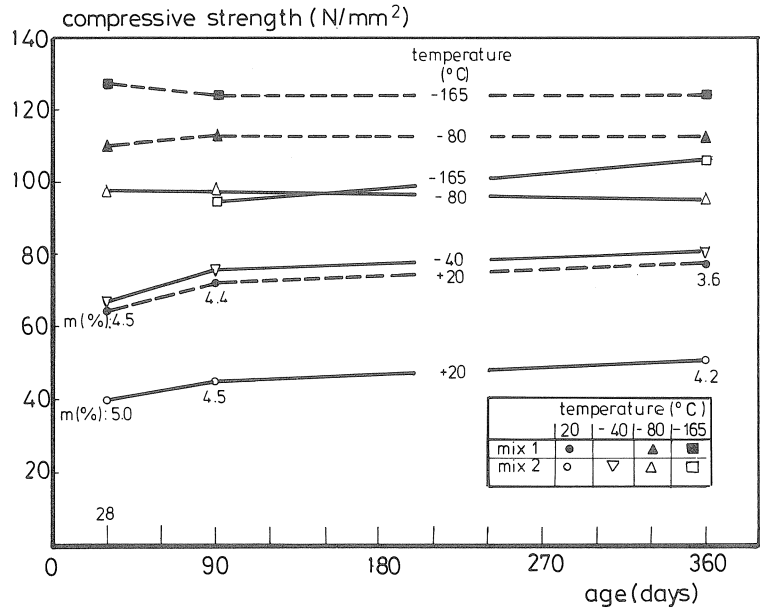

Fig. 5.5 Compressive strength of sealed concrete as a function of temperature and age.

5.3. Modulus of elasticity at different temperatures

The static modulus of elasticity was measured in this experimental programme. This modulus represents the secant modulus and was measured at stresses of one-third of the cylinder strength f_c at 20, -80 and -165°C. Testing started at an age of 90 days and only sealed concrete was investigated. The mean values calculated from two experiments are summarized in Table 5.2.

Table 5.2 Cryogenic properties of the stress-strain relationship.

Mix	T (°C)	f_c (N/mm^2)	E_c	$E_c(T)/E_c(20°C)$ (.)	$f_c(T)/f_c(20°C)$ (.)
1	+ 20	42.02	36125	1.00	1.00
	- 80	72.66	49100	1.36	1.73
	-165	83.56	61475	1.70	1.99
2	+ 20	28.24	34050	1.00	1.00
	- 80	69.04	52425	1.54	2.44
	-165	85.42	66675	1.96	3.02

The static modulus of elasticity was found to increase when the temperature was lowered, but to a far lesser extent than the (cylinder) compressive strength. This is clearly shown in Table 5.2 by the relative modulus of elasticity and strength. For mix 2 with a higher water/cement ratio (0.60) this difference in relative values was more pronounced than for mix 1 (w/c ratio: 0.40).
Stress-strain relationships for both mixes are shown in Figs. 5.6a and 5.6b. An almost linear elastic behaviour was found at -165°C for the stress-strain curve. Failure occurred in a brittle mode at -165°C for both mixes. The same type of failure was observed for mix 1 at -80°C.

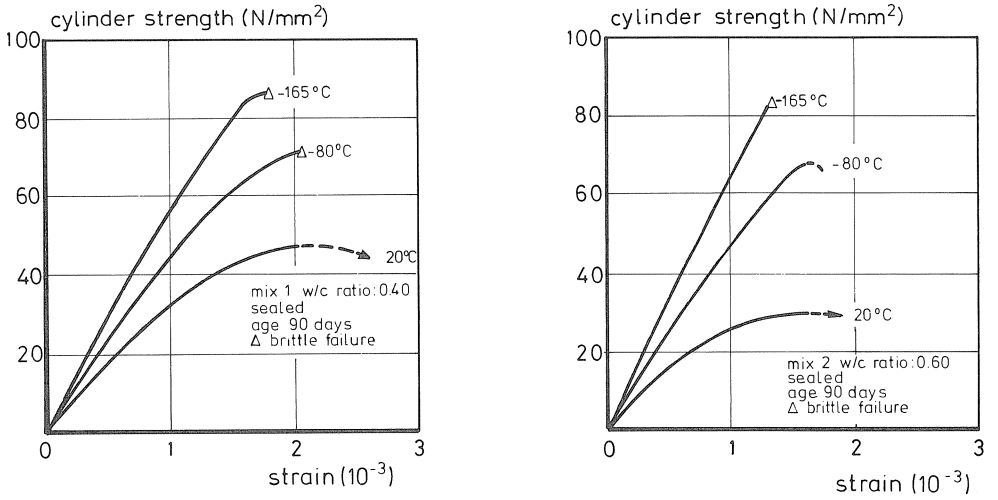

Fig. 5.6 Stress-strain relationship at three temperatures for mix 1 (a) and mix 2 (b).

5.3.1. Influence of thermal cycling on the modulus of elasticity

To investigate the influence of thermal cycling on the static modulus of elasticity of sealed concrete at an age of 90 days, a number of experiments were performed on

cylinders after 0, 5 and 10 thermal cycles. The temperature was lowered to -100°C and after 60 min. raised to +20°C at a rate of 1°C/min. Some typical values of the relative modulus of elasticity and cylinder strength are shown in Fig. 5.7. The concrete with the highest water/cement ratio (mix 2) exhibited the greatest reduction in elasticity and strength after 5 and 10 thermal cycles. For mix 1 no decrease in strength and hardly any decrease in the static modulus was observed.

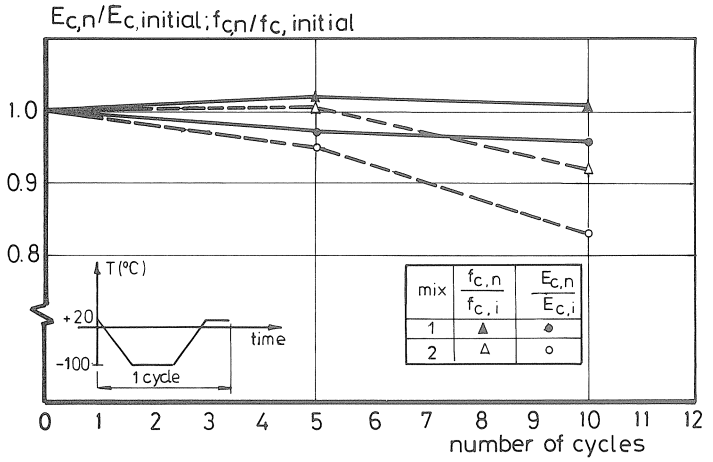

Fig. 5.7 Relative modulus of elasticity and cylinder strength of sealed concrete at 90 days versus the number of temperature cycles.

5.4. Thermal behaviour

The effect of three different sets of curing conditions, namely water-saturated, sealed and air-dry at 50% r.h., on the thermal strain-temperature relationship was investigated. Experimental results for both mixes determined at an age of 90 days are shown in Fig. 5.8, where each curve represents the mean of three different experiments.

Specimens which were sealed or air-dried during the curing time exhibited almost linear thermal deformation and perfect reversibility. The thermal deformations for both mixes were almost identical, i.e. the water/cement ratio did not affect the thermal behaviour. However, the water-saturated specimens showed totally different behaviour. Between -20 and -60°C a pronounced expansion was observed. This expansion in the transition range was clearly influenced by the water/cement ratio and increased for higher ratios, as Fig. 5.8 shows. When the water-saturated specimens were reheated, an even greater expansion occurred, and irreversible strains indicating internal micro-cracking were observed at 20°C after reheating. These irreversible strains are greatest for the concrete mix with the highest water/cement ratio.

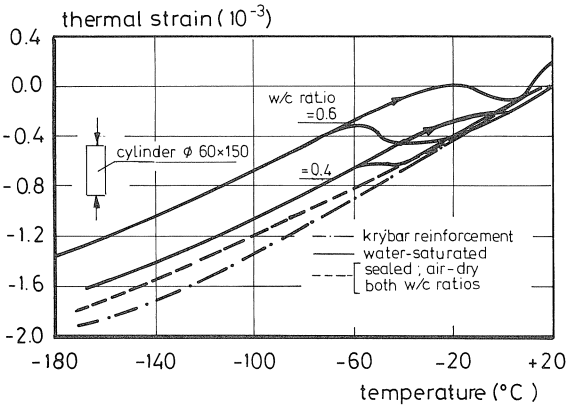

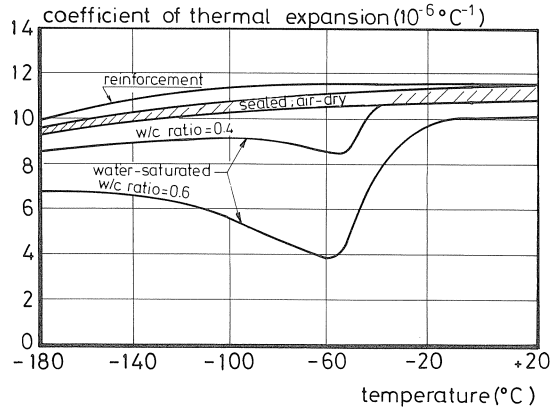

Figure 5.8 Thermal strain and coefficient of thermal expansion as a function of temperature.

The sealed specimens were tested at two different ages, namely 90 and 365 days. The concrete at an age of 365 days was found to have a thermal strain which was slightly greater than that of concrete at an age of 90 days. Furthermore, it showed perfect reversibility from cooling to reheating.

To investigate the influence of the type of steel on the thermal deformation three different steels, namely Krybar, Krybar with 3.5% Ni and Tempcore were tested. Only minor differences between the different types of steel were found to occur during cooling. Some typical results represented by one line are shown in Fig. 5.8.

For engineering calculations it is common to define the coefficient of thermal expansion $\alpha(T)$ as the slope of the secant with the origin at 20°C:

$$\alpha(T) = \frac{\varepsilon(T)}{(T-20^{\circ}C)} \qquad 1/^{\circ}C \qquad (5.5)$$

in which $\varepsilon(T)$= thermal strain and T = temperature.

For air-dry and sealed concrete a continuously decreasing curve was found. The shaded area gives the scatter range for both mixes. It turned out that changes in the moisture content had virtually no effect on the thermal deformation. If we compare the coefficient of expansion of the reinforcement and the concrete, it is clear that only limited stresses will be introduced in a reinforced member.
The water-saturated concrete showed an expansion in the transition range which greatly depended on the water/cement ratio or moisture content (m). For the two concrete mixes investigated, with water/cement ratios of 0.40 and 0.60 respectively, a positive value of $\alpha_c(T)$ was always found, see Fig. 5.8.

5.5 Properties of the reinforcing steel

Krybar reinforcement was used for the pull-out experiments, this being a reinforcing steel which because of its special properties is used in applications as storage tank structures for the containment of liquefied natural gas (LNG). At room temperature the yield and ultimate strength were found to be 471 and 541 N/mm^2 respectively, and the modulus of elasticity was 2.1×10^5 N/mm^2. When the temperature is lowered the yield and ultimate stength increase progressively, as can be seen in Fig. 5.9, [72]. For the 20 mm diameter bar a value of 0.076 was found for f_R. To investigate the bond stress-slip relationship of plain bars some deformed bars were prepared (removing the ribs) to obtain a smooth surface. This preparation resulted in 18 mm plain bars. To characterize the surface roughness the so called R_a-value was determined. This value equals the mean deviation of the surface profile from the average profile depth. The surface profile was recorded by means of a Taylor-Hobson device. Because two batches of reinforcement were smoothed separately, two different values of R_a, namely 9 and 2 μm, were found.

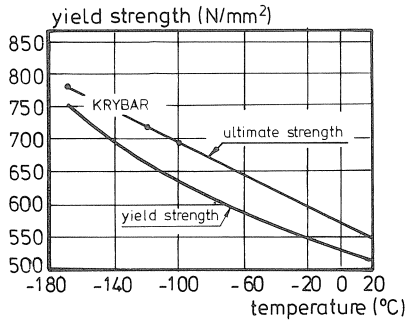

Fig. 5.9 Yield and ultimate strength of Krybar reinforcement versus temperature [72].

5.6. Bond stress-slip relationship at several temperatures

5.6.1. Influence of the curing conditions and concrete grade

In general the results are presented in diagrams where each curve represents a bond stress-slip relationship at a certain temperature. For the temperatures of -165, (-140) and -120°C one experimental result was selected for the curve because of the peculiar results, while for the other temperatures a mean value of the curve has been given.

The experimentally determined bond stress-slip curves are presented in Figs. 5.10, 5.11 and 5.12 for sealed, air-dry and water-saturated concrete respectively. The results of mix 1 and mix 2 are given in the left-hand and right-hand diagrams respectively. In general, the bond stress increased at a certain slip value at lower temperatures. However, the main part of this increase occurred at temperatures down to -120°C. At lower temperatures hardly any increase in bond stress was observed. For both mixes and regardless of the curing condition a continuous curve was observed at -40 and -80°C similar to the curve found at 20°C. A single abrupt change in slip was noticed at -120°C for the tested curing conditions. This large increase in slip values was found at a stress level of about 40 N/mm^2 for both mixes and was initiated at a slip value of approximately 0.10 mm, see Fig. 5.10. A typical phenomenon was also found at -165°C where the slip values changed abruptly and increased instantaneously. These abrupt changes were initiated at slip values of about 0.03 mm and increased rapidly at higher slip values (stress levels). This phenomenon resulted in a large increase in slip values at stress levels of about 30 N/mm^2 for water-saturated and at 40 N/mm^2 for sealed and air-dry concrete. These results are in accordance with the experimental results of Scheuermann [33]. The abrupt changes in slip were probably caused by the initiation of internal radial cracks, which feature occurs in a more brittle mode at low temperatures according to Scheuermann [33].

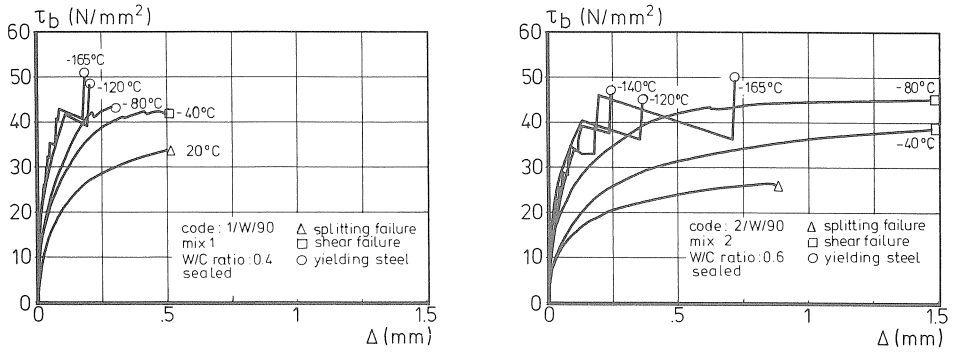

Fig. 5.10 Bond stress-slip relationships for sealed concrete at various temperatures and both mixes.

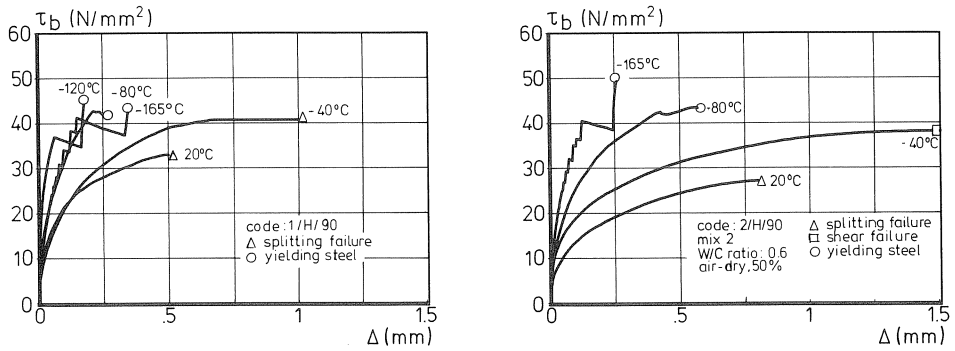

Fig. 5.11 Bond stress-slip relationships for air-dry concrete at various temperatures and both mixes.

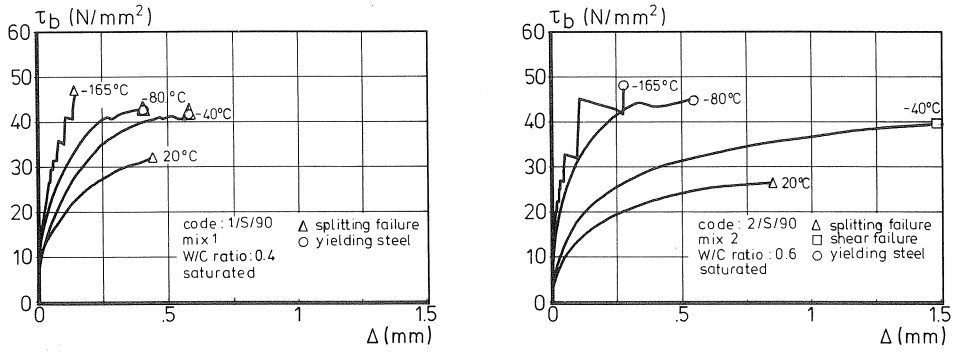

Fig. 5.12 Bond stress-slip relationships for water-saturated concrete at various temperatures and both mixes.

Failure mode

Splitting failure was found to be the failure mechanism at room temperature for all curing conditions. Furthermore, this failure mechanism was observed for mix 1 and air-dry concrete at -40°C and for water-saturated concrete at all testing temperatures. The splitting failure mechanism was in agreement with the tensile splitting strength, see Fig. 5.2, which attained the lowest values for saturated concrete.

Shear failure was mostly observed for mix 2 (lowest grade) at -40°C. However, for sealed concrete this failure mode was also found at -80 and -40°C for mix 1. At the other (lower) temperatures the maximum bond stress was determined by the yield strength of the reinforcement. Consequently, no failure of the concrete was found to occur.

Other aspects of the bond stress-slip relationship and failure mode will be discussed further in Section 6.

Comparison of the bond stress

The bond stresses measured at two slip values, namely, 0.025 and 0.1 mm, are assembled in Fig. 5.13. For mix 1 the sealed concrete attained the highest bond stress for both slip values, while for mix 2 the water-saturated and the sealed concrete exhibited the highest bond stress. Regardless of the curing conditions, a similar increase of bond stresses was observed for lower temperatures. Furthermore, a greater increase in bond stress was observed for mix 2 in comparison with mix 1 when the temperature was lowered. However, the actual values at -165°C were more or less equal.

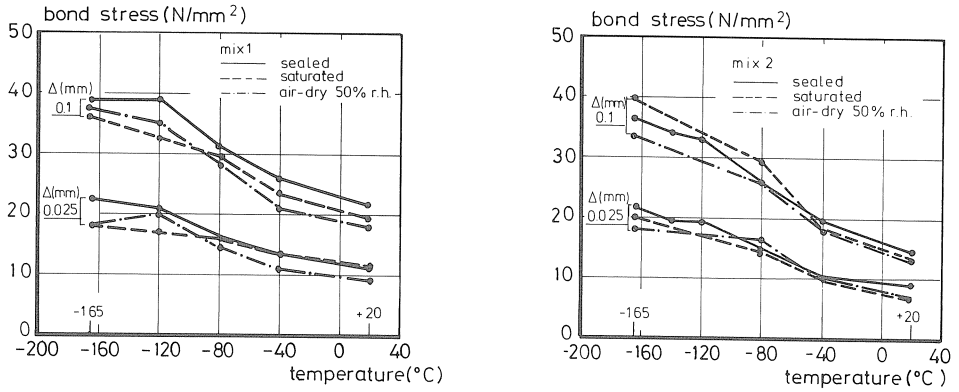

Fig. 5.13 Bond stress determined at 0.025 and 0.10 mm slip versus temperature for different curing conditions.

5.6.2. Influence of the age of the concrete

To investigate the influence of the age of the concrete on the bond stress-slip relationship, experiments were conducted at three different ages, namely 28, 90 and 365 days, and at several temperatures.

The majority of this type of experiments were performed for mix 2 and sealed concrete. Bond stresses measured at two slip values and different ages are assembled in Fig. 5.14.

For ageing concrete an increase in bond stress was found at 20°C which was proportional to the compressive strength. Consequently, the highest bond stress was observed at a concrete age of 1 year. At lower temperatures the highest bond stress at a certain slip value was found at 90 and 28 days at -80 and -165°C respectively. As mentioned above in Section 5.2.1, comparison of the actual compressive strength with the bond stress gives a reasonable correlation at temperatures of 20 and -80°C.

Hence, some relation seems to exist between the actual compressive strength and the bond stress. Furthermore, the effect of the low temperature upon the bond stress-slip curve is most pronounced at a concrete age of 28 days and least pronounced at an age of 365 days, as can be seen in Fig. 5.14 for bond stresses measured at a slip of 0.025 mm.

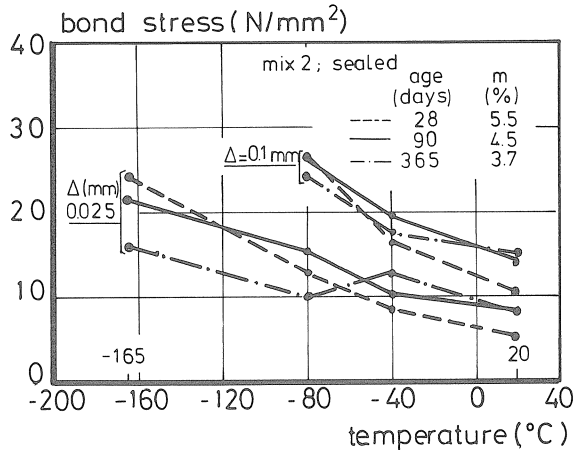

Fig. 5.14 Bond stresses measured at two slip values and different ages versus temperature.

This feature is probably associated with the decreasing free moisture content in the concrete as a result of hydratation. It was found that the extent of the abrupt changes in slip observed at -165°C increase for ageing concrete. For mix 2 even a different failure mode was observed for concrete at an age of 365 days and tested at -165°C. The abrupt changes in slip finally led to splitting failure, which is probably associated with a lower tensile splitting strength found at low temperatures. The splitting strength turned out to be lower for ageing concrete, as mentioned previously in Section 5.2.1. The failure mode was not affected by the age of the concrete at the other temperatures. At room temperature splitting failure was always observed for both mixes, while for mix 2 at -40 and -80°C shear failure occurred.

5.6.3. Influence of some parameters on bond resistance

The influence of the parameters relating to the cooling rate, embedment length and bar diameter are dealt with in succession below. Because the maximum bond stress was mostly determined by the yield strength of the reinforcement, it was decided to minimize the embedment length to 40 mm or $2d_s$. Furthermore, a number of experiments was conducted with 10 mm steel bars which have a f_R value of about 0.067.

Cooling rate and embedment length

The effect of the cooling rate on the bond stress-slip characteristic was investigated by using three different cooling rates, namely 1/3, 1 and 3°C/min. Experiments were performed at two temperatures -80 and -165°C respectively. The results found after a cooling rate of 3°C/min differ from the curves measured at -165°C after cooling at 1°C/min. No significant influence of the cooling rate on the bond stress-slip curve measured at -80°C was found. It was therefore decided to perform the experiments after cooling at a rate of 1°C/min.
To investigate the effect of the embedment length on the bond stress-slip relationship, tests were also performed with a shorter embedment length of 40 mm ($2d_s$). Three different temperatures, namely +20, -80 and -165°C were used in the experiments. The measured curves are shown in Fig. 5.15 for both embedment lengths.

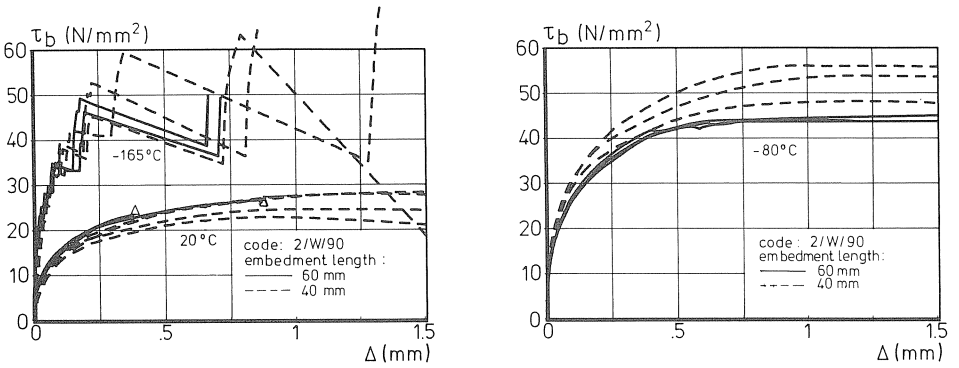

Fig. 5.15 Bond stress-slip curves measured at different bond lengths and temperatures.

A reduced bond stress of about 5% was found at room temperature for the experiments performed with the short bond length, but the failure mode changed. When a short embedment length was used, shear failure was always observed, whereas splitting failure turned out to be the failure mechanism for the tests with a longer bond length ($3d_s$). At -165°C a lower bond resistance was found up to a stress level of approximately 25 N/mm^2 for the tests with a short bond length. At higher stress levels, approximately equal bond stress-slip relationships were observed for both embedment lengths. Note that the extent of the abrupt slip changes was greater for the short embedment length. A different behaviour was observed at -80°C.
In this case the test with the short embedment length attained the highest bond resistance. About 25% higher bond stresses were found in comparison with the test results of the long embedment length ($3d_s$). Hence no general conclusion can be drawn as to the effect of the embedment length on the bond stress-slip relationship, because bond length and temperature simultaneously affect the bond stress-slip curves in different ways.

Bar diameter

Bar diameters within the 8-32 mm range have no significant influence on bond resistance at room temperature in general. To investigate the effect of the bar diameter and the temperature on bond resistance, a number of pull-out experiments were performed with a 10 mm reinforcing bar. This bar had an f_R-value of 0.067 and the embedment length was 40 mm, i.e. kept to a minimum in relation to the maximum particle size of 16 mm. Nevertheless, the bond length was equal to four times the bar diameter, as opposed to a bond length of three times the bar diameter used in the main series for d_s=20 mm. The results measured at three different temperatures are shown in Fig. 5.16.

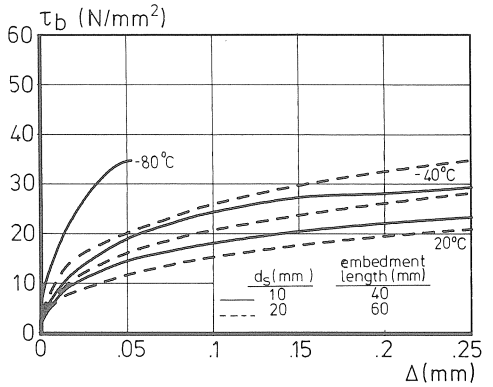

Fig. 5.16 Bond stress-slip curves measured for two bar diameters, namely 10 and 20 mm.

The bond resistance measured in the pull-out experiments for the 10 mm diameter bar turned out to be greater in comparison with the 20 mm diameter bars; see Fig. 5.16. However, this increase of approximately 10%, found at 20 and -40°C, was similar to that for longer embedment lengths, which phenomenon has been mentioned previously. Hence, no conclusion could be drawn regarding the bar diameter and the two above-mentioned temperatures. An increase of about 60% in bond resistance was found at -80°C for the 10 mm diameter bar and bond length of $4d_s$. A pull-out experiment performed at -80°C with an embedment length of $3d_s$ proved to have a lower bond resistance as compared with results found with a bond length of $2d_s$. Therefore, this proves that at -80°C a smaller bar diameter is associated with higher bond resistance.

Tempcore reinforcement

Six pull-out experiments were performed with 20 mm diameter "Tempcore" steel bars with an f_R value of about 0.069. The purpose of these experiments was more

particularly to compare the results that Vandewalle [32] obtained with the aid of a "beam test" with the pull-out results. Therefore different storage conditions and a different test age were used. The tests were performed at 28 days after storage of the specimens in a fog room at 99% r.h. and 20°C. Thus the results could not be directly compared with the other experimental results, because of the different curing conditions.
The effect of three different temperatures, namely 20, -80 and -165°C, on the bond stress-slip relationship was investigated by means of two experiments for each temperature. Some typical results are given in Fig. 5.17.

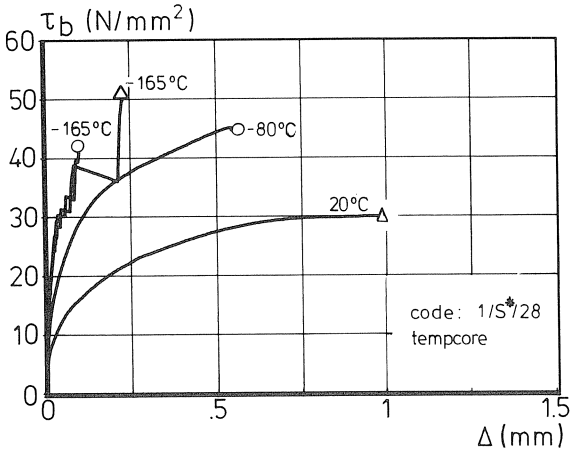

Fig. 5.17 Bond stress-slip relationships measured for three different temperatures and "Tempcore" steel.

Splitting failure turned out to be the main failure mechanism at +20 and -165°C. A similar failure mechanism was found for water-saturated pull-out experiments, as mentioned above in Section 5.6.1. Furthermore, the bond stress-slip relationship measured for "Tempcore" steel developed in a manner similar to that for the curve measured for "Krybar" steel.

5.6.4. Influence of thermal cycling on bond resistance

In order to investigate the influence of thermal cycling on the bond stress-slip relationship, a number of experiments were performed on pull-out specimens at room temperature after 0, 5 and 10 thermal cycles. Only specimens of sealed concrete at an age of 90 days were tested. The temperature was varied from +20 to -100°C at a cooling and heating rate of 1°C/min. After each series of thermal cycles two specimens were used of both mixes. The extent in which the bond stress was affected as a result of the cyclic temperature loading is shown in Fig. 5.18.

The bond strength and the bond stress measured at three different slip values is shown in the diagram. For mix 1 (w/c ratio: 0.40) no influence of the cyclic temperature loading on the bond stress was found. Only a minor decrease in bond strength was observed. However, for mix 2 (w/c ratio: 0.60) a reduction in bond stress was found after 5 and 10 temperature cycles. After 10 cycles this reduction amounts to 11, 7 and 4% at slip values of 0.025, 0.10 and 0.20 mm respectively. The greatest part of this reduction was observed after 5 temperature cycles. No effect on the bond strength was found.
The bond strength was determined for both mixes by the splitting failure mechanism. Furthermore, the ultimate slip value turned out to be smaller after thermal cycling for mix 1.

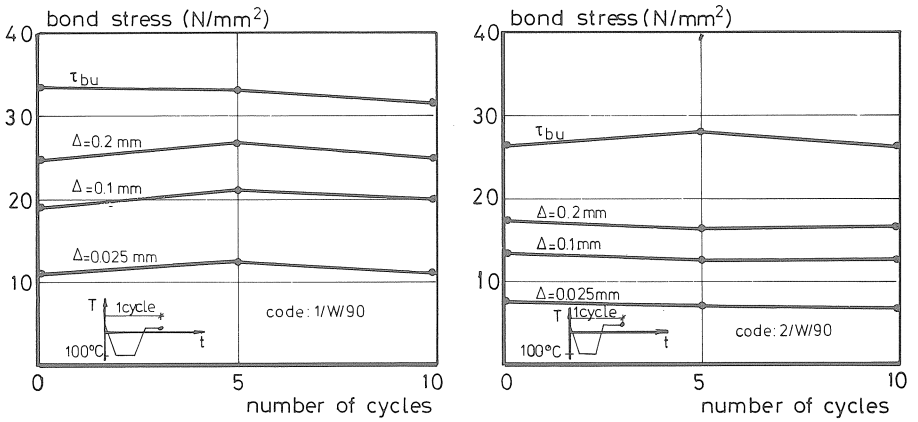

Fig. 5.18 Bond stress measured at different slip values versus the number of temperature cycles.

5.6.5. Results of the plain bars

Pull-out experiments were performed on 18 mm diameter plain bars embedded centrically over a length of 60 mm. The experiments were confined to sealed concrete at an age of 90 days for mix 1 only. The pull-out results exhibited a wide scatter, which phenomenon can be seen in Fig. 5.19 in which the scatter range for each temperature is represented by two curves.
All the experimentally determined curves were situated within this range of scatter. The bond stress-slip curves found at -40 and -80°C were similar in shape to the curve at 20°C. After reaching the maximum bond stress a descending branch was found for greater slip values. The bond stress decreased until it reached a constant value after a total slip of approximately 1.0 mm. This final constant bond stress value seems to be independent of the temperature. However, at -80°C much higher bond stress values were obtained even at slip values of 1.5 mm. A wide scatter range was found for pull-out tests at -120 and -165°C.

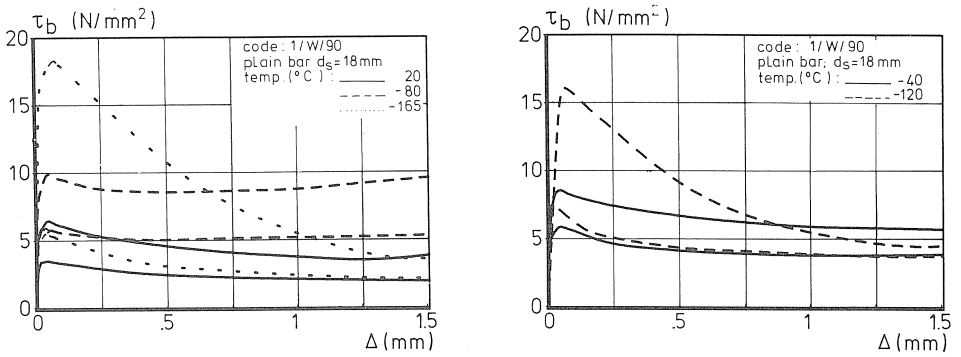

Fig. 5.19 Scatter range of the bond stress-slip curves at various temperatures.

Furthermore, a different shape in the curves was observed. After the maximum bond stress had been reached, a steeply descending branch was found.
On closer examination of the experimental results, it proved possible to make a distinction with respect to the bar surface roughness. The bar surface was given an R_a-value which equals the mean deviation of the surface profile from the average profile depth. Two R_a-values, of 2 and 9 μm respectively, were used in the experiments. Hardly any influence was found to exist at 20°C, while at -165°C an effect of R_a on the bond stress-slip curves was found.
For the plain bars with R_a = 2 μm an increase in bond strength of about 115% in comparison with the bond strength at 20°C was found at -80 and -165°C. The greater part of this increase (90%) was already observed at -40°C. An increase in bond strength of about 135 and 190% was found at -120 and -165°C respectively for the plain bars with a R_a = 9 μm. It should be noted, however, that at -165°C a very wide scatter in results was observed.

5.7. Experimental results of the tension members

This Section is devoted to the experimental results of the reinforced tension members with regard to crack width and crack spacing. First the sealed tension members are dealt with and, second, the water-saturated tension members. More detailed information about the experimental results is given in Romijn [73].

5.7.1. Observations of the sealed tension members

The reinforced tension members were subjected to direct tension at four temperatures, namely +20, -40, -80 and -165°C. The load at which cracking of the member started was found to increase markedly due to the increase in tensile strength at low temperature is shown in Figs. 5.20 and 5.21. At -80°C the greatest

increase in the cracking load was observed for both mixes, which is in accordance with the tensile splitting strength, see Section 5.2. Cracking occurred at a mean tensile stength of 0.75 f_{cspl} which is a mean value for all temperatures. Initially, greater crack widths were found at low temperatures in comparison with crack widths at room temperature for a certain stress at the crack particularly for mix 2. However, for mix 1 the crack width relative to the crack width at room temperature decreased at a higher stress level. Greater crack widths were observed after testing for mix 2 at -40 and -80°C respectively. It should be noted that in the latter case the number of cracks decreased at lower temperatures.

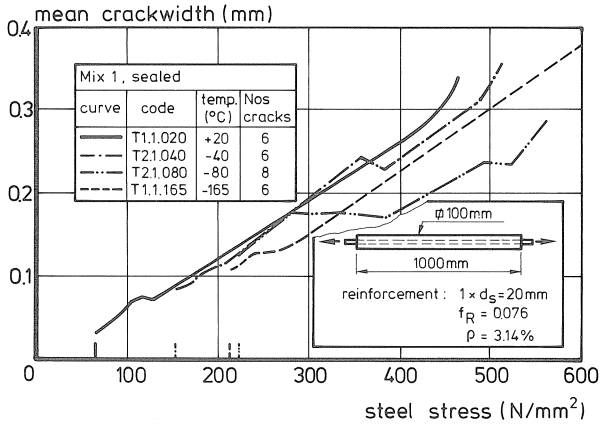

Fig. 5.20 Mean crack width versus steel stress for different temperatures and mix 1.

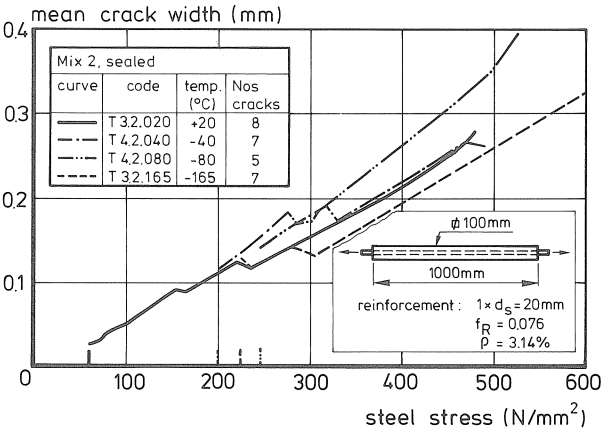

Fig. 5.21 Mean crack width versus steel stress for different temperatures and mix 2.

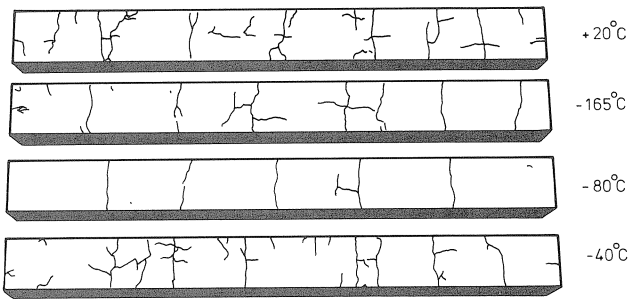

Fig. 5.22 Crack spacing for mix 2 at different temperatures.

Consequently, the crack width increased. It was observed that all the crack widths laid in the scatter range which usually occurred at room temperature. Furthermore, the number of cracks was greatest at -80 for mix 1 and smallest at -80°C for mix 2. For the other temperatures equal crack spacing for mix 1 and some lower crack spacing for mix 2 was observed, see Fig. 5.22.

No abrupt increase in crack width was observed at temperatures below -120°C, and this phenomenon was also found in the local bond stress-slip relationship for slip values greater than 0.1 mm. This phenomenon was reported by Scheuermann [33] based on his observations of tension members reinforced with 1.01 and 1.53% respectively, but was not found when 1.94% reinforcement was used. In the present experiments 3.14% reinforcement was used. Consequently, no abrupt change in crack width is to be expected when the reinforcement ratio is greater than 2%.

The maximum to mean crack width and minimum to mean crack width ratios were calculated from the measured values and assembled in Table 5.3. In general, values of about 1.3 and 0.7 were found for the relative w_{max} and w_{min} respectively. Notice, that only a few experiments were performed. Again an opposite effect was observed at -80°C for mix 1 and mix 2, because the highest and lowest values were found for the relative w_{max}.

Table 5.3 The relative maximum and minimum crack width for sealed concrete at a steel stress level of about 300 N/mm^2.

temperature (°C)	Mix 1 $\frac{w_{max}}{w_{mean}}$ (.)	Mix 1 $\frac{w_{min}}{w_{mean}}$ (.)	Mix 2 $\frac{w_{max}}{w_{mean}}$ (.)	Mix 2 $\frac{w_{min}}{w_{mean}}$ (.)
+ 20	1.2	0.8	1.4	0.6
- 40	1.3	0.8	-	-
- 80	1.6	0.3	1.1	0.8
-165	1.2	0.8	1.4	0.5

Steel stress-strain relationship

The experimentally found steel stress-strain curves are presented in Fig. 5.23 for mix 1 and mix 2 respectively. Notice, that the strain is in fact the mean strain of the tension member. An increase in the cracking load is clearly shown as mentioned above. Furthermore, a marked increase in the tension stiffening ($\Delta\varepsilon$) was observed at lower temperatures. The major part of the increase in tension stiffening occurred in the temperature range from 0 to -80°C. Tension stiffening was greatest at -80°C for mix 1 and at -165°C for mix 2. But only small differences in tension stiffening were found at -165°C and -80°C for mix 1.

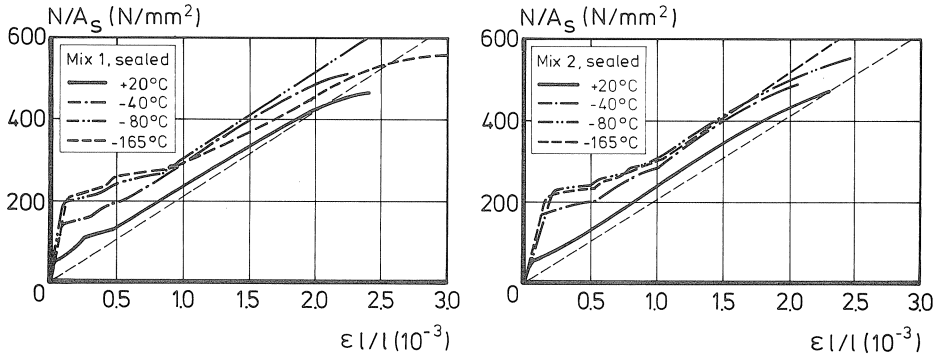

Fig. 5.23 Steel stress-strain relationship for sealed concrete.

5.7.2. Observations of the water-saturated tension members

Experiments were performed at -80 and -165°C for the water-saturated tension members. For mix 1 the measuring system failed at -80°C, and at -165°C two clusters of 3 cracks each occurred on three sides of the tension member. The measuring system was not able to measure the individual crack width. Therefore, the mean crack width for mix 1 at -165°C was calculated from a total of 6 and 8 cracks, see Fig. 5.24. The increase in tensile strength and the prestressing effect as a result of the thermal differences between the reinforcement and the concrete caused a marked increase in cracking load. Consequently, the steel stress after cracking increased strongly up to a stress level between 300 and 360 N/mm^2. The greatest increase was again observed at -80°C.

After the initiation of cracking at a stress level of about 330 N/mm^2 most of the cracks were generated at a stress level of about 400 N/mm^2 and the last crack was found at a steel stress of 540 N/mm^2. Thus, a similar behaviour like the tension member at room temperature was found. In the beginning of the formation of cracks a greater crack width was observed for mix 1, because only a few cracks exist at that time. Depending on the number of cracks a greater or smaller crack width was found for mix 1 compared to the crack width for mix 2 at higher stress levels.

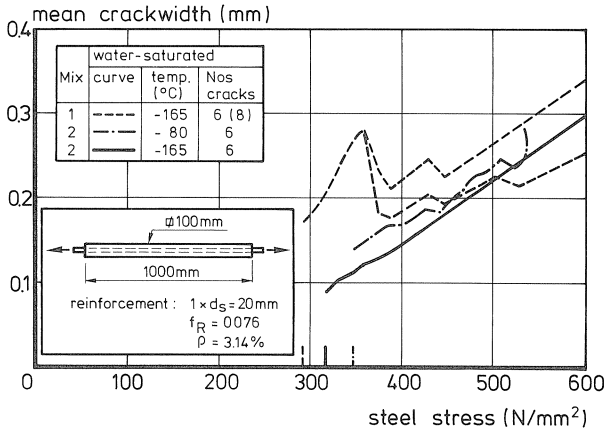

Fig. 5.24 Mean crack width versus steel stress for water-saturated concrete.

Steel stress-strain relationship

The steel stress-strain curves found are shown in Fig. 5.25, which includes the curve observed at 20°C for sealed concrete. For mix 1 only the curve observed at -165°C could be measured, because at -80°C the measuring system failed after the initiation of the first crack.
The cracking load and the tension stiffening increased even more than the sealed tension members showed, probably as a result of the "prestressing effect". For mix 2 the greatest increase in tension stiffening was observed.

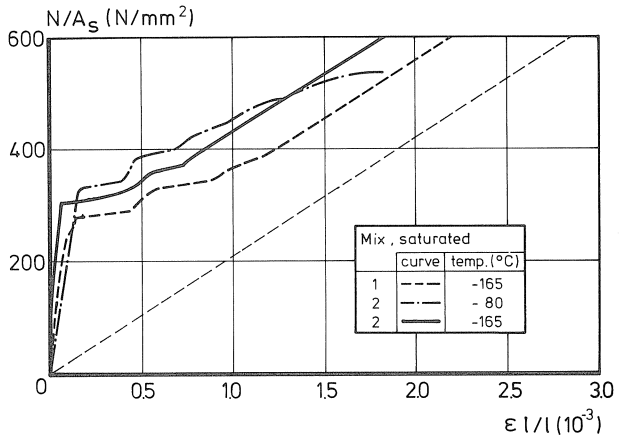

Fig. 5.25 Steel stress-strain relationship for water-saturated concrete.

Remark: The measuring system for crack width and the total elongation of the tension member appeared to be sensitive to shock loading caused by the abrupt cracking of the member, particularly at low temperatures and in the case of water-saturated concrete.

5.8. Concluding remarks

On the basis of the experimental results mentioned above, the following main conclusions can be drawn:

- The increase in the compressive strength and the tensile splitting strength of concrete with lowering of the temperature is primarily a function of the free moisture content and is independent of the grade and age of the concrete.

- The compressive strength increase due to low temperature can be predicted fairly accurately, whereas only a rough approximation is possible for the cryogenic tensile splitting strength, see formula (5.4).

- In general, the greater part of the increase in splitting strength occurs in the temperature range from 0 to -40°C, as contrasted with the increase in compressive strength, which mainly occurs from 0 to -120°C.

- In general, a maximum splitting strength is found at -80°C. At lower temperatures the cryogenic splitting strength remains constant, or even a small reduction is observed.

- Concrete tested at three different ages, namely 28, 90 and 365 days, possesses actual strengths which are about equal at -80 and -165°C, while a higher actual strength is found at -40°C for the oldest concrete. For the concrete with a low w/c ratio (0.40) equal splitting strength is found at -80 and -165°C for three different ages. However, for the concrete mix with a high w/c ratio (0.60) the actual cryogenic splitting strength showed a small decrease, which was greater for an age of 28, 90 and 365 days, in that order.

- The static modulus of elasticity is found to increase at low temperatures, but to a far lesser extent than the (cylinder) compressive strength. Despite this feature, an increase in the static modulus of 70 and 95% is observed for mix 1 and mix 2 respectively.

- After thermal cycling a reduction in strength of the sealed concrete is observed, which is most significant for the modulus of elasticity and least significant for the compressive strength. Note that for mix 1 (low w/c ratio) hardly any reduction in strength is observed, as opposed to the results of mix 2 (high w/c ratio), which exhibits losses in strength up to about 20% after 10 thermal cycles.

- An almost linear elastic stress-strain relationship is found for concrete tested at -165°C.

- Sealed and air-dry concrete exhibits thermal behaviour characterized by almost linear thermal deformation and perfect reversibility. This behaviour proved to be independent of the w/c ratio and the moisture content. However, water-saturated concrete turned out to undergo thermal expansion in the temperature range between -20 and -60°C. This expansion is clearly affected by the w/c ratio and increases for higher ratios. After reheating, irreversible strains are found at 20°C. These are greater for concrete with higher w/c ratios.

- Sealed concrete tested at 365 days exhibits thermal behaviour characterized by a slightly greater thermal strain in relation to the thermal strain observed at 90 days.

- Only small differences in thermal behaviour are found between the three types of steel referred to as Krybar, Krybar with 3.5% Ni, and Tempcore. This strain always remains in excess of the concrete strain and shows perfect reversibility.

- Only limited stresses will be introduced in a reinforced concrete member during cooling as a result of the small differences between the coefficients of thermal expansion of the reinforcement and of the air-dry or sealed concrete. However, considerable stresses may develop in reinforced water-saturated concrete.

- It has been proved that the bond stress increases when the temperature is lowered. The main part of this increase takes place in the temperature range from 20 to -120°C. For lower temperatures hardly any further increase in bond resistance is found.

- A typical phenomenon is observed at -165°C for all three sets of curing conditions, i.e. sealed, water-saturated and air-dry concrete, for slip values generally exceeding 0.02mm. For higher bond stresses these slip values increase instantaneously, and these abrupt changes in the slip rapidly become larger.

- For mix 1 in the case of water-saturated concrete splitting failure is nearly always found to be the governing failure mechanism, whereas for the other specimens at low temperatures shear failure or yielding of the reinforcement determines the bond strength.

- The cooling rate in the range from 1/3°C/min. to 3°C/min. turns out to have only a small influence on the bond stress-slip relationship. It has been proved that the embedment length and the temperature affect the bond stress-slip curves in different ways. Therefore no general conclusion can be drawn. Detailed information is given in Section 5.6.3.

- For the one year old concrete a less pronounced effect of the temperature on the bond stress-slip relationship is observed. Furthermore, a different failure mode, namely splitting failure, is observed at -165°C for concrete tested at an age of 365 days.

- At -80°C a 10mm diameter reinforcing bar turns out to have a bond resistance about 60% higher than a 20mm diameter bar, but at 20 and -40°C the bar diameter has no significant effect on the bond resistance.

- "Tempcore" steel exhibits a bond stress-slip relationship similar to that for "Krybar" steel.

- Thermal cycling proved to have no significant effect on the bond resistance for mix 1 even after 10 temperature cycles. For mix 2 a reduction in bond resistance is found. This reduction becomes smaller when determined at greater slip values and varies from 11 to 4% for slip values from 0.025 to 0.20 mm.

- It is found that the bond strength of plain bars increases by about 115% at -80 and -165°C in comparison with the bond strength found at 20°C. The main part of this increase takes place in the temperature range from +20 to -40°C, because at -40°C an increase of 90% is observed. The surface roughness very greatly affects the bond resistance at low temperatures only. An increase of 190% in bond strength is found for R_a = 9 μm as against an increase of 115% for R_a = 2μm . However, the bond stress measured at a slip value of 1.5 mm turns out to be independent of the temperature.

- The load at which cracking started in a concrete element subjected to direct tension was found to increase markedly, particularly for water-saturated concrete. The highest cracking load is found at -80°C.

- Always smaller crack widths are found at low temperatures in comparison with crack widths found at room temperature for the mix with the low w/c ratio (0.40).

- Tension stiffening increases at lower temperatures, and the major part of this increase occurs in the temperature range from 0 to -80°C. The greatest tension stiffening is observed for the water-saturated concrete tension members.

6. ANALYSIS OF THE RESULTS AND VERIFICATION OF THE MODELS

6.1. Introduction

The experimentally found bond stress slip curves are predicted analytically by means of a regression analysis. In order to use the valid slip values of the determined bond stress-slip curves for practical circumstances, i.e. a smaller concrete cover than in

the actual experiment, the bond strength is predicted as a function of the concrete cover with the aid of the model described in Section 3.3. The magnitude of the ultimate bond stress of deformed bars depends on the failure mode, i.e. splitting failure or shear failure. Shear failure is predicted as a linear function of the actual compressive strength based on the experimental results.
The reinforced tension member model is used to predict crack width and crack spacing and the results are compared with the experimentally found values.

6.2. Bond stress-slip relationship

6.2.1. Analytical prediction of the bond stress slip curve

An attempt was made to predict the local bond stress-slip curves analytically. Therefore the curves were approximated by the expression:

$$\tau_b(T) = a(T)\ \Delta^{b(T)} \qquad N/mm^2 \qquad (6.1)$$

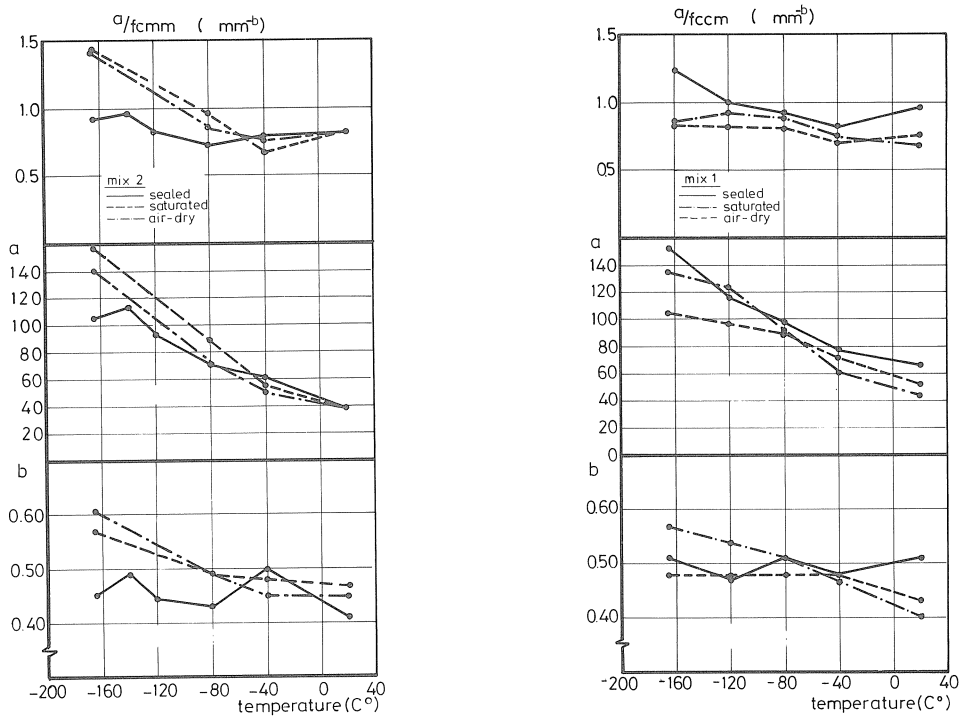

Fig. 6.1 Factors of the bond stress-slip relationship for both mixes versus temperature.

Because expression (6.1) increases continuously and therefore comprises no maximum the slip value is limited to 0.25 mm. In spite of this feature, it is possible to predict realistic crack widths up to 0.5 mm. Typical factors of the bond stress-slip relationships are shown in Fig. 6.1.
No constant value for the exponent b could be found. Particularly, the values observed at -165°C deviate from the other values of the exponent. We have to bear in mind, however, the typical bond stress-strain curves found at -165°C; not only did abrupt changes in slip occur, but the ultimate slip was usually also less than 0.25 mm. It is clear that both features could, along with other factors, affect the exponent b. Nevertheless, it proved possible to find a single approximate and generally applicable value, valid for the whole temperature range, for the sealed and water-saturated specimens and for the sealed specimens for mix 1 and mix 2 respectively.
Some relation seems to exist between the bond stress and the actual compressive strength, at least for the air-dry and the water-saturated concrete for mix 1 and the sealed concrete for mix 2, which feature can be seen in Fig. 6.1, represented by the ratio $a(T)/f_{ccm}(T)$. This ratio varied between 0.7 and 1.4 and in general no constant value was obtained. However, for application in arctic areas (-40°C) a mean value of 0.75 could be adopted for this ratio, which approximation gives reasonable crack widths, Van der Veen and Reinhardt [74,75].

6.2.2. Comparison of the bond stress-slip relationship with other research

Comparable pull-out experiments were performed by Scheuermann [33]. The researcher derived a formula to predict the bond stress-slip relationship, which can be described as follows:

$$\tau_b(T) = f_{ccm}(T)\, f_1(T)\, \Delta^{b_o f_2(T)} \qquad N/mm^2 \qquad (6.2)$$

in which

$$f_1(T) = 0.71 - 0.49\,(\frac{T - 20}{190}) \qquad (6.2a)$$

$$b_o f_2(T) = 0.46\,\{1 - 0.39\,(\frac{T - 20}{190})\} \qquad (6.2b)$$

Expression 6.2 was converted to the cube compressive strength using the relation $1.1\, f_{cm}(T) = f_{ccm}(T)$ between the cylindrical and the cubic compressive strength as was found in Section 5.2. Furthermore, typical factors mentioned by Scheuermann [33] ($C_1 = 0.06$, $C_2 = 9.64$ and $f_R = 0.076$) are used.

If the same prediction as mentioned above is used for comparison purposes, the following expressions are found for mix 1 and mix 2:

$$f_1(T) = 0.73 - 0.39\,(\frac{T - 20}{190}) \qquad (6.3a)$$

$$b_o f_2(T) = 0.45 \left\{1 - 0.19 \left(\frac{T - 20}{190}\right)\right\} \qquad (6.3b)$$

It should be noted that only a poor prediction is found for $f_1(T)$. On the other hand $b_o f_2(T)$ fits rather closely. The predictions are more or less in accordance. However, a stronger influence of the temperature was found by Scheuermann at lower temperatures. This feature could be the result of the high water/cement ratio of 0.80 and the sealed curing condition which were used in the major part of the experiments. A closer examination of our results also reveals this tendency: a stronger influence of the temperature is found for mix 2 with a w/c ratio 0.60 as represented in the formulae 6.4 and 6.5 and in Fig. 6.2. Formulae 6.4 and 6.5 give the predictions for mix 1 and mix 2 respectively.

$$f_1(T) = 0.74 - 0.33 \left(\frac{T - 20}{190}\right) \qquad \text{mix 1} \qquad (6.4a)$$

$$b_o f_2(T) = 0.45 \left\{1 - 0.16 \left(\frac{T - 20}{190}\right)\right\} \qquad \text{mix 1} \qquad (6.4b)$$

$$f_1(T) = 0.72 - 0.45 \left(\frac{T - 20}{190}\right) \qquad \text{mix 2} \qquad (6.5a)$$

$$b_o f_2(T) = 0.44 \left\{1 - 0.22 \left(\frac{T - 20}{190}\right)\right\} \qquad \text{mix 2} \qquad (6.5b)$$

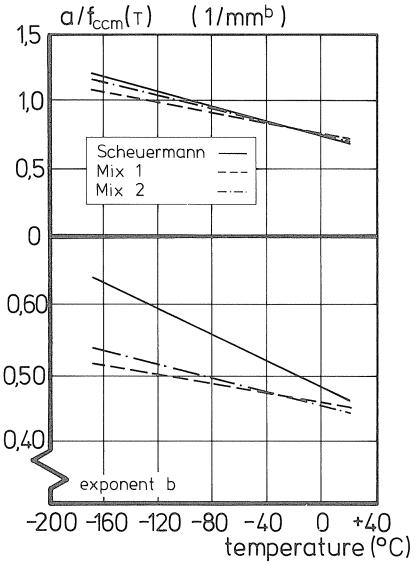

Fig. 6.2 Comparison of the prediction for the bond stress-slip relationship.

It should be mentioned, however, that there is one main difference between the pull-out experiments because in Scheuermann's experiment the loading direction coincides with the direction of casting. In our experiments the pull acts in the opposite direction to the casting direction. Consequently, a higher bond resistance is

expected, at least at room temperature. Indeed for sealed concrete a 40 and 20% higher bond resistance for mix 1 and mix 2 respectively is found at room temperature, see Fig. 6.1. As a result of the poor fit of $f_1(T)$, an underestimation at room temperature is predicted. Nevertheless, the differences in bond resistance vanish at lower temperatures. Furthermore, the exponent b proved to be rather independent of the pull-direction to the casting direction.
The bond stress-slip results obtained with the aid of the beam test by Vandewalle [32] and the pull-out results, see Section 5.6.3, are shown in Fig. 6.3. It is clearly shown that for crack widths greater than 0.1 mm higher bond stresses are found with the aid of the pull-out test. However, the same tendency was found and a reasonable agreement is obtained for small slip values. One should realize that Vandewalle used a practical concrete cover of 1.5 d_s and stirrups as against the large concrete cover of 4.5 d_s in the pull-out experiments.

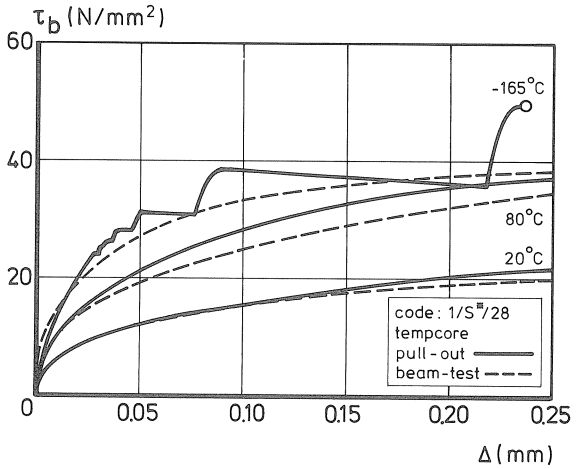

Fig. 6.3 Comparison of the bond stress-slip curves.

The effect of the concrete cover on the bond stress-slip curve was investigated by Scheuermann [33]. Scheuermann performed tests on pull-out specimens with a concrete cover of 2 d_s and with or without stirrups. Only small differences in the bond stress-slip curve were found for small slip values ($\Delta < 0.3$ mm), which is in accordance with the results mentioned above. However, the failure mode was strongly affected by the concrete cover and the amount of stirrup reinforcement applied. Specimens without stirrup reinforcement always failed due to splitting of the concrete cover. When 6 mm diameter stirrup reinforcement ($A_{ss} = 0.15\ A_s$) was used, splitting failure only occurred at temperatures below -100°C and where a 10 mm diameter stirrup ($A_{ss} = 0.40\ A_s$) was used, splitting failure was always prevented. Although the concrete cover split, the stirrup was able to prevent splitting failure and failure occurred due to slip-through of the bar (shear failure). This phenomenon of "shear failure" is dealt with in the next Section.

6.3. Shear failure mode

Shear failure was observed mostly for mix 2 and only at -40 and -80°C. For lower temperatures no failure of the concrete occurred, because the yield strength of the reinforcement was reached. Nevertheless, a relation between the actual compressive strength and the ultimate bond stress τ_{bs} is derived, and this relation is assumed to be valid for the whole temperature range and both mixes. The ratios experimentally found are collected in Fig. 6.4 and a mean ratio of 0.51 is calculated for the bond strength to the actual cubic compressive strength.

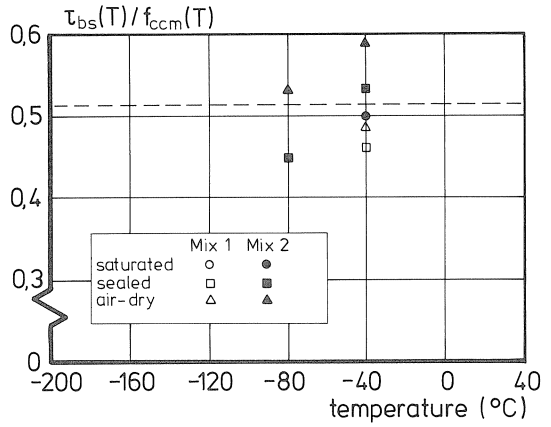

Fig. 6.4 Relationship between the bond strength determined by shear failure and the actual compressive strength.

Thus the following relation holds true:

$$\tau_{bs}(T) = 0.51\ f_{ccm}(T) \qquad N/mm^2 \qquad (6.6)$$

A similar relationship was derived by Scheuermann [33]. Based on his pull-out experiments expression 6.7 was calculated.

$$\tau_{bs}(T) = 0.47\ f_{cm}(T) \qquad N/mm^2 \qquad (6.7)$$

In order to compare both expressions the cylindrical strength has been converted to the cubic strength with the aid of formulae 5.2 and 5.3, which gives expression 6.8.

$$\tau_{bs}(T) = 0.43\ f_{ccm}(T) \qquad N/mm^2 \qquad (6.8)$$

It appeared from expressions 6.6 and 6.8 that Scheuermann [33] found a 12% smaller bond resistance before shear failure occurred. However, Scheuermann used a smaller bar diameter (16 mm) and the load direction of the pull-out specimen was parallel to the settling direction of the concrete.

Hungspreug [76] mentioned that if bond failure is caused by shearing out of a cylindrical surface of the concrete, the bond strength depends on the bar diameter. This feature was found experimentally by Lutz et al. [45] who observed a higher bond resistance for a greater bar diameter. However, the differences in bond resistance were only small.

6.4. Verification of the splitting failure model

6.4.1. Verification of the model at various temperatures

The experimentally found bond stresses at which level splitting failure occurred are compared with the predicted values with the aid of formula 3.50 and n = 1. Thus the bond stress at the occurrence of cracking is predicted. First, the experimental results found at room temperature are assembled in Table 6.1. It is found that the ultimate load τ_{bu} is approximately 15% higher than the "cracking" load τ_{br}, which is in close agreement with the experimental results of Schmidt-Thrö [65] and Tepfers [53]. When 3 cracks are assumed (n = 3) in formula 3.50 an increase in τ_{br} of about 14% is calculated which is again in close agreement with the experimental results.

Table 6.1 Bond stress at splitting failure τ_{bu} and the occurrence of cracking τ_{br}

	Mix 1			Mix 2		
curing conditions	τ_{bu} (f_{ctm})	τ_{br} (f_{ctm})	$\frac{\tau_{bu}}{\tau_{br}}$ (.)	τ_{bu} (f_{ctm})	τ_{br} (f_{ctm})	$\frac{\tau_{bu}}{\tau_{br}}$ (.)
saturated	8.56	7.57	1.13	8.35	7.71	1.08
sealed	8.84	7.57	1.14	8.33	7.68	1.08
air-dry	9.28	7.55	1.23	8.98	7.37	1.22

τ_{br} calculated with formula 3.50 and $\alpha = 35°$; n = 1
f_{ctm} = f_{csp1}

Splitting failure at low temperatures was only observed for mix 1. Thus only the results of mix 1 are assembled in Fig. 6.5.
As can be seen from Fig. 6.5 the lowest relative crack resistance is found experimentally and theoretically at -40 and -80°C. However, the experimental values are much more pronounced than the predicted values. The difference between the cracking load τ_{br} and the ultimate load τ_{bu} at room temperature has already been discussed above. The predicted values τ_{br} at -40 and -80°C are more or less the same as the experimentally found ultimate load, which is surprising because lower values for the prediction are expected. The same phenomenon was found experimentally by Scheuermann [33] who measured the load at which level

longitudinal splitting cracks occurred and the failure load. He observed that in the case of a pull-out test with a concrete cover of 2 d_s at -40 and -80°C the cracking load τ_{br} equals almost the ultimate load τ_{bu}. For all the other temperatures an increase of about 10% in load after cracking was possible.

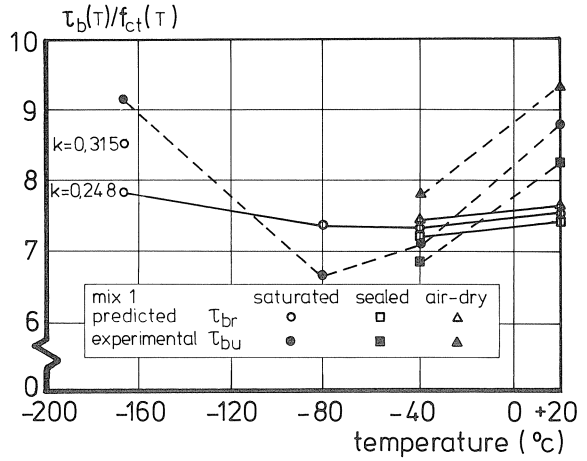

Fig. 6.5 Relative bond stress at which splitting failure was observed and the predicted values at which splitting cracks start.

Only at -165°C is more information available about the softening of the concrete. The factor k increases to 0.315, see Section 3.3.5, and when the cracking resistance is again calculated, an increase of about 8% is found, see Fig. 6.5 ($\tau_{br} = 8.53\ f_{ctm}$). Furthermore, the increase of the load from $\tau_{br}(n = 1)$ to $\tau_{bu}(n = 3)$ becomes less; it decreases from 14 to 11%.

Another feature was also found as a result of a higher k-value. The crack depth increases by about 10 per cent, i.e. less concrete remains elastic. However, more information about the softening behaviour of concrete at low temperatures is necessary to draw general conclusions.

To be on the safe side the best way to predict the failure load is to calculate the cracking load (n = 1) instead. Then a behaviour similar to the experimentally found ultimate load is obtained, but less pronounced.

Failure modes are predicted and compared with the experimentally found modes. The results are collected in Table 6.2. Many failure modes at low temperatures are confined to the yield strength of the reinforcement. Thus, no failure of the concrete was able to occur. All the actual failure modes of the concrete are predicted correctly. If it is assumed that the bond stress level could be raised until concrete failure occurred, then splitting failure is predicted in all cases for the highest concrete grade (mix 1), and shear failure for the lowest concrete grade (mix 2). This feature is in accordance with the observations of Scheuermann [33] who found only shear failure and used a low concrete grade (w/c ratio = 0.80).

Table 6.2 Failure modes for both concrete mixes at an age of 90 days

	Mix 1						Mix 2					
	prediction			experimental			prediction			experimental		
Temp. (°C)	τ_{br}/f_{ct}	τ_{bs}/f_{ct}	failure mode	τ_{bu}/f_{ct}	τ_{bu} N/mm^2	failure mode	τ_{br}/f_{ct}	τ_{bs}/f_{ct}	failure mode	τ_{bu}/f_{ct}	τ_{bu} N/mm^2	failure mode
sealed												
+20	7.57	9.86	split	8.84	33.6	split	7.68	7.93	split	8.30	24.3	split
-40	7.23	7.60	split	6.89	41.6	yi/sp	7.07	5.50	shear	5.65	39.8	shear
-80	7.10	7.28	split*	5.48	43.7	yield	7.01	5.66	shear	4.89	43.6	shear
-120	7.28	8.24	split*	6.30	46.2	yield	7.17	6.67	shear*	5.05	44.3	yield
-140	-	-	-	-	-	-	7.20	6.87	shear*	5.27	47.0	yield
-165	7.48	9.48	split*	7.36	49.4	yield	7.35	7.21	shear*	5.95	49.3	yield
saturated												
+20	7.57	9.36	split	8.56	42.0	split	7.71	8.04	split	8.14	25.0	split
-40	7.34	9.36	split	7.18	40.4	split	7.11	5.52	shear	5.43	40.3	shear
-80	7.36	9.39	split	6.71	42.4	split	7.30	6.17	shear*	5.76	44.3	yield
-165	7.87	13.76	split	9.07	43.0	split	7.41	7.21	shear*	5.81	45.7	yield
air-dry												
+20	7.64	9.56	split	9.28	30.8	split	7.63	7.64	split	9.03	27.1	split
-40	7.38	8.16	split	7.79	40.3	split	7.25	6.07	shear	7.21	39.2	shear
-80	7.30	8.20	split*	6.74	43.2	yield	7.15	6.04	shear*	6.15	44.1	yield
-120	7.34	8.24	split*	6.56	45.8	yield	-	-	-	-	-	-
-165	7.55	9.35	split*	7.39	46.2	yield	7.37	7.97	split*	7.64	49.8	yield

Note f_{ct} = $f_{c,spl}$

τ_{br} calculated with formula 3.50; (n = 1); $\alpha = 35°$

τ_{bs} calculated with formula 6.6

* it is assumed that the bond stress level could be raised up to concrete failure.

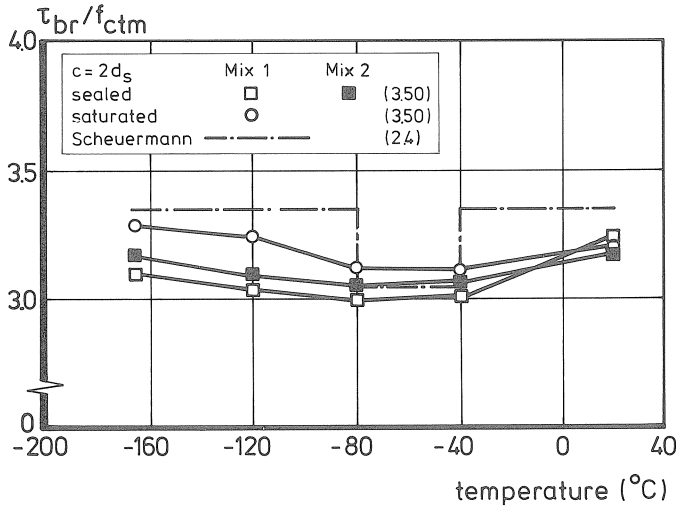

Fig. 6.6 The calculated (relative) splitting failure load for a concrete cover $c = 2\,d_s$.

Scheuermann [33] performed pull-out experiments with a concrete cover of 2 d_s and derived a formula to predict the splitting failure load, see formula 2.4. In the present experimental study only pull-out experiments with a large concrete cover c = 4.5 d_s were carried out. The results of the derived theoretical formula 3.50 (n = 1, tan α = 40°) are compared with the results of Scheuermann's formula for a practical concrete cover c = 2 d_s. The theoretical calculated results are assembled in Fig. 6.6. To keep the diagram clear the results of the water-saturated specimens of mix 2 have been left out, because these revealed the same tendency as the results of the sealed specimens. As mentioned previously, the lowest bond strength ratio τ_{br}/f_{ctm} was found at -40 and -80°C, which results were in close agreement with the prediction of Scheuermann. Higher bond strength ratios were calculated for the other temperatures which were slightly smaller than Scheuermann's ratios. Thus a reasonable agreement is obtained for small concrete covers with formula 3.50.

6.4.2. Application of the model

The predicted bond stress-slip relationships are shown in Fig. 6.7 for mix 1 and mix 2 respectively. At -120°C and lower temperatures the predictions are not valid for slip values larger than 0.1 mm, because at these low temperatures an abrupt and large change in slip occurred at this slip value.
The occurrence of longitudinal (splitting) cracks is calculated for a concrete cover c = 2 d_s with formula (3.50), assuming tan α = 40° and one crack (n = 1). It is clearly shown in Fig. 6.7 that in general cracking starts at slip values of at most 0.05 and 0.1 mm for mix 1 and mix 2 respectively. The failure load is about 10 to 20% higher (except for -40 and -80°C, as discussed previously). Consequently, if no transverse reinforcement is applied only small slip values (crack widths) are allowed.

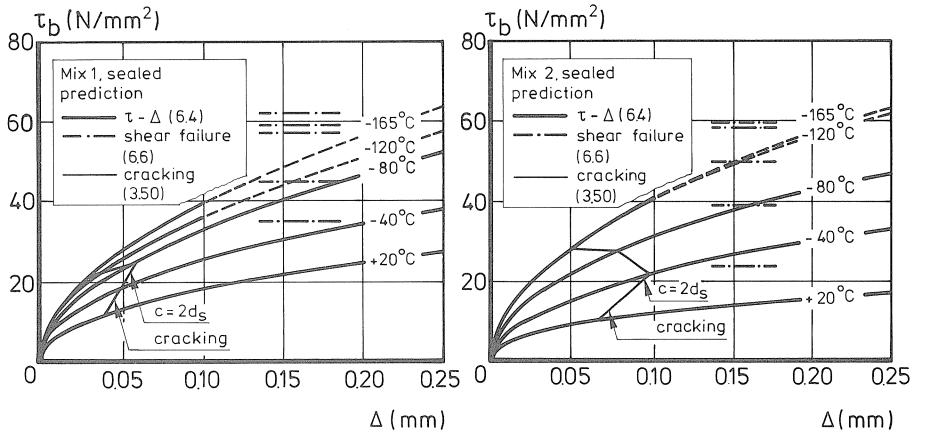

Fig. 6.7 Predicted bond stress-slip curves and the occurrence of cracking for a concrete cover c = 2 d_s.

Therefore it is necessary to use transverse reinforcement (stirrups) in order to use the bond stress-slip curves up to 0.25 mm at 20, -40 and -80°C and up to 0.10 mm at -120 and -165°C, particularly for high concrete grades. It is possible to raise the failure load by using sufficient transverse reinforcement until another failure mode (shear failure) is reached, see Fig. 6.7. The shear failure mode gives the highest possible bond strength.

6.5. Verification of the reinforced tension member model

This Section is devoted to the reinforced tension member model which was discussed in Section 3.2.2. First the sealed tension members are calculated and second, the water-saturated members are calculated and analyzed. It should be noted that no stirrups were used in the reinforced tension member, because only one bar was embedded.

6.5.1. Analysis of the sealed tension members

The mean crack width and mean crack spacing are calculated using the bond stress-slip relationship which was approximated in Section 6.2.1. To enable a distinction to be made in this relationship between the sealed specimens and water-saturated specimens, the factors shown in Fig. 6.1 are used.

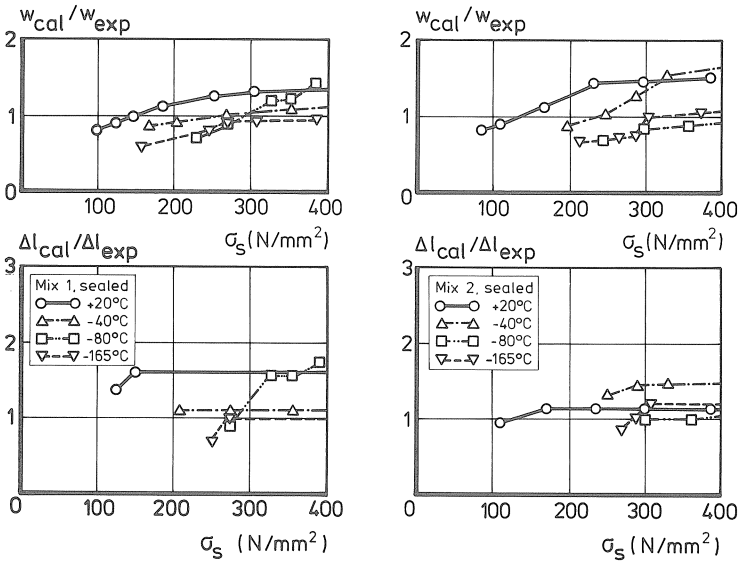

Fig. 6.8 Comparison of the calculated and experimentally found crack width and crack spacing.

The relative crack width ratio w_{cal}/w_{exp} and the relative crack distance ratio $\Delta\ell_{cal}/\Delta\ell_{exp}$ were calculated for a number of steel stresses in the case of a fully developed crack pattern and the results are shown in Fig. 6.8. Thus formulae (3.26) and (3.8) were used for the calculated crack width (w_{cal}) and crack spacing ($\Delta\ell_{cal} = 1.5\ \ell_{st}$). The tensile strength was kept constant from the initiation of the first crack until a fully developed crack pattern ($\sigma_{cr-1} = \sigma_{cr-2} = 0.75\ f_{ctm}$).
It turned out that at low temperatures the predicted crack widths mostly underestimate the actual ones for steel stresses from about 100 to 300 N/mm^2. For higher steel stresses too high a value was predicted at -40°C for both mixes. The ratio w_{cal}/w_{exp} increases for higher steel stresses, because the predicted crack distance ($\Delta\ell_{cal}$) was too high in general. However, reasonable crack widths were predicted for practical steel stresses around 300 N/mm^2. If the crack width is calculated at a steel stress of 300 N/mm^2 a smaller crack width was always calculated for lower temperatures for mix 1. For mix 2 the greatest crack width was calculated at -40°C, which feature was also experimentally found, see Fig. 5.21. Some typical results are given in Table 6.3.

It appears that the smallest crack distance was calculated at -165°C for both mixes and the greatest crack distance at -40°C for mix 2.
An equal and greatest crack distance was found experimentally at -40°C for mix 1 and mix 2 respectively, see Figs. 5.20 and 5.21. Fewer differences in crack distance were calculated for mix 1, which was also observed experimentally. The calculated steel stress-strain curves are presented in Fig. 6.9. The same characteristics were found when these curves were compared with the experimentally found curves, see Fig. 5.23. Thus, the major part of the increase in tension stiffening again occurred in the temperature range from 0 to -80°C. The highest tension stiffening was observed and calculated at -80°C for mix 1. Furthermore, only small differences in tension stiffening were calculated at low temperatures for mix 2.

Table 6.3 Results of the tension member model.

Temp. (°C)	$\sigma_{s,cr}$ (N/mm^2)	w_{cr} (mm)	$w_x(\sigma_s = 300$ N/mm^2) (mm)	$\Delta\ell$ (mm)	ε_{max} (10^{-6})	$\Delta\varepsilon$ (10^{-6})
Mix 1						
+20	101	0.04	0.25	231	198	281
-40	166	0.06	0.20	223	326	464
-80	216	0.08	0.17	233	400	629
-165	176	0.05	0.14	166	314	525
Mix 2						
+20	83	0.03	0.22	191	186	211
-40	193	0.09	0.24	295	367	551
-80	240	0.09	0.15	215	485	655
-165	218	0.07	0.14	184	415	621

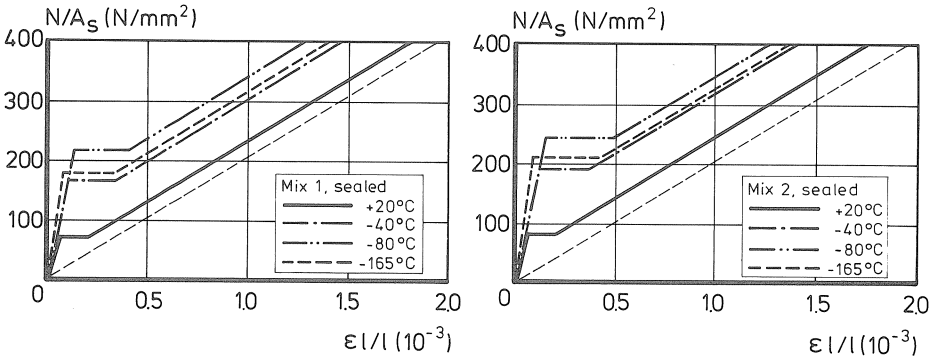

Fig. 6.9 Predicted steel stress-strain relationship for sealed concrete.

6.5.2. Analysis of the water-saturated tension members

In order to calculate the mean crack width and the mean crack spacing the water-saturated tension members are considered to be prestressed due to the thermal differences between the reinforcement and the concrete. This calculation method has been dealt with in Section 3.2.3. An important factor is the jump in steel stress $\Delta\sigma_{s,cr}$ after cracking of the tension member. This steel stress jump and other related values are collected in Table 6.4.

Table 6.4 Results of the tension model for water-saturated concrete.

Mix	Temp. (°)	$\varepsilon_s-\varepsilon_c$ 10^{-3}	σ_{cT} N/mm²	σ_{sT} N/mm²	$\Delta\sigma_{s,cr}$ N/mm²	$\Delta\ell$ mm	$\frac{\Delta\ell(T)}{\Delta\ell(20^\circ C)}$ (.)	w_x* mm
1	- 80	0.27	-1.58	50.3	177.0	190	2.07	0.163
1	-165	0.31	-1.85	59.0	130.8	176	1.91	0.177
2	- 80	0.66	-3.89	123.8	220.6	247	1.94	0.176
2	-165	0.67	-4.01	127.6	221.4	217	1.71	0.143

* σ_s = 300 N/mm²

The differences in thermal strain ($\varepsilon_s-\varepsilon_c$) can be calculated from Fig. 5.8. The stresses, namely σ_{cT}, σ_{sT} and $\Delta\sigma_{s,cr}$ are calculated with formulae (2.6), (2.7) and (3.30).

The smallest crack distance is calculated for mix 1, which feature was found experimentally because 8 and 6 cracks were found for mix 1 and mix 2 respectively. Since no experiments were performed at room temperature, the crack distance at room temperature was calculated and compared with the crack distance determined at the other temperatures. A substantial increase in crack distance was calculated as

expressed by the ratio $\Delta\ell(T)/\Delta\ell(20°C)$, see Table 6.4. Thus, a larger crack spacing at low temperatures is calculated for the water-saturated tension member as opposed to the smaller crack spacing for the sealed tension members. This conclusion is in agreement with the ratios found for $\Delta\ell(T)/\Delta\ell(20°C)$, which are collected in Table 2.1. They vary between 1.4 and 1.8 for the water-saturated specimens, and are 0.9 for the sealed specimens. For the actual experiments a mean value of 1.9 was calculated for the ratio $\Delta\ell(T)/\Delta\ell(20°C)$, which is in agreement with the ratios found in the literature. However, as discussed previously in Section 3.2.3, it is not the prestress itself which caused the greater crack distance. The main cause is the changing bond stress-slip relationship and the increase in tensile strength at low temperatures.
The relative crack width ratio w_{cal}/w_{exp} is calculated for a number of steel stresses for a fully developed crack pattern and the results are shown in Fig. 6.10.

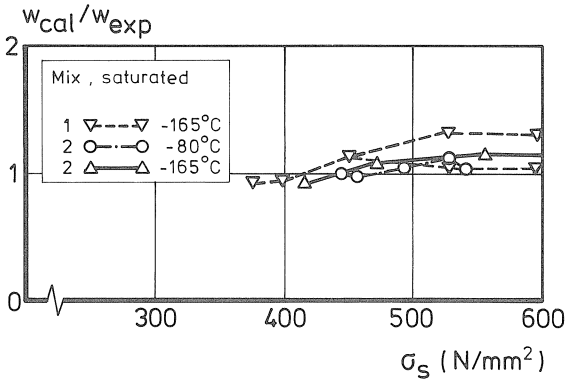

Fig. 6.10 Comparison of the calculated and experimentally found crack width for water-saturated concrete.

Reasonably predicted crack widths were found for mix 2 and too high crack widths were predicted for mix 1 for steel stresses above 400 N/mm^2. However, this stress level is far above the practical range from 300 to 350 N/mm^2. When the crack width was calculated at a steel stress of 300 N/mm^2, values of 0.10 and 0.15 mm were found at room temperature for mix 1 and mix 2 respectively. At low temperatures a greater crack width is calculated for mix 1 and a greater and smaller crack width is calculated for mix 2 at -80 and -165°C respectively. These calculated crack widths are in close agreement with the experimentally found crack widths, see Fig. 5.24, and the same tendency in crack width is observed.
The calculated steel stress-strain curves are presented in Fig. 6.11. First, the diagrams are calculated without the "prestress effect". Second, the steel stress σ_{sT}, due to the thermal differences between the reinforcement and the concrete ("prestress effect"), is added to $\Delta\sigma_{s,cr}$, which gives the actual diagrams shown on the right in Fig. 6.11. It is clearly shown that σ_{sT} caused a strong increase in tension stiffening ($\Delta\varepsilon$), which is the most pronounced for the greatest value of σ_{sT}.

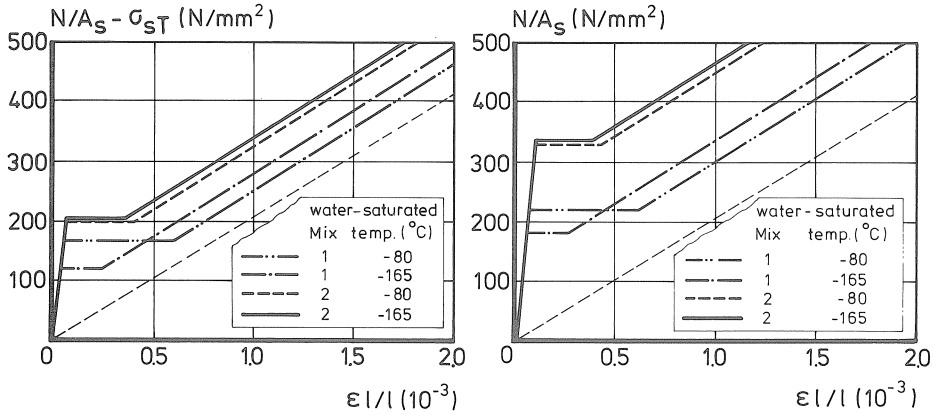

Fig. 6.11 Steel stress-strain curves without and with the "prestress effect".

Consequently, the greatest tension stiffening is calculated for mix 2, which feature was also experimentally found, see Fig. 5.25.
That water-saturated reinforced tension members have a greater tension stiffening than the sealed members was found experimentally as well. Thus, a fairly good agreement was found between the experimental results and the predicted results.

6.6. Discussion and concluding remarks

It has been proven that realistic crack widths can be calculated as a function of temperature using the tension member model. Though no stirrups were applied in the actual experiments it is strongly advised to use transverse reinforcement, particularly at low temperatures. Nevertheless, the crack width was predicted fairly well, but the majority of the calculated mean crack widths was smaller than 0.2 mm. The tension member model is capable of predicting realistic crack widths even when thermal differences occur between the reinforcement and the concrete. In that case the tension member should be considered as a prestressed member. The mean crack spacing decreases slightly at -165°C for sealed concrete. However, a strong increase in crack spacing occurred for water-saturated concrete at lower temperatures, mainly caused by the changing bond stress-slip relationship and tensile strength and not due to the "prestressing effect". Furthermore, the tension stiffening increases at lower temperatures, but it increases very strongly as a result of the "prestressing effect".

On the basis of the results set out above, the following main conclusions can be drawn:

- The bond stress-slip relationships are predicted analytically and a reasonable agreement with the results obtained from other research is found.

- The bond strength limited by the shear failure mode is expressed as a bond strength to compressive strength ratio and this ratio is found experimentally.
- Splitting failure can be predicted theoretically with the model and the typical phenomenon (a lower bond strength to tensile strength ratio found at -40 and -80°C) is predicted as well.
- Crack width can be calculated as a function of temperature with the aid of the tension member model. It can also take into account the "prestressing effect" in the case of water-saturated concrete.
- It is necessary to apply transverse reinforcement at low temperatures to avoid splitting failure and thus extend the valid slip values of the predicted bond stress-slip curves.
- Based on the local bond stress-slip curves the maximum crack width is limited to 0.2 mm at -120 and -165°C, and to 0.5 mm at the other (higher) temperatures.

7. CONCLUSIONS AND OUTLOOK

The aim of the present study was to prove that the crack width and the crack spacing can be predicted with the aid of the classical bond stress-slip theory. An engineering model of the reinforced tension member was further developed and formulae were derived to predict the crack width and crack spacing. This classical bond stress-slip theory is based on the local bond stress-slip relationship, which was determined experimentally as a function of temperature and curing conditions. A model was derived to predict the ultimate bond stress in cases where splitting failure occurred as a function of concrete cover and temperature. The lowest bond strength relative to the actual splitting strength is predicted at -40 and -80°C. This phenomenon was in agreement with the experimental results found in the literature. For a practical cover ($c = 2d_s$) the occurrence of splitting cracks was already predicted at small crack widths (0.1 to 0.2 mm) particularly for high concrete grades and the lowest temperature. Consequently, transverse reinforcement (A_{ss}) is necessary to allow greater crack widths. The failure mode changes from splitting failure to shear failure, if the transverse reinforcement amounts at least $A_{ss} = 0.15\ A_s$ for temperatures down to -100°C and $A_{ss} = 0.4\ A_s$ for lower temperatures, Scheuermann [33]. The bond strength determined by shear failure is expressed as a linear function of the actual compressive strength which was based on the results found experimentally. It was proved that the crack width and crack distance were predicted fairly accurately.
The mechanical properties of two concrete mixes were determined as a function of temperature and moisture content. Predictions were given for the compressive strength and the tensile splitting strength. It should be noted that a great scatter was found in the tensile splitting strength, thus making an accurate prediction impossible.

Sealed and air-dry concrete exhibited thermal behaviour characterized by almost linear thermal deformation and perfect reversibility. Only small differences in thermal behaviour were found between the reinforcement and the concrete.

However, water-saturated concrete was found to undergo thermal expansion in the temperature range between -20 and -60°C. Considerable stresses may develop in reinforced water-saturated concrete as a result of the thermal differences between the reinforcement and the water-saturated concrete. To calculate crack width and crack spacing correctly a reinforced tension member should be conceived as a prestressed member.

Supplementary research may focus on the following subjects:

- The stress-elongation diagram of a deformation-controlled uniaxial test of concrete and the relationship between the uniaxial tensile strength and the tensile splitting strength as a function of temperature and moisture content (curing conditions). In the present study it is assumed that the fracture energy depends linearly on the tensile strength and the shape of the stress-deformation diagram, represented by the coefficient k, has been kept constant. It was shown in Section 6 that the splitting failure load is affected by the factor k and the fracture energy. Furthermore, the same relationship at room temperature between the uniaxial and the splitting strength is assumed at low temperatures.
- The effect of post-tensioning on the crack width and the crack spacing at low temperatures. The tension member model used for water-saturated concrete includes the prestressing effect. In fact, the model was originally developed for structural concrete, Bruggeling [7], at room temperature and takes into account the effect of reinforcement and tendons. Based on the observations of the sealed concrete (mix 1) pull-out specimens, it is recommended that a constant exponent b and the same ratio $a(T)/f_{ccm}(T)$ as sealed concrete be applied for the local bond stress-slip relationship at low temperatures in the case of tendons.
- The effect of dynamic loading at low temperatures on the crack width and crack spacing and the deformation capacity of the reinforced member. It was found that deformed bars showed a higher bond resistance with increasing loading rate, Vos [78]. However, this loading rate effect is less pronounced for high concrete grades as compared to the low-strength concrete. As a result of the increase in compressive strength at low temperatures only a small increase (10%) in bond resistance is expected under dynamic loading. It was found that the tension stiffening, represented by the factor $\Delta\varepsilon$ (Table 6.3), increased significantly at low temperatures. Consequently, the steel stress in a crack caused by an imposed deformation will be much higher at low temperatures than the associated steel stress at room temperature.
- Structural behaviour of reinforced concrete at low temperatures can be analyzed with the aid of a finite element method (F.E.M). It has already been proven that the local bond stress-slip relationship can be predicted numerically as a function of temperature, Wang and Van der Veen [79]. The experimentally found bond stress-slip relationship can be used in the so-called interface elements, which make it possible for a construction to be analyzed for cracking with F.E.M. at low temperatures.

8. NOTATION

A_c	=	cross-sectional area of concrete	[mm^2]
A_s	=	cross-sectional area of reinforcement	[mm^2]
A_{ss}	=	cross-sectional area of stirrups	[mm^2]
B	=	concrete grade	[N/mm^2]
E_c	=	static modulus of elasticity	[N/mm^2]
E_{co}	=	initial tangent modulus of elasticity	[N/mm^2]
$E_{c,n}$	=	residual modulus of elasticity after n thermal cycles	[N/mm^2]
E_s	=	modulus of elasticity of steel	[N/mm^2]
G_F	=	fracture energy	[N/m]
N	=	normal force	[N]
N_{cr-1}	=	normal force at which the first crack is initiated	[N]
N_{cr-2}	=	normal force at which the crack pattern is fully developed	[N]
R_a	=	surface roughness	[μm]
T	=	temperature	[°C]
$\dot{T}$	=	cooling rate	[°C/min]
a(T)	=	proportionality factor for bond stress-slip relation versus temperature	[N/mm^{2+b}]
b(T)	=	factor as a function of temperature for bond stress-slip relation	[.]
c	=	concrete cover	[mm]
d_s	=	bar diameter	[mm]
$\frac{d(.)}{dx}$	=	first derivative with respect to x	[./mm]
e	=	crack depth	[mm]
f_c	=	cylinder compressive strength	[N/mm^2]
f_{cc}	=	cube compressive strength	[N/mm^2]
f_{cm}	=	mean cylinder compressive strength	[N/mm^2]
$f_{c,n}$	=	residual cylinder compressive strength after n thermal cycles	[N/mm^2]
f_{ccm}	=	mean cube compressive strength	[N/mm^2]
f_{cspl}	=	tensile splitting strength	[N/mm^2]
f_{sy}	=	yield strength of reinforcement	[N/mm^2]
f_R	=	specific rib area	[-]
k	=	factor for stress-crack opening relation	[-]
ℓ_{st}	=	transfer length	[mm]

ℓ_{sT}	=	transfer length caused by a drop in temperature ΔT	[mm]
m	=	free moisture content	[%]
n	=	modular ratio E_s/E_c	[-]
r	=	radius	[mm]
t	=	time	[s]
w/c	=	water/cement ratio	[-]
w_{cr}	=	mean crack width if the crack pattern is just fully developed	[mm]
w_{cr-1}	=	mean crack width for the "first generation cracks"	[mm]
w_{cr-2}	=	mean crack width for the "second generation cracks"	[mm]
w_x	=	mean crack width	[mm]
$\alpha(T)$	=	coefficient of thermal expansion	[1/°C]
δ	=	crack opening displacement	[mm]
δ_o	=	stress free crack opening	[mm]
δ_{tot}	=	total deformation	[mm]
δ_t	=	deformation in tangential direction	[mm]
ε ℓ/ℓ	=	mean value of strain of an element	[-]
ε_c	=	concrete strain	[-]
ε_{cr}	=	ultimate concrete strain	[-]
ε_{max}	=	the maximum mean strain of a structural concrete tension member if the crack pattern is just fully developed	[-]
ε_{meanl}	=	the mean strain of the distortion zone	[-]
$\varepsilon_{s,cr}$	=	steel strain at the crack	[-]
ν	=	Poisson's ratio	[-]
ρ	=	reinforcement ratio	[-]
σ_c	=	concrete stress	[N/mm^2]
σ_{cr}	=	tensile strength of concrete	[N/mm^2]
σ_{cT}	=	concrete tensile stress caused by a drop in temperature	[N/mm^2]
σ_s	=	steel stress	[N/mm^2]
$\sigma_{s,cr}$	=	steel stress at the crack just after cracking	[N/mm^2]
σ_{sT}	=	steel stress due to drop in temperature	[N/mm^2]
τ_b	=	bond stress	[N/mm^2]
$\tau_{b,av}$	=	mean bond stress	[N/mm^2]
τ_{br}	=	bond stress at the initiation of splitting cracks	[N/mm^2]
τ_{bs}	=	bond stress in case of shear failure	[N/mm^2]
τ_{bu}	=	bond strength	[N/mm^2]

ΔT	=	temperature difference	[°C]
Δ_{cr}	=	relative displacement (slip)	[mm]
$\Delta \ell$	=	mean crack spacing	[mm]
$\Delta \varepsilon$	=	tension stiffening	[-]
$\Delta \sigma_{s,cr}$	=	jump in steel stress after cracking	[N/mm^2]

9. REFERENCES

1. Turner, F.H.; Concrete and Cryogenics, Cement and Concrete Association, Wexham Springs (1979), 99 pp.
2. Bruggeling, A.S.G.; Concrete storage vessels, State of the art report, Stevin report, University of Technology, Delft (1979), 265 pp.
3. Breugel, K. van; Potentialities of concrete for storage systems for liquefied gases and hazardous products, Post. Proceedings 10th International Congress of the FIP, New Delhi (1986).
4. Storage tanks for refrigerated liquefied gases with an outer concrete container, Committee for cryogenic storage in concrete tanks, Final Report, Rijnmond (1985), 42 pp.
5. Veen, C. van der; Double wall tank constructed completely in prestressed concrete, IFHP-IULA Symposium, Rotterdam (1987), pp. 148-152.
6. Noakowski, P.; Die Bewehrung von Stahlbetonbauteilen bei Zwangsbeanspruchung infolge Temperatur, Deutscher Ausschuss für Stahlbeton 296 (1978), 153 pp.
7. Bruggeling, A.S.G.; Structural concrete; science into practice, Heron (1987), 67 pp.
8. Veen, C. van der; Properties of concrete at very low temperatures, A survey of the literature, University of Technology, Delft (1987), 121 pp.
9. Bamforth, P.B., Murray, W.T., Browne, R.D.; The application of concrete property data at cryogenic temperature to LNG tank design, Proceedings Second International Conference on Cryogenic Concrete, Amsterdam (1983), session 4, 17 pp.
10. Breugel, K. van, et al.; Betonconstructies voor de opslag van tot vloeistof gekoelde gassen, Stuvo-rapport no. 70 (1983), 251 pp.
11. FIP; Cryogenic behaviour of materials for prestressed concrete; State of the art report, Wexham Springs (1982), 84 pp.
12. Wischers, G., Dahms, J.; Das Verhalten des Betons bei sehr niedrigen Temperaturen, Beton (1970), no. 4, pp. 135-139.
13. Kordina, K., Neisecke, J.; Die Ermittlung der Gebrauchseigenschaften von Beton und Spannstahl bei extrem tiefen Temperaturen, Betonwerk + Fertigteil-Technik (1978), no. 4, pp. 191-197.
14. Reinhardt, H.W.; Mechanische en fysische eigenschappen van beton tussen -190°C en +400°C, Cement 31 (1979), no. 1, pp. 7-13.

15. Browne, R.D., Bamforth, P.B.; The use of concrete for cryogenic storage; A summary of research, past and present, Proceedings First International Conference on Cryogenic Concrete, Newcastle upon Tyne (1981), 27 pp.
16. Hohberg, I.M.; Flüssiggasbehälter aus Spannbeton; Darstellung des gegenwärtigen Wissenstandes über Materialverhalten und Entwurfskriterien bei Tieftemperatur, Thesis, Technische Universität Berlin (1980), 260 pp.
17. Schäper, M.; Tieftemperaturbeanspruchte Spannbetonbehälter, Forschungsbericht Universität Essen (1984), 220 pp.
18. Schnell, J.R.; Zur Bemessung von Stahlbetonteilen unter Last, Vorspannung und Zwang bei Tieftemperatur, Dissertation Technische Universität Darmstadt (1985), 230 pp.
19. Rostásy, F.S., Scheuermann, J.; Verbund und innerer Zwang von einbetoniertem Bewehrungsstahl bei tiefer Temperatur, Forschungsbericht Technische Universität Braunschweig (1984), 92 pp.
20. Monfore, G.E., Lentz, A.E.; Physical properties of concrete at very low temperatures, Journal of the PCA, Research and Development Laboratories (1962), pp. 33-39.
21. Goto, Y., Miura, T.; Experimental studies on properties on concrete cooled to about minus 160°C, Technology Reports, Tohoku University, 44 (1979), no. 2, pp. 359-381.
22. Goto, Y., Miura, T.; Mechanical properties of concrete at very low temperatures, Proceedings 21th Japanese Congress on Material Research, Kyoto (1978), pp. 157-159.
23. Yamane, S., Kasami, H., Okuno, T.; Properties of concrete at very low temperatures, ACI, Proceedings Conf. Mexico City (1977) pp. 67-78.
24. Elices, M., Planas, I.; Measurement of tensile strength of concrete at very low temperatures, ACI Journal (1982), no. 79-21, pp. 195-200.
25. Tognon, G.; Behaviour of mortars and concretes in the temperature range from +20°C to -196°C, Proceedings of the Fifth International Symposium on the Chemistry of Cement, Tokyo (1968), III-24, pp. 229-249.
26. Miura, T.; Deterioration of concrete cooled to very low temperatures, Transactions of the Japan Concrete Institute, 4(1982), pp. 57-64.
27. Rostásy, F.S., Schneider, U., Wiedemann, G.; Festigkeitsverhalten hydraulischer Baustoffe unter konstanter und wechselnder Temperatureinwirkung im Bereich von -200°C, Arbeitsbericht III Technische Universität Braunschweig (1979), 32 pp.
28. Lambotte, H., Cocquyt, F.; The influence of low and very low temperatures on mechanical and thermal characteristics of concrete, Proceedings Transport and Storage of LPG & LNG, Bruges (1984), pp. 365-375.
29. Rostásy, F.S., Wiedemann, G.; Strength and deformability of concrete after low temperature cycles, Proceedings Second International Conference on Cryogenic Concrete, Amsterdam (1983), 8 pp.
30. Wiedemann, G.; Zum Einfluss tiefer Temperaturen auf Festigkeit und Verformung von Beton, Dissertation Technische Universität Braunschweig (1982), 149 pp.

31. Vandewalle, L.; Hechting tussen staal en beton in cryogene omstandigheden, Cement 38 (1986), no. 9, pp. 56-59.
32. Vandewalle, L.; Hechting tussen wapening met verbeterde hechting en beton bij gewone en cryogene omstandigheden, Dissertation Universiteit Leuven (1988), 327 pp.
33. Scheuermann, J.; Zum Einfluss tiefer Temperaturen auf Verbund und Rissbildung von Stahlbetonbauteilen, Dissertation Technische Universität Braunschweig (1987), 224 pp.
34. Bamforth, P.B.; The structural permeability of concrete at cryogenic temperatures, Dissertation, University of Aston, Birmingham (1987), 370 pp.
35. Rehm, G.; Über die Grundlagen des Verbundes zwischen Stahl und Beton, Deutscher Ausschuss für Stahlbeton, 138 (1961), 59 pp.
36. Kasami, H., Tanaka, Y., Kishima, Y., Yamane, S.; Properties of concrete at very low temperatures, Proceedings First International Conference on Cryogenic Concrete, Newcastle upon Tyne (1981), 11 pp.
37. Pfützenreuter, K.H.; Verbundverhalten von Betonstahl im Tieftemperaturbereich, Graduation work, Universität Essen (1982).
38. Vandewalle, L., Mortelmans, F.; Investigation of the bond stress between a reinforcement bar and concrete under cryogenic conditions, Proceedings of the Second International Conference on cryogenic Concrete, Amsterdam (1983), 8 pp.
39. Scheuermann, J.; Untersuchung von Konstruktionswerkstoffen bei tiefen Temperaturen, Verbund und Rissbildung in Stahlbetonbauteilen, Forschungskolloquium des Deutschen Ausschusses für Stahlbeton, Braunschweig 17 (1986), pp. 115-120.
40. Iványi, G., Fastabend, M.; Biegeversuche an hohen Stahlbetonbalken bei tiefen Temperaturen, Forschungsbericht, Universität Essen, 34 (1985), 113 pp.
41. Schnell, J.; Rissbildung und Steifigkeit bei tiefen Temperaturen, Forschungskolloquium des Deutschen Ausschusses für Stahlbeton, Technische Hochschule Darmstadt 18 (1986), pp. 41-43.
42. Iványi, G., Schäper, M.; Biegerissbildung von Stahlbetonbalken bei tiefen Temperaturen, Bauingenieur 58 (1983), pp. 135-142.
43. Bruggeling, A.S.G., Bruijn, W.A. de; Theorie en praktijk van het gewapend beton, University of Technology, Delft (1985), 1333 pp.
44. Krips, M.; Rissbreitenbeschränkung im Stahlbeton und Spannbeton, Dissertation, Technische Hochschule Darmstadt (1984), 250 pp.
45. Lutz, A., Gergely, P.; Mechanics of bond and slip of deformed bars in concrete, ACI-Journal (1967), pp. 711-721.
46. Tanner, J.A.; An experimental investigation of bond slip in reinforced concrete, Thesis Cornell University (1971).
47. Nilson, A.H.; Bond stress-slip relations in reinforced concrete, Report 358, Cornell University (1971).
48. Martin, H.; Zusammenhang zwischen Oberflächenbeschaffenheit, Verbund und Sprengwirkung von Bewehrungsstählen unter Kurzzeitbelastung, Deutscher Ausschuss für Stahlbeton, 228 (1973), 50 pp.

49. Bruggeling, A.S.G.; Imposed deformations and crack width, University of Technology, Delft (1980), 141 pp.
50. Veen, C. van der; Trekkracht; van τ-δ relatie tot overdrachtslengte, in Theorie en praktijk van het gewapend beton, University of Technology (ed. Bruggeling, A.S.G. and Bruijn, W.A. de) Delft (1985), pp. 263-344.
51. Veen, C. van der, Pruijssers, A.P.; Scheurvorming in een trekstaaf c.q. buigligger, University of Technology, Delft (1985), 59 pp.
52. Bruggeling, A.S.G.; Die Übertragungslänge von Spannstahl bei Vorspannung mit sofortigem Verbund, Betonwerk + Fertigteil Technik (1986), pp. 298-302.
53. Tepfers, R.; A theory of bond applied to overlapped tensile reinforcement splices for deformed bars, Report 73-2, Chalmers University of Technology, Göteborg (1973), 328 pp.
54. Reinhardt, H.W., Cornelissen, H.A.W., Hordijk, D.A.; Tensile tests and failure analysis of concrete, Journal of Structural Engineering, 112 (1986), pp. 2462-2477.
55. Wolinski, S., Hordijk, D.A., Reinhardt, H.W., Cornelissen, H.A.W.; Influence of aggregate size on fracture mechanics parameters of concrete, International Journal of Cement Composites and Lightweight Concrete, 9 (1987), pp. 95-103.
56. Reinhardt, H.W.; Fracture mechanics of an elastic softening material like concrete, Heron, 29 (1984), 42 pp.
57. Petterson, P.E.; Crack growth and development of fracture zones in plain concrete and similar materials, Report TVBM-1006, Lund Institute of Technology (1981), 174 pp.
58. Hordijk, D.A., Mier, J.G.M. van, Reinhardt, H.W.; Chapter 4, Material properties, pp. 67-127, in RILEM Report Fracture mechanics of concrete structures, from theory to applications, ed. Elfgren, L., Chapman & Hall, London (1989), 407 pp.
59. Timoshenko, S.; Strength of Materials, part II, Advanced theory and problems, Princeton, New Yersey (1956), pp. 205-210.
60. Heilmann, H.G.; Beziehungen zwischen Zug- und Druckfestigkeit des Betons, Beton, 2 (1969), pp. 68-70.
61. Tepfers, R. et al.; Bond action and bond behaviour of reinforcement, State of the art, Bulletin d'information No. 151, CEB (1982), 153 pp.
62. Urban, V.; Anchorage length and bond stress calculation, Research Report 458, Technical University Prague (1980) (Reference from [61]).
63. Tilanterä, T., Rechardt, T.; Bond of Reinforcement in Lightweight Aggregate Concrete, University of Technology, Helsinki (1977), pp. 1-36 (Reference from [61]).
64. Eligehausen, R.; Übergreifungsstösse zugbeanspruchter Rippenstäbe mit geraden Stabenden, Deutscher Ausschuss für Stahlbeton, 301, Berlin (1979), 118 pp.
65. Schmidt-Thrö, G.; Verbundverhalten von Rippenstählen im Beton unter besonderer Berücksichtigung einer einachsigen Querpressung, Dissertation, München (1987), 211 pp.
66. Körmeling, H.A.; Strain rate and temperature behaviour of steel fibre concrete in tension, Dissertation, Delft (1986), 140 pp.

67. Veen, C. van der; Bond stress-slip relationship at very low temperatures, Part I, Experimental results, Stevin Report 25-87-43, University of Technology, Delft (1987), 70 pp.
68. Veen, C. van der; Aanhechting van staal in beton onder cryogene omstandigheden, Cement, 8 (1986), pp. 18-24.
69. Veen, C. van der; Bond stress-slip relationship at very low temperatures, Part II, Appendices, Stevin Report 25-88-2, University of Technology, Delft (1988), 69 pp.
70. RILEM/CEB/FIP committee; Tests and specifications of reinforcements for reinforced and prestressed concrete. Bond test for reinforcing steel, 2. Pull-out test. Materials and Structures; Research and Testing 3 (1970), no. 15, pp. 175-178.
71. Neville, A.M.; Properties of Concrete, Pitman, London (1982), 779 pp.
72. Lessel, G., Bernard, A.; Mechanical properties of concrete reinforcing bars used for liquefied gas storage tanks, Proceedings Second International Conference on Cryogenic Concrete, Amsterdam (1983), 11 pp.
73. Romijn, P.E.; Experimenteel onderzoek aan gewapend betonnen trekstaven bij lage temperaturen, Graduate thesis, Delft University of Technology, Delft (1990).
74. Veen, C. van der, Reinhardt, H.W.; Bond behaviour of reinforced concrete at low temperatures, The 10th International Conference on Port and Ocean Engineering under Arctic Conditions, Sweden, Lulea (1989), pp. 852-861.
75. Veen, C. van der, Reinhardt, H.W.; Bond strength in reinforced concrete at low temperatures, Proceedings of the eight International Conference on Offshore Mechanics and Arctic Engineering, The Hague (1989), pp. 573-582.
76. Hungspreug, S.; Local bond between a reinforcing bar and concrete under high intensity cyclic load, Report 81-6 Cornell University, Ithaca (1981), 449 pp.
77. Thormählen, U.; Zum Einfluss von Spanngliedern mit nachträglichem Verbund auf Rissbildung und Rissbreitenbeschränkung bei teilweise vorgespannten Konstruktionen, Dissertation Technische Hochschule Aachen (1978), 319 pp.
78. Vos, E.; Influence of loading rate and radial pressure on bond in reinforced concrete, A numerical and experimental approach, Dissertation, Delft (1983), 235 pp.
79. Wang, Q., Veen, C. van der; Numerical analysis for pull-out test at low temperature, Report 25.2-89-516, University of Technology, Delft (1989), 25 pp.

APPENDIX I MIX Proportions

MIX Code B1640040 (MIX 1) strength $f_{ccm} \approx 60$ N/mm^2 (at 28 days)

Components		Sieve analysis of aggregate Sieve opening	
	[kg/m^3]	[mm]	[kg]
sand	807	8-16	595
glacial river gravel	1017	4-8	422
Portland cement B	400	2-4	299
water	160	1-2	209
		0.5-1	150
		0.25-0.50	104
		0.10-0.25	45
calc. density	2384		1824

MIX Code B1627560 (MIX 2) strength $f_{ccm} \approx 40$ N/mm^2 (at 28 days)

Components		Sieve analysis of aggregate Sieve opening	
	[kg/m^3]	[mm]	[kg]
sand	973	8-16	563
glacial river gravel	971	4-18	408
Portland cement B	275	2-4	272
water	165	1-2	214
		0.5-1	136
		0.25-0.50	215
		0.10-0.25	136
calc. density	2384		1944

Sieve analysis of aggregate

Sieve opening [mm]	Füller [cum. %]	MIX 1 [cum. %]	MIX 2 [cum. %]
8-16	100.0	100.0	100.0
4-8	70.7	67.4	71.0
2-4	50.0	44.2	50.0
1-2	35.4	27.9	36.1
0.5-1	25.0	16.4	25.1
0.25-0.50	17.7	8.2	18.1
0.10-0.25	12.5	2.5	7.0